PSEUDOPHOSPHORYLATION OF TAU MODULATES ITS FUNCTION AND INDUCES AD-LIKE CHANGES

BY

Qian Sun

M.S., Nanjing University, 2003

Submitted to the graduate degree program in Molecular Biosciences
and the Graduate Faculty of the University of Kansas
in partial fulfillment of the requirements for the degree of
Doctor of Philosophy

Committee members: _____
Chairperson – T. Chris Gamblin

_____
William Dentler

_____
Mary L. Michaelis

_____
Kristi Neufeld

_____
Mark Richter

Date defended: 8/7/2009

The Dissertation Committee for Qian Sun certifies

that this is the approved version of the following dissertation:

PSEUDOPHOSPHORYLATION OF TAU MODULATES ITS FUNCTION AND INDUCES AD-LIKE CHANGES

Committee members: _____
Chairperson* – T. Chris Gamblin

Date approved: 8/7/2009

_____

Abstract

The microtubule associate protein tau, in a hyperphosphorylated form, loses its normal function and aggregates into insoluble paired-helical filaments (PHFs) in Alzheimer's disease (AD) and other tauopathies. The stoichiometry of phosphorylation is increased from 2-3 mol of phosphate per mole of tau in normal brain to 5-9 mol of phosphate per mole of tau in AD. In AD, the deregulation of kinases, such as glycogen synthase kinase-3β (GSK-3β), is believed to be associated with the generation of hyperphosphorylated tau. However, the functional contribution of hyperphosphorylation on AD is not well understood. Therefore, pseudohyperphosphorylation mutants at six or sever GSK-3β phosphorylation sites were generated by amino acid substitution. In addition, several single, double and triple pseudophosphorylation mutants at these sites were also generated and used as controls. I studied the changes on mobility on SDS-PAGE, microtubule (MT) binding and arachidonic acid (ARA) induced polymerization. Four pseudophosphorylation mutants induced an SDS-resistant mobility change. All but three mutants had a reduced MT binding affinity and pseudohyperphosphorylation mutants did not have a greater effect compared with pseudophosphorylation mutants at single or double sites. Three pseudohyperphosphorylation mutants with retarded SDS mobility had a greater effect on ARA-induced polymerization, with reduced nucleation and elongation rate. Some pseudophosphorylation mutants had a significantly increased polymerization at high ARA concentrations compared with wild type tau. The tangle like aggregates similar to those isolated from AD brain

were formed in the mixture of six pseudophosphorylation mutants. These observations suggest the increased toxicity of hyperphosphorylated tau may be induced by decreased MT binding affinity and reduced nucleation and polymerization rate. These observations also explain the potentially beneficial role of tau polymerization and NFT formation.

I also studied the mechanism of ARA-induced tau polymerization. The results suggest that ARA can induce tau polymerization both as large micelles and monomers (or small micelles) and molecular nature of tau can affect the morphology of tau filament. The amount and morphology of tau filament can also be affected by surface area : inducer ratio.

Dedicated to my parents

给我亲爱的爸爸妈妈

Acknowledgements

First and foremost I would like to express the deepest appreciation to my mentor Dr. Chris Gamblin, who supported me throughout my dissertation with his patience and knowledge and gave me the room to work in my own way at the same time. He taught me how to be a scientist and helped me to gain the confidence in science. He has made available his support in numerous ways. Without his encouragement and effort, I would not be able to complete this work and write this dissertation. I feel extremely fortunate to have him as my mentor and to be guided by him in my graduate school.

I would also like to show my gratitude to members of my graduate committee, Dr. William Dentler, Dr. Erick Floor, Dr. Kristi Neufeld, Dr. Mary Michaelis and Dr. Mark Richter for all their advice. They helped me to pass through the difficult time in my graduate school. They also showed me a way to science and helped me build the enthusiasm in research. I owe my deepest gratitude to their encouragement and support.

In my daily work, I have been supported by a friendly and cheerful group of labmates from the Gamblin lab. I am indebted to them for all the helpful discussions and suggestions, and for making the lab a fun place to work every day. Especially, I would like to thank Dr. Carolyn Rankin, who has been working together with me in the lab during my graduate school. She not only taught me a lot of techniques I used in this dissertation but also has been supportive in my life. I would also like to

thank Kellen Voss, the graduate student from the Gamblin lab, to read and correct my dissertation.

I would also like to thank Dr. Lester Binder (Northwestern University) for providing the constructs for S396/404E and P301L, and Dr. Richard Himes for providing purified tubulins.

The Department of Molecular Biosciences has provided the support and equipment I have needed to complete my dissertation. I would like to thank Dr. David Moore from Microscopy and Analysis Imaging Laboratory for his help in tutoring me in the use of Transmission Electron Microscopy.

Finally, I thank my parents for supporting me throughout all my studies at graduate school. They have always been my primary source of courage and motivation in my life.

Table of Contents

List of Figures

List of Tables

List of Abbreviations

AA	Amino acid
Aβ	β amyloid peptide
AD	Alzheimer's disease
AI	htau40$^{I277/308P}$ mutant tau
APP	Aβ precursor protein
ARA	Arachidonic acid
CaMPK	Ca^{2+}/calmodulin-dependent protein kinase
CBD	Corticobasal degeneration
CMC	Critical micelle concentration
cdk	Cyclin-dependent kinase
CNS	Central nervous system
FPLC	Fast protein liquid chromatography
FTDP-17	Frontotemporal dementia with Parkinsonism linked to chromosome 17
GSK3	Glycogen synthase kinase 3
GSK-3β	Glycogen synthase kinase 3β
JNK	c-Jun NH_2-terminal kinase
LB	Luria broth
LLS	Laser light scattering
MAPK	Mitogen activated protein kinase
MARK	Microtubule-affinity regulating kinase
MT	Microtubule

NFTs	Neurofibrillary tangles
NPN	N-phenyl-1-napthylamine
PDPK	Proline-directed protein kinase
PHFs	paired helical filaments
pI	Isoelectric points
PiD	Pick's disease
PKA	cyclic-AMP-dependent kinase
PP1	Ser/Thr phosphatase protein 1
PP2A	Ser/Thr phosphatase protein 2A
PP2B	Ser/Thr phosphatase protein 2B
PP2C	Ser/Thr phosphatase protein 2C
PP5	Ser/Thr phosphatase protein 5
PSP	Progressive supranuclear palsy
SFs	Straight filaments
SAPK	Stress activated kinase
SDS-PAGE	Sodium dodecyl sulfate-polyacrylamide gel electrophoresis
TEM	Transmission electron microscopy
Tg	Transgenic
ThS	Thioflavine S
TTK	Tau-tubulin kinase
Wt	Wild type tau

CHAPTER 1 INTRODUCTION

In 1975, Tau protein was first isolated by Weingarten and colleagues as a protein factor that co-purified with tubulin and was able to promote microtubule assembly (*1, 2*). About ten years later, tau was found to be the major component of neurofibrillary tangles (NFTs), one of the hallmarks of Alzheimer's disease (AD), by several groups (*3-7*). This finding evoked new interest in the study of tau protein.

1.1 The structure and function of human tau in normal neurons

In human brain, there are six different isoforms of tau protein, which are all translated from a single gene on chromosome 17 at position 17q21, named *MAPT* (*8, 9*). The *MAPT* gene contains 16 exons and the alternative splicing of exon 2, 3 and 10 results in the generation of 6 tau isoforms, ranging from 352 to 441 amino acids (Figure 1.1)(reviewed in (*8*)). These isoforms differ by the presence of 3 or 4 microtubule binding repeats combined with the presence of 0, 1 or 2 N-terminal insertions (reviewed in (*8*)). The additional microtubule binding repeat R2 is encoded by exon 10 and the two N-terminal insertions are encoded by exon 2 and exon 3 (Figure 1.1). These tau isoforms are named ht23 (0N3R), ht24 (0N4R), ht34 (1N4R), ht37 (1N3R), ht39 (2N3R), and ht40 (2N4R), where N represents the N-terminal insertions and R represents the microtubule binding repeats (*10, 11*). Human tau protein mainly locates in neurons with high concentrations of tau observed in axons. The expression of these tau isoforms is developmentally regulated, with ht23 (0N3R) being the only isoform present in fetal brain (also called fetal tau) and all six isoforms

being present in adult brain (reviewed in (*8*)). Furthermore, there are about equal amounts of 3R and 4R isoforms in adult brain (*12*).

The major functions of tau are to bind and stabilize microtubules and to promote microtubule assembly. The C-terminal part of tau binds to microtubules (reviewed in (*8*)), and is named the microtubule binding domain (Figure 1.2). The microtubule binding domain has 3 or 4 microtubule binding repeats (R1 – R4), which are encoded by exons 9-12. These microtubule binding repeats and the regions in between these repeats contribute to the binding between tau and microtubules (reviewed in (*13*)). The 4R isoforms have a higher binding affinity compared with 3R isoforms due to the presence of an additional binding repeat and strong interactions between microtubules and the internal regions between R1 and R2 (reviewed in (*8*)). The proline-rich region also contributes to the binding between tau and microtubules (*14*).

The rest of the tau protein, the projection domain, projects from the surface of the microtubules. This domain includes the N-terminal part of the protein and the following proline-rich region (Figure 1.2). The major function of the projection domain is to control the spacing between microtubules in the axon (*15*), therefore controlling the diameter of the axon (reviewed in (*8*)). Tau has other functions in cells including interactions with cytoskeleton components (actins and neurofilaments), cytoplasmic organelles, the plasma membrane and regulatory functions during development (reviewed in (*8, 16*)).

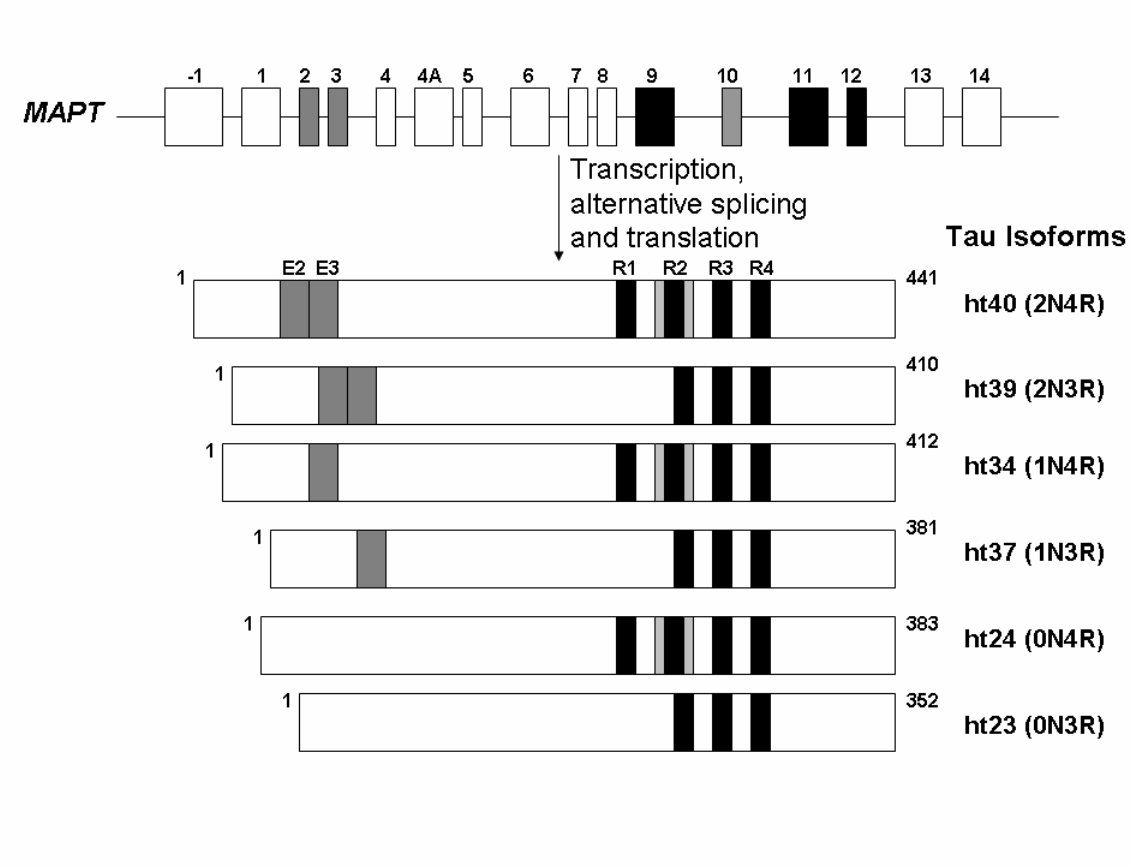

Figure 1.1. Schematic representation of human tau gene and the six tau isoforms found in human central nervous system (CNS). Human tau gene is located on chromosome 17 at position 17q21 and contains 16 exons. Exon 1 is a part of the promoter. Exon 4A, 6 and 8 are not transcribed in human CNS. Alternative splicing of exon 2, 3 and 10 produces the six tau isoforms in human brain. These isoforms differ by the absence or presence of one or two N-terminal 29 amino acids inserts (dark gray box), encoded by exon 2 and 3, in combination with three or four 18 amino acid microtubule binding repeats (black box and light gray box, R1 to R4) in the C-terminus. The relative sizes of the exons are not drawn to scale.

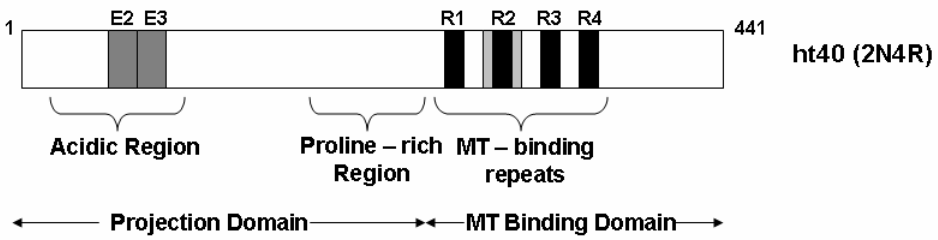

Figure 1.2. Schematic representation of the functional domains on the longest human tau isoform (2N4R). The microtubule binding domain is the C-terminal part of the protein and contains four microtubule-binding repeats. The function of this domain is to bind and stabilize microtubules. The projection domain contains N-terminal acidic region and the following proline-rich region. This domain interacts with cytoskeletal elements and determines the spacing between microtubules in axons.

Tau loses its normal functions in some neurodegenerative diseases and aggregates into insoluble paired helical filaments (PHFs), straight filaments (SFs) and neurofibrillary tangles (NFTs) (reviewed in (*8*)). The neurodegenerative diseases include: Alzheimer's disease (AD), Pick's disease (PiD), progressive supranuclear palsy (PSP), corticobasal degeneration (CBD) and frontotemporal dementia with Parkinsonism linked to chromosome 17 (FTDP-17).

1.2 Alzheimer's Disease and tauopathies

1.2.1 Alzheimer's Disease

Alzheimer's disease (AD) was first described by Dr. Alois Alzheimer in 1906. AD is a progressive dementia characterized by the presence of amyloid plaques and neurofibrillary tangles (reviewed in (*8*)). AD is the most common form of dementia and accounting up to 50 - 70 percent of all dementia cases (http://www.alz.org). There were approximately 18 million AD patients worldwide by 2007. Today, in the US, as many as 5.3 million people are living with AD and AD is the 6th-leading cause of death in the US (http://www.alz.org). In a conservative estimation, 1 in 10 of those over 65 and 1 in 5 of those over 85 years old are likely to have AD (reviewed in (*17*)). With the extension of the average life span, we are facing an increasing number of AD cases.

With the progression of AD, some pathological changes occur in the brain. These include, but are not limited to, reduced brain size, neuronal loss, the presence of amyloid plaques and the presence of neurofibrillary tangles. Among these

pathological changes, amyloid plaques and neurofibrillary tangles are the two most prominent and are used as the diagnostic hallmarks of AD (reviewed in (*17*)).

The major component of amyloid plaques is β amyloid peptide (Aβ), which homogenously distributes in the plaques (reviewed in (*17*)).

The second most distinctive pathological component of AD is neurofibrillary tangles (NFTs). NFTs are mainly found in the cortex and hippocampus (*18*). Most NFTs are intracellular, although some extracellular "ghost tangles" are also present in AD brain. These "ghost tangles" are the insoluble components of dead neurons (reviewed in (*17*)). The number and distribution of NFTs relate to the type and degree of dementia, and the spreading of NFTs has been used as a diagnostic sign of the stage of the dementia (*19*). NFTs are Thioflavine S (ThS) positive and tau is the major component of NFTs. Tau protein isolated from NFTs is abnormally hyperphosphorylated and is in the form of insoluble paired helical filaments (PHFs) and straight filaments (SFs) (*20, 21*). PHFs are the wound helices of a pair of unbranched filaments. PHFs are approximately 20 nm across and 80 nm long per period. SFs are filaments with a width between 5 - 20 nm, with no periodical changes in the width. Both PHFs and SFs in AD contain all six isoforms of tau (reviewed (*17*)). In addition to tau, other components are found in NFTs, including ubiquitin (*22*), RNA (*23*), α-synuclein (*24*), GSK-3β (*25*) and apolipoprotein E (*26*).

In AD, tau pathology was found to be associated with Aβ pathology in neuritic plaques. Aβ peptides are in the center of neuritic plaques. Other components, such as apolipoprotein E and amyloid precursor protein, form a less condensed halo around

the plaques (reviewed in (*17*)). Tau, in the form of insoluble paired helical filaments (PHF), is also found to be present in the halo (*27*).

Neuron loss is also observed in AD. There is as high as a 70% reduction in the number of neurons in AD (reviewed in (*17*)). Most of these neurons are the neurons prone to NFT formation, such as the disrupted neurons that result in "ghost tangles" (*28, 29*). Also, the shrinkage of the remaining neurons happens frequently in AD (*28*). Besides the changes to neuronal cells, abnormal glial cells are observed in AD. The activated glial cells, mainly astrocytes and microglial cells, are found in AD brains (reviewed in (*17*)).

1.2.2 Other tauopathies

Alzheimer's disease is associated with both extracellular Aβ deposits and intracellular NFTs. Therefore, it has been questioned whether the changes in tau function contribute to dementia or are a non-specific event associated with Aβ deposits. The finding of pathological tau deposits in a group of neurodegenerative diseases in which Aβ deposits are totally or mostly absent, suggests that the changes in tau function alone is sufficient to cause neurodegenerative diseases. Tau deposits in these diseases are different in morphology and the percentage of each isoform (see below). These diseases include: Pick's disease (PiD), progressive supranuclear palsy (PSP), corticobasal degeneration (CBD) and frontotemporal dementia with Parkinsonism linked to chromosome 17 (FTDP-17). These diseases are collectively termed tauopathies (reviewed in (*30*)).

1.2.2.1 Pick's Disease (PiD)

PiD is a neurodegenerative disease characterized by the presence of Pick bodies. Pick bodies are intracellular, anti-PHFs-tau antibody positive inclusions in brains (reviewed in (*30*)). Close examination of Pick bodies showed that tau in Pick bodies is a mix of straight filaments (SFs) and twisted ribbon filaments with long-periods (*31*). Tau isolated from Pick bodies is also abnormally hyperphosphorylated, similar to tau isolated from AD (reviewed in (*30*)).

1.2.2.2 Progressive supranuclear palsy (PSP) and corticobasal degeneration (CBD)

In PSP and CBD, tau deposits form in both neurons and glial cells. Progressive supranuclear palsy (PSP) and corticobasal degeneration (CBD) are late onset, neurodegenerative diseases with neuronal loss and NFT formation in neurons and glial cells (reviewed in (*13*)). The major component of NFTs is hyperphosphorylated tau protein but in different forms in PSP and CBD. In PSP, straight filaments are the major forms of tau in NFTs, and twisted ribbons with a long period are also observed in tangles (reviewed in (*8*)). In CBD, tau filaments are in the form of paired helical filaments (PHFs) and straight filaments (SFs) (reviewed in (*13*)).

1.2.2.3 Frontotemporal dementia with Parkinsonism linked to chromosome 17 (FTDP-17)

Although tau positive inclusions are found in these tauopathies, they were first thought of as a non-specific event accompanying neurodegeneration. The causative role of tau in AD was bolstered by the discovery of mutations in the tau gene in inherited FTDP-17, which are autosomal dominant, adult-onset, neurodegenerative disorders (*32*). Because similar changes in tau function and neuropathologies were observed in FTDP-17 as in AD and other tauopathies, studies on these FTDP-17 mutations contribute to the understanding of the role of tau protein in non-familial tauopathies.

To date, 38 mutations of the tau (*MAPT*) gene have been identified from studies of over 100 families with FTDP-17 (Figure 1.3) (*32*). The pathologies vary within and between different families with the same or different mutations (reviewed in (*33*)). The formation of tau deposits in neurons and/or glial cells is one of the major characteristics of FTDP-17 ((reviewed in (*34*)). Other general characteristics include neuronal atrophy, neuronal loss and active glial cell (reviewed in (*33*)). The neuropathology may resemble that of AD or PiD because of the presence of NFTs in neurons or resemble those of PSP or CBD because of tau deposits in glial cells (reviewed in (*33*)). Usually little or no amyloid deposition is observed in FTDP-17. Most of the FTDP-17 mutations are in the coding region of tau (Figure 1.3). All of the exonal mutations are located in the MT-binding region (exons 9-12) or close to it, with R5H/L to be the only exception. The rest of the mutations (E9+33, +3, +11, +12, +13, +14, +16, +19, +29) occur in the introns downstream of exon 9 and exon 10, affecting splicing regulation.

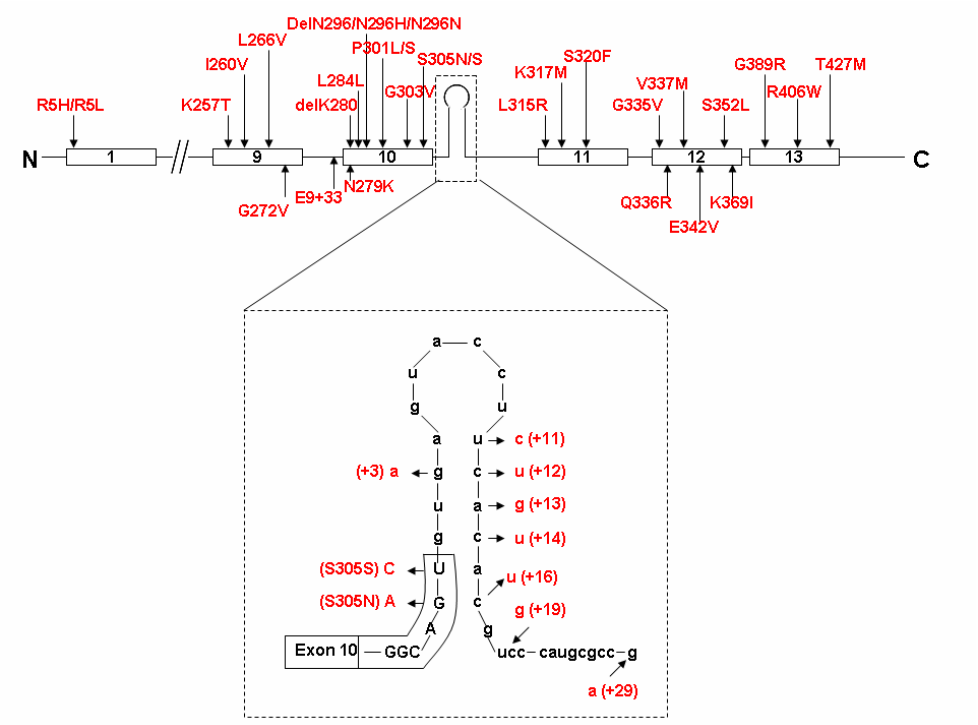

Figure 1.3. Schematic representation of mutations in human *MAPT* gene associated with FTDP-17. FTDP-17 mutations are listed in the figure and labeled with red. The mutations on the pre-mRNA stem-loop and the downstream intron are shown in the insertion. The mutations in this region affect the splicing of the gene. Exonic sequences are labeled with uppercase letters and intronic sequences in lowercase. The relative sizes of the exons are not drawn to scale. Modified from Gasparini *et al.*, 2007.

All these mutations can be classified into three groups: mutations altering the tau-microtubule interactions; mutations altering tau mRNA splicing; and mutations altering both tau-microtubule interactions and tau RNA splicing. The mutants in the first group, such as P301L and P301S decrease the binding affinity of tau to microtubules and/or reduce their ability to promote microtubule assembly (*32*). Most of the mutants with reduced tau-microtubule interactions also more readily aggregated into filaments (*35*). The second group is the mutations that alter tau mRNA splicing. This group includes all of the mutations in the intron downstream of exon 10 and most of the coding mutations in exon 10 (*36*). Several deletion and missense mutations in exon 10 affect both the splicing of mRNA and tau protein function, and belong to the third group. These mutations are DelK280, N296H and S305N (*8, 13, 30, 32-34*).

The link between tau mutations and FTDP-17 phenotypes emphasizes that tau dysfunction itself can cause neurodegenerative disorders. The reduced microtubule binding activity and the subsequent aggregation are key events in the progression of neurodegeneration.

1.3 Pathological tau deposits:

The presence of tau deposits in AD and other tauopathies is one of the prominent characteristics of these neurodegenerative diseases. However, the tau deposits in different tauopathies are different not only in the ultrastructure of the deposits, but the percentage of each isoform (reviewed in (*13*)).

In AD and some of the FTDP-17 resembling AD, such as tau mutants L266V, L315R, S320F, V337M, K369I, R406W (reviewed in (*32, 37*)), a small number of SFs and a large number of PHFs are present and all six brain tau isoforms can be isolated from the tau deposits (reviewed in (*13*)). The core of a PHF is composed of the microtubule binding region of tau (*38*). When separation by SDS-PAGE, tau in PHFs and SFs from AD is present in three major bands (68, 64 and 60 kDa) and a minor band at 72kDa (Figure 1.4) and all tau is hyperphosphorylated (*39, 40*). When de-phosphorylated by alkaline phosphatase, the four bands resolve into six bands corresponding to the six isoforms (Figure 1.4) (*41, 42*).

In PiD and some of the FTDP-17 mutations (i.e. K257T, G272V, DelK280 and G389R), twisted ribbons and SFs are the major forms of insoluble tau and only 3R isoforms are present in the tau deposits. SDS-PAGE analysis of the insoluble tau reveals two major bands (64 kDa and 60 kDa) and a minor band (68 kDa), and all of which are hyperphosphorylated (Figure 1.4) (reviewed in (*13*)). Dephosphorylation of the insoluble tau results in 3 bands corresponding to the three 3R isoforms (Figure 1.4). However, all six brain isoforms are expressed and found in soluble components in brain (reviewed in (*32, 37*)).

Another pattern of the insoluble tau is seen in CBD, PSP and some FTDP-17 (such as R5H/L, I260V, N279K, N296H/N, P301L, E342V, +3, +12, +13, +14 and +16) (reviewed in (*13*)). In these cases, tau deposits are in the form of twisted ribbons and SFs, and only hyperphosphorylated 4R isoforms are found in the deposits (reviewed in (*32, 37*)). Insoluble tau deposits electrophorese as two major bands at

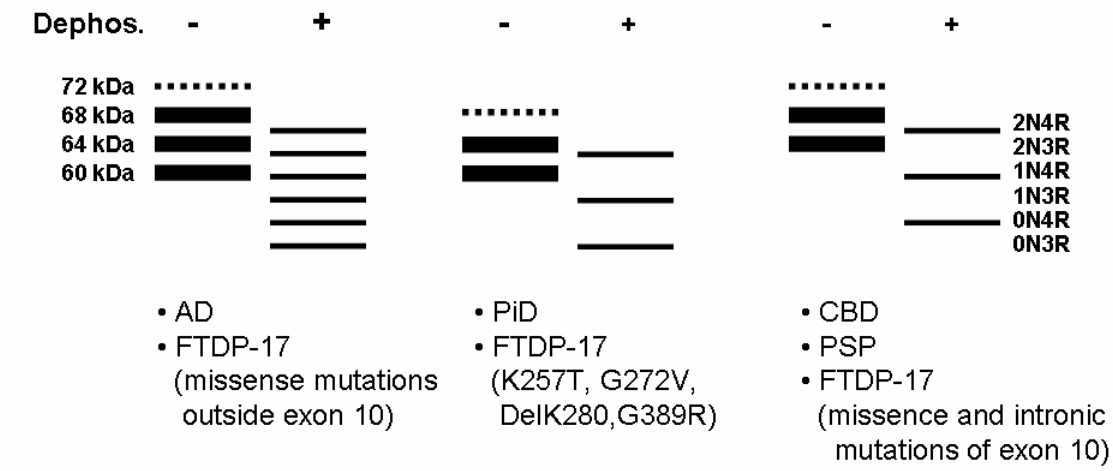

Figure 1.4. Schematic representation of western blot patterns of insoluble tau bands in AD and different tauopathies. The diagram describes the typical patterns of the insoluble tau deposits on SDS-PAGE in AD and various tauopathies. The sarkosyl-insoluble tau is separated by SDS-PAGE and immunoblotted with anti-tau antibodies before (-) and after (+) dephosphorylation. The molecular weights of the bands are labeled on the left and the different tau isoforms on the right. The 1st, 2nd and 3rd pattern of tau bands are mainly found in AD, PiD, and CBD and PSP, respectively. The patterns of FTDP-17 mutations differ according to the type and position of the mutations. Modified from Lee *et al.,* 2001.

68 kDa and 64 kDa and a minor band at 72 kDa (Figure 1.4). The dephosphorylated samples resolve into 3 bands corresponding to the three 4R isoforms. However, the expression patterns of tau in CBD, PSP and the FTDP-17 mutants are different. In CBD and PSP, all six isoforms are expressed in the patients' brains. In the FTDP-17 mutations, the expression levels of the 4R isoforms are much higher than those of the 3R isoforms, due to the changes in mRNA splicing in these FTDP-17 mutants (reviewed in (*32, 37*)).

One thing that should be mentioned about the tau deposits is that it is not clear if these tau deposits are neurotoxic or neuroprotective. Evidence from cell models and animal models supports the idea that NFTs are neuroprotective (see below).

1.4 Phosphorylation of tau

A distinct feature of tau isolated from pathological tau deposits in AD and tauopathies is that it is abnormally hyperphosphorylated. The hyperphosphorylated tau has similar changes in MT binding and self-aggregation as observed in FTDP-17 mutations. Therefore, hyperphosphorylation has been suggested as an early event in the progression of AD and tauopathies. The phosphorylation of tau was also observed in normal brain and its function is to regulate tau function.

There are 85 potential phosphorylation sites on the longest tau isoform. These include 79 serine or threonine sites and 6 tyrosine sites. Currently, 71 of these 85 potential sites have been shown to be phosphorylated in physiological or pathological conditions. Most of these sites locate in the proline-rich region and C-terminal region

outside of the microtubule binding repeats. These sites are Thr17, Try18, Try29, Thr39, Ser46, Thr50, Thr52, Ser56, Ser68, Thr69, Thr71, Thr95, Thr101, Thr102, Thr113, Thr123, Thr131, Thr149, Thr153, Thr169, Thr175, Thr181, Ser184, Ser191, Try197, Ser198, Ser199, Ser202, Thr205, Ser208, Ser210, Thr212, Thr214, Ser217, Thr220, Ser231, Thr235, Ser237, Ser238, Ser241, Ser245, Ser258, Ser262, Ser263, Ser285, Ser289, Ser293, Ser305, Ser316, Ser320, Ser324, Ser341, Ser352, Ser356, Thr361, Thr373, Thr386, Try394, Ser396, Ser400, Thr403, Ser404, Ser409, Ser412, Ser413, Thr414, Ser416, Ser422, Thr427, Ser433 and Ser435.

1.4.1 Phosphorylation regulates tau function under physiological conditions

Tau is phosphorylated to 2-3 mol of phosphate per mole of tau in normal brain and phosphorylation of tau regulates its function, such as microtubule binding and cell sorting (*8, 43*). At least 30 sites have been reported to be phosphorylated on normal tau (reviewed in (*8*)). Stabilizing microtubules and promoting the assembly of microtubules are the major functions of tau in neurons. Phosphorylation of tau can negatively regulate tau-microtubule binding affinity as well as its ability to promote tubulin assembly (*44-46*). The phosphorylation of tau at the sites outside of MT-binding repeats decreases tau-MT binding in a 2-3 fold range (*47*). Phosphorylation at the sites inside MT-binding repeats, for example S262, drastically reduces tau-MT binding. However, none of these phosphorylation sites alone is sufficient to totally abolish the binding between tau and MTs (*48*). The phosphorylation at certain sites

could reduce the ability of tau to stimulate tubulin assembly without drastically changing the binding affinity between tau and microtubules (*49-51*).

The phosphorylation level changes in different developmental stages. In fetal brain, tau is phosphorylated in a higher stoichiometry but not as high as in AD (*8, 52, 53*). The mechanism of transient hyperphosphorylation during development is not clear. The transient hyperphosphorylation may relate to the higher concentration of tubulins and higher degree of plasticity of microtubules required during neuron development in fetal brain (*54*). The concentration of tubulin in fetal brain is about 1.5 times higher than that in adult brain and the presence of hyperphosphorylated tau may reduce the chance of MT bundling (*53*). The de-phosphorylation of hyperphosphorylated fetal tau is most likely due to the increase of phosphatase activation when maturity (*8, 52, 53*).

1.4.2 Pathological phosphorylation of tau

Phosphorylation of tau happens under both physiological and pathological conditions. However, the stoichiometries of phosphorylation are different under these two conditions. In AD brain, the stoichiometry of phosphorylation is drastically increased from 2-3 mol phosphate per mole of tau in normal brain to 5-9 mol (*55*). Hyperphosphorylated tau is the major component of PHFs, SFs and NFTs, and phosphorylation is considered one of the trigger events of AD and tauopathies. Hyperphosphorylated tau is also found in the cytosol from AD brain (*55*). In AD brain, the expression level and the concentration of normal tau are as high as the

concentration in age-matched control (*56*). However, in addition to the normal tau, the concentration of abnormally hyperphosphorylated tau is several fold higher than normal tau (*55*).

Tau protein in AD and tauopathies is not only hyperphosphorylated but also abnormally phosphorylated. About 45 sites have been found to be phosphorylated in PHF tau (Figure 1.5) (*53, 57*). Most of these phosphorylation sites cluster in the proline-rich region and C-terminal region (*53, 57*). The hyperphosphorylation and abnormal phosphorylation of pathological tau were first suggested by the following findings. First, the results of 2D gel electrophoresis showed PHF tau was more acidic than normal tau. This increase in acidity was due to the hyperphosphorylation (*58*). Second, the increased phosphorylation levels were all confirmed by the upward band shift on the SDS-PAGE exclusively in pathological tau. Third, by using mass spectrometry and antibodies to PHF-tau, pathological tau was found to be hyperphosphorylated at both native phosphorylation sites and abnormal pathological sites. Antibodies to PHF-tau, such as AT100 and TG3, can react with tau isolated from AD patients but not normal tau (*59, 60*).

1.4.3 Tau phosphorylation and tau aggregation

Because hyperphosphorylated tau is found in insoluble and cytosolic forms from the brains of AD and other tauopathy patients, hyperphosphorylation is considered an early event in the development of NFTs. This idea is supported by the fact that the hyperphosphorylated tau isolated from AD is able to self-aggregate into

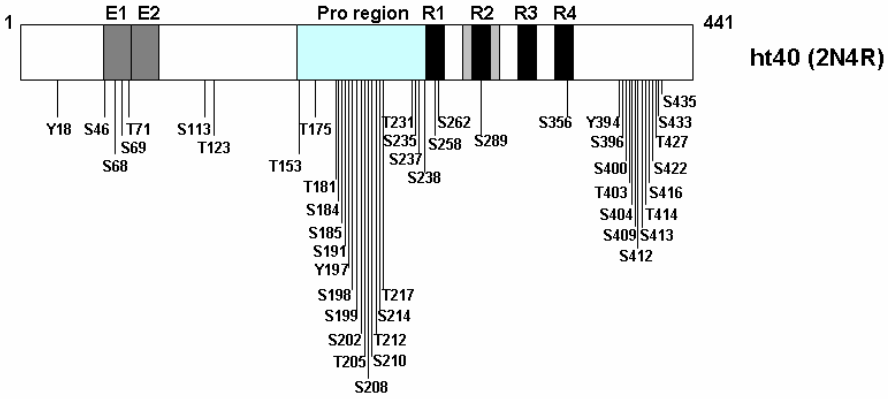

Figure 1.5. Schematic representation of phosphorylation sites on the longest tau isoform from AD. Approximately 45 phosphorylation sites have been identified on PHF tau from AD by phosphorylation-specific antibodies and mass spectrometry. Most of these sites cluster in the proline-rich region (light blue box) and C-terminal region. Black boxes represent microtubule binding repeats (R1- R4) and gray boxes represent N-terminal inserts. The boxed regions are not drawn to scale.

PHFs and SFs under physiological conditions (*61*). The dephosphorylation with PP2A alone is enough to inhibit the self-aggregation of AD tau (*62*). Recent results showed that re-phosphorylation of PP2A de-phosphorylated AD tau with several combinations of kinases can restore the ability of tau to self-aggregate (*63*).

How hyperphosphorylation leads to the formation of filaments and NFTs is not clear. It may come from the following changes. First, the hyperphosphorylated tau has a lower affinity for MT (*63*). Because it is released from MT, the concentration of soluble cytosolic tau is drastically increased and this is a more favorable condition for tau self-polymerization. Second, the conformational changes induced by phosphorylation make phosphorylated tau a better substrate of kinases and further increase its tendency for self-aggregation. Similarly, all known FTDP-17 mutations can alter their conformations to the more favorable ones for the interaction with kinases and more readily for self-aggregation (*64*). Third, the abnormal hyperphosphorylation of tau can neutralize inhibitory factors of tau. Although tau is a natively unfolded protein, β-sheet fragments form in its microtubule-binding repeats (*65*). R3 in 3R isoforms and R2 and R3 in 4R isoforms can self-aggregate because of the presence of these β-structures (*65*). However, there are negatively charged or positively charged amino acids clusters in tau (Figure 1.6). Because of the positions where these charged regions are located, the hydrophobic interactions between tau are inhibited and this makes it impossible for normal tau to self-aggregate. The inhibitory effects of these structural elements on tau self-aggregation have been confirmed by studies on *in vitro* tau aggregation (see below). The phosphorylation

sites of tau mainly cluster in the proline rich region and C-terminal region and the phosphorylation in these two parts can promote tau self-aggregation by removing these inhibitory factors. In Figure 1.6, a mechanism hypothesized by K. Iqbal explains how phosphorylation removes inhibitory factors for tau aggregation (*53*). The charge distributions on tau protein are demonstrated by the calculated different isoelectric points (pIs) in different parts. The proline rich region locates in the N-terminal side of the MT-binding repeats and is a very basic fragment with pI > 9. At the same time, the presence of proline residues bends the protein and masks the intermolecular attractions between microtubule binding repeats. Phosphorylation in the proline-rich region can neutralize the basic charges in this region and remove the inhibitory effect (Figure 1.6). The C-terminal part after Pro-397 is highly acidic. This part has been shown to inhibit the self-aggregation of tau (*66*). One hypothesis for the inhibitory effect of the C-terminal part is that it can mask the region that is required for tau- tau interactions (*64*). The phosphorylation of S396 and/or S404 can open up this region and allow the interactions between microtubule repeats (Figure 1.6). This hypothesis is supported by the increased polymerization rate of the S396/S404E pseudophosphorylation mutant (*67*).

The fact that hyperphosphorylation can promote tau self-aggregation demonstrates AD and tauopathies have impaired phosphorylation and de-phosphorylation processes. Therefore, it is of great interest to determine the kinases and phosphatases involved in tau phosphorylation/dephosphorylation and their roles in AD and tauopathies.

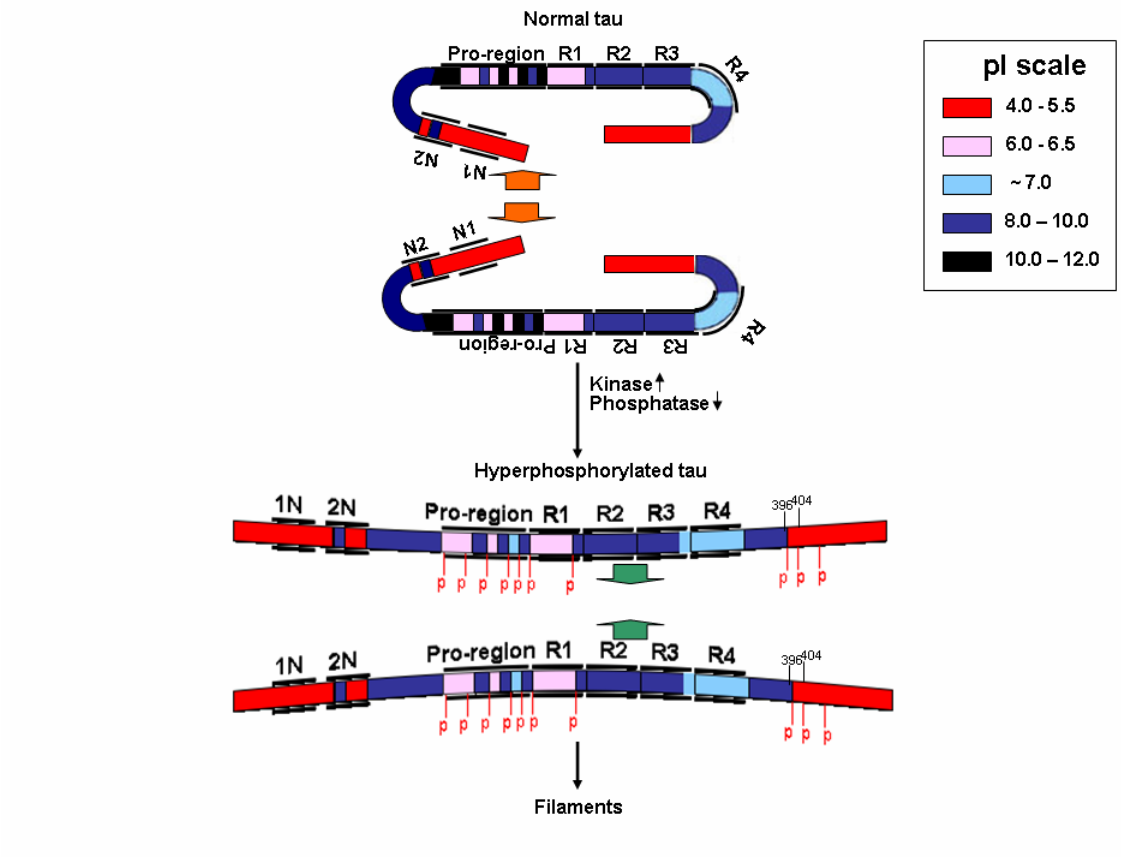

Figure 1.6. Schematic representation of a hypothesis of hyperphosphorylation induced tau self-aggregation. The calculated pIs for different regions of the longest tau isoform are labeled with different colors. In normal tau, the highly positively charged proline-rich region in the N-terminal side of the microtubule binding repeats inhibits intermolecular attractions through R2 and R3. The phosphorylation in this region due to increased kinase activities and/or decreased phosphatase activities neutralizes the positive charges and promotes tau self-aggregation. The C-terminus of tau inhibits tau-tau interaction by masking R2 and R3 regions. The phosphorylation at S396 and/or S404 removes the mask and facilitates filament formation. The boxes representing each region are not drawn to scale. Modified from Iqbal *et al.,* 2009.

1.4.4 Tau kinases

More than 20 kinases can phosphorylate tau protein, but it is not clear which are responsible for the pathological phosphorylation of tau. It has been suggested that more than one combination of protein kinases is involved in transforming normal tau to pathologically hyperphosphorylated tau (*63*). The kinases known to phosphorylate tau can be classified into three groups: 1) proline-directed protein kinases (PDPK), which phosphorylate a serine or threonine followed by a proline residue. About half of the known tau phosphorylation sites are proline-directed sites. Mitogen activated protein kinase (MAPK), cyclin-dependent kinase (cdk1 and 5) and stress activated kinases (SAPKs) belong to this group. Glycogen synthase kinase 3 (GSK3) is included in this group as well, although it can also phosphorylate tau at some of the serine or threonine residues not followed by a proline residue by recognizing a specific Ser-X-X-X-pSer or Ser-X-X-X-D/E motif (*68*). 2) Non-proline-directed protein kinases, which do not require the presence of a proline residue following Ser or Thr. Tau-tubulin kinase (TTK) 1 and 2, microtubule-affinity regulating kinase (MARK), cyclic-AMP-dependent kinase (PKA), protein kinase B (PKB/AKT), protein kinase C and Ca^{2+}/calmodulin-dependent protein kinase II (CaMPK II) (*57, 69*). MARK is the kinase that phosphorylates tau in the MT-binding repeats, such as Ser262, and reduced tau-MT binding by about 10-fold. 3) Tyrosine protein kinases such as Src kinase (*70*).

1.4.5 Tau phosphatases

Under physiological conditions, the phosphorylation of tau is maintained through the balance between kinases and phosphatases. Ser/Thr phosphatase protein 1, 2A, 2B, 2C and 5 (PP1, PP2A, PP2B, PP2C and PP5) are the protein phosphatases that are responsible for the dephosphorylation of tau (*71*). *In vitro* reactions have shown that these protein phosphatases can de-phosphorylate tau at different sites (*57, 69*). Among these phosphatases, PP2A is the most important one for tau de-phosphorylation. PP2A accounts for over 70% of tau phosphatase activity in brain (*71*). PP2A can counterbalance tau phosphorylation not only by directly dephosphorylating tau but also indirectly by reducing tau phosphorylation by inhibiting the activity of kinases, such as PKA, CaMPK II and MAP kinase (*53*).

1.5 Current research on tau aggregation and phosphorylation

1.5.1 In vitro tau aggregation

Tau filaments, with similar structure, morphology and immunoacitivity as AD tau filaments were formed *in vitro* (*67*). The results of *in vitro* tau aggregation studies suggest that the structural elements of tau contribute differently to its aggregation. The results also explain how tau phosphorylation and FTDP-17 mutations change its self-aggregation.

The microtubule binding repeat region is the core part of paired helical filaments (reviewed in (*72*)). This region alone is sufficient to aggregate into PHFs, with two hexapeptide motifs at the beginning of R2 and R3 being the most important part in promoting PHF formation by inducing β-structure (reviewed in (*73*)). Two

FTDP-17 mutants, P301L and DelK280 in the microtubule binding repeats can enhance the rate of aggregation by increasing the tendency for forming β-structure in this region (reviewed in (*74*)). The proline rich region in the N-terminal part of the microtubule binding repeats has been shown to inhibit tau aggregation (reviewed in (*53*)). The electronic repulsion between the positively charged amino acids in this region inhibits the stacking of β-structure and the presence of proline residues bends the protein and masks the microtubule binding repeats (reviewed in (*53*)). This inhibition can be neutralized by phosphorylation in this region (see below). The extreme N-terminus of tau facilitates the aggregation of tau. The formation of an Alz50 conformation through the binding of the extreme N-terminus and the microtubule binding repeats region is an important early step in tau aggregation and NFT formation (reviewed in (*66*)). The cleavage of the extreme N-terminus will abolish the formation of the Alz50 conformation and disrupt PHF formation *in vitro* (*75*). The C-terminal region of tau has the opposite effect on tau aggregation. Tau lacking its C-terminal tail has an increased rate of polymerization and more filaments were observed compared with full length tau (*76*). Tau has been suggested to adopt a hairpin structure with C-terminal tails covering the microtubule binding repeats and therefore inhibiting the interactions between microtubule binding repeats (reviewed in (*74*)). This inhibitory effect can be removed by phosphorylation (see above).

Due to the inhibitory effects of these structural elements on tau aggregation, tau does not aggregate spontaneously under physiological pH, temperature, ionic strength and concentration *in vitro* (reviewed in (*77*)). Polyanionic compounds such

as heparin (*78*), polyglutamate (*79*), RNA (*80*) and fatty acids (*81*) need to be present to induce tau aggregation. The aggregation process is a typical nucleation-elongation process (reviewed in (*77*)). The presence of these molecules could overcome the energy barriers for aggregation and therefore facilitate tau aggregation. *In vitro* tau aggregation may involve the formation of a stabilized assembly competent conformation, the formation of oligomers and the formation of filaments (reviewed in (*77, 82*)). The assembly of cysteine-dependent dimers in oxidative conditions has been suggested to increase the rate of aggregation, although the dimerization is not required for tau aggregation (*83, 84*). In addition, the cysteine-independent dimers also contribute to tau filament formation (*85*). However, because the normal physiological condition is reducing, dimer formation may only have subtle contributions to tau aggregation.

1.5.2 tau phosphorylation

Because of the observation that hyperphosphorylated tau is the major component of the PHFs and SFs in AD, much effort has been focused on determining how phosphorylation changes tau normal function and causes neuronal loss and dementia. Although no clear answer for this question is currently known, progress has been achieved in this field by using *in vitro* models or more physiologically relevant animal models.

1.5.2.1 In vitro studies

1.5.2.1.1 The studies on tau phosphorylation by pseudophosphorylation tau mutants

Pseudophosphorylation has been used in other systems to mimic the changes induced by phosphorylation (*86, 87*). Due to the complexity of tau phosphorylation sites, the diversity of tau phosphorylation sites and the highly dynamic turnover of phosphorylation *in vivo*, it is virtually impossible to control the phosphorylation on a specific residue or a combination of specific residues by kinase(s). Therefore, phosphorylation is mimicked by replacing serine or threonine residues with negatively charged glutamic acid or aspartic acid (*76, 88-91*). This replacement imitates the changes induced by phosphorylation in the aspects of conformational change, microtubule binding and antibody reactivity (*88, 92*). Using tau aggregation assays, there are some conflicts between the results from different reports. The conflicts between each report may due to the different methods used for assaying the amount of polymerization (Thioflavine S fluorescence vs. laser light scattering vs. transmission electron microscopy) and/or different reaction conditions, such as protein concentration and/or inducer concentration. The results obtained from the studies on pseudophosphorylation are listed in Table 1.1. In addition to the changes on conformation, tau self-aggregation, MT binding and stimulation of MT assembly, pseudophosphorylated tau was also shown to have lower binding affinity for PP2A and neural membrane cortex, and have increased phosphorylation at other sites (*90, 91, 93*). At the same time, cells expressing pseudophosphorylated tau were also found to have increased caspase 3 activity, increased cytotoxicity and increased apoptosis with or without detectable tau aggregates (*94-96*). These results also

suggest that the toxicity of phosphorylated tau might not depend on the formation of tau aggregates.

Considering the difference between heterogeneous phosphorylation by kinases and homogeneous pseudophosphorylation, pseudophosphorylation can not completely mimic the phosphorylation changes. However, it is still an invaluable tool to answer the questions of phosphorylation at specific sites in tau functions.

1.5.2.1.2 The studies on kinases and phosphatases

1.5.2.1.2.1 Glycogen synthase kinase - 3β (GSK-3β)

GSK-3β is a constitutively active kinase involved in many of the physiological processes from glycogen metabolism to gene transcription (*97*). It is a proline directed protein kinase (*68*). It has been shown to play roles in both familial and sporadic forms of AD (*97*). GSK-3β is highly expressed in neuronal cell bodies and their processes, and also co-localizes with NFTs in AD brain (*97*). In addition, the expression level of GSK-3β is significantly increased in AD brain compared with control brains (*98*). After examining the sites on tau that are phosphorylated by GSK-3β, at least 23 sites (T69, T175, T181, S184, S198, S199, S202, S210, T212, S214, T217, T231, S235, S237, S258, S262, S289, S356, S396, S400 and S413) are phosphorylated by GSK-3β and most of the sites overlap with those found in PHF tau (*99*). This evidence makes GSK-3β a leading candidate for inducing the progression of AD. The *in vitro* studies on GSK-3β and its inhibitor lithium further support this hypothesis. Our *in vitro* study with GSK-3β phosphorylated tau showed that GSK-3β

Table 1.1. Results on pseudophosphorylation research

Site(s)	Conformational change	MT-binding Affinity	Promote MT – assembly	Self-aggregation
175[96]	n/d	▼	n/d	▲
199[100]	n/d	n/d	n/d	▲
202[101]	■	▼	n/d	■
205[101]	■	▼	n/d	■
212[100]	n/d	n/d	n/d	▲
214[100]	n/d	n/d	n/d	▲
217[92, 102]	n/d	n/d	▼	▼[92]/■[102]
231[100]	n/d	n/d	n/d	■
235[100]	n/d	n/d	n/d	▼
262[100, 102]	n/d	n/d	n/d	■
327[88]	▼	■	■	n/d
396[92]	n/d	n/d	n/d	■
409[100]	n/d	n/d	n/d	■
422[92, 100, 102]	n/d	n/d	■	▲[92]/■[100, 102]
111/153[92, 102]	n/d	n/d	▼	▼[92]/■[102]
202/205[101]	■	▼	n/d	■
212/214[100, 103]	■	n/d	n/d	▲
231/235[92, 93, 100]	n/d	▼	■[92]/▼[93]	▲[100]/■[102]
156/327[88]	▼	■	▼	n/d
262/356[92]	n/d	n/d	▼	■
396/404[76, 93, 100, 103]	▼	■	▼	▲
403/404[92, 102]	n/d	n/d	■	■
175/176/181[92]	n/d	n/d	▼	▼
199/202/205[100]	n/d	n/d	n/d	▲
396/403/404[102]	n/d	n/d	n/d	▲
400/403/404[92]	n/d	n/d	▼	■
409/412/413[92]	n/d	n/d	■	▼
208/210/212/214[92]	n/d	n/d	▼	▼
231/235/393/404[93]	▼	▼	▼	■
396/400/403/409[92]	n/d	n/d	■	■
195/198/199/202/205[92]	n/d	n/d	▼	▼
208/210/212/214/217[92]	n/d	n/d	▼	■
198/199/202/231/235[91]	▼	n/d	▼	▼
396/404/409/413/422[91, 94]	▼	n/d	■	■
199/202/205/212/214/396/404[103]	▼	n/d	■	▲
198/199/202/231/235/396/404/409/413/422[89-91, 94]	▼	▼	▼	▼

■: no significant change was observed;

▼: significantly decreased; In the column on conformational change, ▼ represents decreased electrophoresis mobility/ opened conformation (*103*).

▲: significantly increased.

n/d: not determined

can induce an SDS-resistant conformational change similar to PHF tau. GSK-3β phosphorylation is sufficient to promote the formation of tangle-like aggregates from arachidonic acid (ARA) induced tau filaments or concurrently with tau fibrillation (*104, 105*) . GSK-3β phosphorylation also decreases the microtubule binding ability of tau, the ability of tau to promote MT assembly and to stabilize MT (*106*), and therefore changes the cellular microtubule organization and axon dynamics (*53, 107*). These changes in tau function can be reduced by lithium which inhibits GSK-3β activity. By introducing lithium to the cultured human NT2N neurons to reduce the phosphorylation of tau, tau had an enhanced binding to MT and increased ability to promote MT assembly (*108*).

1.5.2.1.2.2 Cyclin-dependent kinase (cdk5)

Cdk5, a proline-directed protein kinase, is a member of the cyclin-dependent kinase family (*109*). Unlike other cyclin-dependent kinases, cdk5 is not directly involved in cell cycle control. Cdk5 is present in post-mitotic neurons, concentrated in axons and is essential for embryonic development (*110, 111*). Cdk5 activity requires the presence of its activator (p39 or p35) or their proteolytic products (p35 or p25) which are exclusively present in post-mitotic neurons (*112*). Like GSK-3β, cdk5 and its activator have been found in brain and to be physical interacting with MT (*113*). Cdk5 can phosphorylate tau at sites that are phosphorylated in AD (S113, S184, S198, S208, S214, T231, S235, S396, and S404). Cdk5 phosphorylated tau shows a band shift on SDS-PAGE similar to PHF tau (*113-115*). Deregulation of

cdk5 has been found in human neurodegeneration, with an increased expression level of cdk5 and p25 in neurons bearing early stage NFTs (*109, 116*). The phosphorylation of tau with cdk5 can also promote the subsequent phosphorylation by GSK-3β (*117*). The combination of cdk5 and GSK-3β can convert normal tau to PHF tau and can restore the ability of self-aggregation and microtubule inhibitory activities (*63*). These features make cdk5 another attractive candidate responsible for disease related abnormal hyperphosphorylation. An *in vitro* phosphorylation study of cdk5 on tau showed that phosphorylation severely inhibited the ability of tau to promote microtubule assembly. Phosphorylated tau was released from MT and resulted in the depolymerization of tubulin (*49*). In primary cultured neurons, constitutive activation and mislocalization of cdk5 induced by the presence of p25 resulted in the hyperphosphorylation of tau and these changes were sufficient to disrupt the cytoskeleton, disrupt neuron morphologies and promote the apoptosis of primary neurons (*118, 119*).

1.5.2.1.2.3 Ser/Thr phosphatase protein 2A (PP2A)

PP2A accounts for over 70% of tau phosphatase activity (*71, 120*). It is a multimeric enzyme with three subunits: a scaffolding A-subunit, a large regulatory B-subunit and a catalytic subunit C (*121*). Site-specific de-phosphorylation of tau by PP2A *in vitro* has been observed at S46, T188, S199, S202, T205, T212, S214, T217, T231, S256, S262, S396, T403, S404 and S422 (*63*). PP2A was found to localize on MT and bind directly to tau (*122, 123*). PP2A is thought to be related to AD because

its expression level and activity are decreased in AD brain (*124, 125*). And the down-regulated PP2A is selectively found in the neurons with pre-tangles and tangles (*126, 127*). In addition to the overall mRNA level, mRNAs of catalytic and regulatory subunits are also selectively decreased in these neurons (*128*). The activity of PP2A is negatively correlated to the increase of tau phosphorylation at most of the AD sites (*71, 129*).

In vitro studies showed PP2A can de-phosphorylate PHF tau or pre-phosphorylated recombinant tau. The de-phosphorylation of tau by PP2A removes most of the phosphates from tau and restores its biological characteristics, such as SDS-resistant conformational change, MT binding activity and promoting MT assembly. At the same time the de-phosphorylated PHF tau loses its ability to aggregate into PHFs and NFTs (*62, 120, 130*). PP2A inhibitors such as okadaic acid, I1PP2A and I2PP2A can increase the abnormal hyperphosphorylation of tau in cultured cells or in rat brain slices. Tau in rat brain slices treated with the PP2A inhibitor, okadaic acid, had pathological changes that resembled the pathologies of AD. These changes included an increased AD-like hyperphosphorylation, decreased MT binding and MT assembly, and the accumulation of tau in tangle-prone neurons (*131*). Further examination of kinase activities showed the increase in tau phosphorylation was not only through the direct down-regulation of de-phosphorylation but indirectly through the regulation of the activity of GSK-3, cdk5 and other kinases (*132-135*). I1PP2A and I2PP2A are endogenous PP2A inhibitors. Their expression levels in AD are also changed together with the level of PP2A (*136*).

The increased level of I1PP2A and I2PP2A can further decrease the PP2A activity and this idea was confirmed in cultured cells (*137*). PC12 cells doubly transfected with tau ht40 and I1PP2A/I2PP2A had increased tau phosphorylation and impaired MT networks. Increased cell death was also observed in this model (*138, 139*).

1.5.2.2 In vivo animal models

In vivo animal models were used to study the link between tau and neuron pathology. The results from these studies shed light on the understanding of toxic species in AD and tauopathies.

1.5.2.2.1 Transgenic C. elegans models

C. elegans is a short-lived, small animal with a central nervous system and a brain. Current results from *C. elegans* expressing human tau partially resembled the situation in human neurodegeneration (*140-142*). Therefore, *C. elegans* can be used as a simplified animal model to study tauopathies. In the *C. elegans* models expressing wild type (1N4R, 0N4R or 0N3R) and FTDP-17 mutant (P301L, V337M and R406W) tau, hyperphosphorylated tau, impaired neuronal function and abnormal neuron morphology were observed (*140-142*). The mutant tau had more severe phenotypes compared with wild type tau. Tau was phosphorylated at many of the sites found in AD tau, such as S199, S202, T231, S396 and S404. The SDS-resistant conformational change was also observed in these phosphorylated tau (*140*). In the 0N3R or 0N4R tau expressing *C. elegans*, no neuronal degeneration happened (*141*).

However, in the 1N4R tau expression worms, loss of axons and neurons, and structural damage to axonal tracks were observed (*142*). A decreased life span was also associated with these changes. Insoluble PHF-like tau accumulations were found in these models but after the appearance of abnormal behavior (*142*). This observation suggested that aggregation may not be required for tau-induced neuronal dysfunction and soluble hyperphosphorylated tau may be the neurotoxic species. The effect of phosphorylation on tau function was also tested in *C. elegans* model with co-expression of GSK-3/cdk5 and tau (*141*). More severe phenotypes were observed compared with *C. elegans* expressing wild type tau alone. The *C. elegans* expressing a pseudohyperphosphorylated form of tau showed similar changes as the double transgenic (Tg) worms (*140*).

1.5.2.2.2 Transgenic Drosophila models

Human genes and *Drosophila* genes have high similarities. At least 50% of *Drosophila* genes have a human homologs and more than 70% of human disease genes, including *MAPT* (human tau gene), have *Drosophila* homologs (*143, 144*). This makes *Drosophila* a good model to study human disease. Some fundamental characteristics of tauopathies were recapitulated in *Drosophila* expressing a human tau gene, including abnormal tau phosphorylation and adult onset, progressive neurodegeneration (*144, 145*). In *Drosophila* models expressing wild type or mutant (R406W, V337M) human tau, neurodegeneration was observed. Both wild type and mutant tau in these models showed an AD-like abnormal hyperphosphorylation and

conformational change with tau concentrating abnormally in the areas of neurodegeneration. These transgenic fruit flies also had a shorter life span compared to non-transgenic controls. All these changes were greater in *Drosophila* expressing mutant tau than those expressing wild type tau (*146*). However, neurofibrillary tangles were not found in this model, not even in the degenerative neuronal cells. A similar result was reported by another group (*147*). In this model, the observed neurodegeneration was dissociated from the presence of NFTs. However, when human tau was co-expressed with GSK-3 *Drosophila* homolog, Shaggy, they observed a severe neurodegeneration induced by tau and a NFT-like pathology composed of hyperphosphorylated tau was observed (*147*).

In two other *Drosophila* models with motor neuron dysfunction, no neuronal death was observed. The malfunction in motor neurons was associated with disrupted axonal transportation, such as: loss of axons, abnormal axon bundling and axonal swelling (*148, 149*). These pathological changes were phosphorylation dependent and were enhanced by co-expression of GSK-3β (*149*). The results from these *Drosophila* models suggested that the early modifications of tau, such as phosphorylation and conformational changes may be the toxic substrates of tauopathies and NFT formation may not be necessary for neurodegeneration.

Drosophila models were also used to study tau phosphorylation and screen for kinases and phosphatases involved in neurodegeneration. From the result of the *Drosophila* expressing a pseudophosphorylated form of tau, phosphorylation was found to directly precede apoptosis and none of the fourteen sites they checked (T111,

T153, S175, T181, S199, S202, T205, T212, T217, T231, S235, S396, S404 and S422) played a dominant role in controlling tau toxicity(*150, 151*). From the results of a genetic modifier screen and other biochemical approaches, PAR-1 kinase (the *Drosophila* homolog of MARK kinase), GSK-3, cdk5/p35, PKA, JNK(c-Jun NH_2-terminal kinase) and PP2A were thought to be important for neurodegeneration, as have been reported for the *in vitro* studies (*152-154*).

1.5.2.2.3 Transgenic mouse models

Transgenic (Tg) mouse models have been used to model the human neurodegenerative diseases and have successfully recapitulated the pathological changes in human tauopathies. However, since mouse brain has its own endogenous tau and conserved phosphorylation sites are the same as those in AD tau, many aspects need to be taken into consideration when interpreting these tau-expressing mouse models. In mouse brain, only 4R isoforms are expressed and the results from some of the Tg mouse models suggest that the presence of endogenous tau may affect expression or splicing of the exogenous tau, thereby affecting the phenotype and pathology of exogenous human tau (*155, 156*). However, mice with endogenous tau deleted by knock-out seem to be normal immunohistologically and functionally, and showed no changes in axonal elongation (*157*). This may due to the presence of other microtubule binding proteins, such as MAP1 and MAP2. Secondly, the promoters used in different Tg mouse models will change the location and level of tau

expression, which has been proven to be extremely relevant to the pathologies observed.

The first Tg mouse model was generated in 1995 by Gotz J with his colleagues. The longest human wild type tau (2N4R) was expressed in Tg mouse brain under the control of human Thy-1 promoter (*158*). A relatively low level of tau was expressed in nerve cell bodies, axons and dendrites (*158*). The antibody studies showed exogenous human tau was phosphorylated at many AD-related sites. However, NFTs did not form in this model (*158*). After this, other Tg mouse models were generated expressing different wild type tau isoforms and with different promoters. With two exceptions, most of these wild type human tau expression mice failed to produce NFTs (*156, 159*). Different types of neurodysfunctions to different levels were observed in these mouse models. The pathologies included but were not limited to: axonal degeneration in brain and spinal cord associated with progressive nerve cell dysfunction, amyotrophy and motor deficits, tau mislocated in somatodendrites, astrocytic expression of tau, AD-like tau hyperphosphorylation, abnormal conformational change and ubiquitination (*160-162*). The presence of abnormal neuronal function without formation of NFTs in the CNS of mice expressing human tau suggested NFT might not be necessary for neuron malfunction.

In a Tg mouse model expressing human 0N3R tau under the control of mouse prion promoter (MoPrP), NFT pathologies occurred for the first time (*159*). Tau expression was observed in CNS and the insoluble, hyperphosphorylated tau coalesced in intraneuronal inclusions in cortical and brainstem neurons in an age-

dependent manner (*159*). NFT-like inclusions were observed in the hippocampus of the aged mice at around 18 to 20 months (*163*). Axon degeneration, diminished axonal transport and motor weakness associated with the age-dependent CNS pathologies were also observed in this model (*159*). This model was the first Tg mouse model recapitulating key features of tauopathies.

Instead of expressing only one of the tau isoforms, Tg mice expressing all six tau isoforms were generated on the background of endogenous mouse tau or the murine tau-null background (*155, 156*). With the presence of endogenous murine tau, although axonal swelling correlatting with a hind-limb abnormality were observed, no NFTs formed in mouse brain. Human tau expressed in mouse brain was hyperphosphorylated and in an abnormal conformation, but neuromorphology was essentially normal (*155*). However, all six human isoforms expressing on the murine tau-null background induced an age-related neuropathology with the presence of PHFs in the cell bodies and dendrites of neurons. Tau in mice brain was hyperphosphorylated at AD-relevant sites and had an AD-like conformational change (*156*). The comparison between these two models suggested the endogenous 3R murine tau may have an inhibitory effect on the neuropathologies induced by the presence of exogenous human tau.

Because most of the Tg mouse models expressing wild type tau failed to recapitulate the human tauopathies, Tg mouse models expressing FTDP-17 mutants in wt tau background were generated. FTDP-17 mutants resulted in an early-onset of neurodegeneration and had an increased tendency to be phosphorylated and aggregate

in vitro, and NFT formation was achieved in most of these Tg mouse models. P301L/S were the two FTDP-17 mutants used most frequently, at least seven Tg mouse lines expressing these two mutants have been generated.

The first Tg mouse model of human P301L used 0N4R human tau isoform under the control of MoPrP (*164, 165*). The mice had a shortened life span with NFT formation and neuronal loss. An age- and gene-dose-dependent motor and behavioral deficit was associated with the formation of NFT and Pick body like neuronal lesions in brain (*164, 165*). Pre-tangle tau filaments were also found in the cortex, hippocampus and basal ganglia. Tau in filaments and NFTs was hyperphosphorylated and had an AD-like conformational change (*164, 165*). Axonal degeneration, neurogenic atrophy and gliosis were also observed in the areas associated with NFTs and tau filaments (*164, 165*). A tetracycline-regulated 0N4R P301L human tau-expressing Tg mouse model, controlled under CaMK-II promoter, was generated by SantaCruz and his colleagues (*166-168*). In this model, continued expression of human P301L resulted in an age-dependent development of dementia. In the young Tg mice, motor defects were observed. Tau in this stage was hyperphosphorylated and had a conformational change. As the mice aged, NFTs were observed in the neocortex and hippocampus (*166-168*). The accumulation of sarkosyl-insoluble tau was observed and the transmission electron microscopy (TEM) examination of this insoluble tau showed it was in the form of SFs. In later stages, forebrain atrophy and up to 80% neuronal loss in the hippocampus were associated with cognitive impairments. These neurodegenerative phenotypes were recovered

and further neuronal loss was stopped by suppressing of the expression of human P301L tau, although NFTs continued to accumulate. The dissociation of neurofibrillary pathology with NFTs in this model again suggested NFTs were not sufficient to cause cognitive decline or neuronal death, at least in this model. The Tg mouse models expressing the P301L/S mutant on other human tau isoforms (2N4R and 1N4R) under the control of other promoters (mThy-1.2, MoPrP and *murine thyl* promoter) also formed NFTs and different types of neurofibrillary pathologies (*169-175*). The mislocated, hyperphosphorylated tau formed SFs and twisted ribbons, which further clustered into NFTs. Some of the mouse endogenous tau also co-aggregated with exogenous human tau. Astrocytosis and neuronal apoptosis, neuron loss, synapse loss and impaired synaptic function, neuron atrophy, motor malfunction and reduced life span were observed in these Tg mouse models. In some cases, microglial activation and neuroinflammation associated with these changes (*169, 172*).

Other FTDP-17 mutants such as V337M, R406W and DelK280 tau were also used in Tg mouse models. Most of the phenotypes were similar as those observed in P301L/S tau Tg mice (*176-180*). In the Tg mouse model generated by Mocanu *et al.*, instead of using full length tau, the MT binding repeat domain of human tau with DelK280 mutation was used. The MT-binding repeat region has been shown to have a higher tendency to self-aggregate *in vitro* and cultured cells (*181*). Abnormal tau aggregation and NFT formation associated with missorting of tau in the somatodendritic compartment, astrogliosis, loss of synapses and neurons were observed in this model.

In addition, human tau with more than one site of mutation was expressed in some of the Tg mouse models (*182-184*). Most of the neurofibrillary phenotypes were similar as these in the Tg mice expressing human tau with a single mutation. In the Tg mouse model with double mutant tau (G272V/P301S), no motor dysfunction appeared (*182*). This made it possible to study the Tg mice with behavioral experiments and the Tg mice in the late stages of tau pathology. NFT-like inclusions, ghost tangles, PHF-like filaments and mild astrogliosis were observed in this Tg mouse model. Other pathologies associated with tauopathies such as impaired behavioral characteristics, increased anxiety, delayed learning and reduced spatial memory were observed in this model with no change in motor activity.

Glial pathologies occur in some of the tauopathies, such as FTDP-17, PSP and CBD. Some Tg mice expressing wild type or mutant tau recapitulated the glial side of the tauopathies (*185-188*). Phosphorylated fibrillary tau was found in astrocytes and oligodendrocytes associated with degeneration of these cells. The ultrastructure of the tau filaments found in glials was similar to those found in neurons and these tau filaments were ubiquitin positive (*185-188*).

Aβ deposition is another diagnostic characteristic of AD. To study the link between Aβ and tau aggregation, double or triple Tg mouse models were generated by crossing the Tg mice. Some conflicting results were shown in these studies. In some studies, Aβ was not necessarily associated with NFT pathologies (*189*). However, in other studies, Aβ was shown to influence NFT formation, even by injecting Aβ oligomers into brains of human tau expressing mice (*184, 190-193*).

CHAPTER 2 RATIONALE AND AIMS

The microtubule associate protein tau loses its normal function and aggregates into insoluble filaments (PHFs and SFs) in Alzheimer's disease (1.2.1). These insoluble filaments can further aggregate into intracellular neurofibrillary tangles (NFTs) and the number of NFTs is closely related to the severity of dementia (1.2.1). NFTs are also found in some other neurodegenerative diseases such as progressive supranuclear palsy (PSP), corticobasal degeneration (CBD), Pick's disease (PiD) and frontotemporal dementia with Parkinsonism linked to chromosome 17 (FTDP-17) (1.2.2, 1.3). A distinct feature of tau isolated from NFTs is abnormal hyperphosphorylation (1.3.2). The abnormal hyperphosphorylation of tau is thought to be a key event in the progression of AD and tauopathies (1.5.2). Hyperphosphorylated tau has a reduced MT binding affinity and a reduced ability to promote MT assembly (1.5.3). In addition, hyperphosphorylated tau is prone to self-aggregate (1.5.3).

To date, about 45 sites have been identified to be phosphorylated in PHF tau (1.3.2). However, it is not clear which kinase(s) is responsible for the hyperphosphorylation of tau. At least 20 kinases can phosphorylate tau and most likely there are more than one combinations of kinases that might be involved in this process (1.5.4). Among these kinases, glycogen synthase kinase - 3β (GSK-3β) is an attractive candidate (1.6.1.2). According to our previous observation, GSK-3β can phosphorylate monomeric or polymerized tau at eleven or five sites respectively (*104, 105*). Phosphorylation at these sites did not change the amount of tau polymerization

induced with arachidonic acid (ARA), but was sufficient to cause tau filaments to coalesce into tangle-like aggregates similar to those isolated from AD brain.

The general aim of this study is to understand the effect of pseudohyperphosphorylation at GSK-3β sites on tau function. Our previous studies showed the pseudophosphorylation at S202 and T205, which are GSK-3β phosphorylation sites, resulted in only subtle effects on tau function (*101*). However, it is not clear whether the pseudohyperphosphorylation at multiple GSK-3β phosphorylation sites will induce a greater change. We hypothesize that the pseudohyperphosphorylation at multiple sites will change tau function more significanlty than pseudophosphorylation at single or double sites. To test this hypothesis, we generated variants with six (6-Phos) or seven (7-Phos) pseudophosphorylation changes. These sites are S199, S202, T205, T231, S235, S396 and S404. Five of these seven sites (S199, T205, T231, S396 and S404) are the five sites identified to be phosphorylated by GSK-3β when polymerized tau was used as the substrate. S202 was added to the core five sites since the antibody AT8 recognizes phosphorylation at both S199 and S202 (*43*). For similar reasons, S235, which is recognized by antibody TG-3 together with T231, was added to 6-Phos to generate 7-Phos (*13*). Single, double and triple pseudophosphorylation mutants were generated and used to test the possibility that fewer sites could have similar effects on tau function as the pseudohyperphosphorylated tau. The pseudophosphorylation mutants at other sites (T212, S208 and S210) were included in the study as well. T212E was included because it was shown in another study to significantly increase

the amount of ARA-induced tau polymerization (1.5.1.1). S208 and S210 are the sites phosphorylated by a non-proline directed protein kinase, tau-tubulin kinase (TTK). These two sites locate in the same region as GSK-3β phosphorylation sites and are also found to be phosphorylated in AD.

These pseudophosphorylation variants were assayed for changes on electrophoretic mobility, microtubule binding and ARA-induced polymerization. The results from this study showed that pseudohyperphosphorylation can decrease the binding affinity of tau to MT and reduce ARA-initiated rates of nucleation and polymerization. The combination of these changes could explain the increased cytotoxicity of hyperphosphorylated tau. The observation of tangle like tau aggregates in our study also explains the potential beneficial role of tau polymerization and NFT formation.

In vitro ARA-induced tau polymerization has previously been shown to depend both on tau concentration and the inducer concentration (1.5.1). The biphasic dependence is also observed in all of our pseudophosphorylation mutants. However, the mechanism of ARA-induced tau polymerization is not understood. In the appendix, the mechanism of ARA-induced tau polymerization is studied. The results suggest that ARA can induce tau polymerization both as large micelles and as monomers (or small micelles). The morphology of ARA-induced filaments is affected by the molecular nature of ARA. I also found that the amount and morphology of tau filaments were affected by surface area : volume ratio of the reaction.

CHAPTER 3 MATERALS AND METHODS

3.1 Tau protein purification

3.1.1 Generation of mutant tau constructs

As mentioned above, 9 sites (S199, S202, T205, S208, S210, T212, T231 and S235) were chosen to generate the pseudophosphorylation mutants. Fifteen mutants from the combination of these 9 sites were generated by replacing serine/threonine with glutamic acid/aspartic acid on the longest isoform of human tau (ht40, 441 amino acids). QuikChange Site-Directed Mutagenesis Kit from Stratagene (La Jolla, CA) was used to generate these site-directed mutants. The single mutants were constructed first and confirmed by sequence analysis. The primers used for site-directed mutagenesis were:

S199E: 5'-GCA GCG GCT ACA GCG AGC CCG GCT CCC CAG G-3' and

5'-CCT GGG GAG CCG GGC TCG CTG TAG CCG CTG C-3'

S202E: 5'-CAG CAG CCC CGG CGA ACC AGG CAC TCC CG-3' and

5'-CGG GAG TGC CTG GTT CGC CGG GGC TGC TG-3'

T205E: 5'-CCG GCT CCC CAG GCG AAC CCG GCA GCC GCT C-3' and

5'-GAG CGG CTG CCG GGT TCG CCT GGG GAG CCG G-3'

S208D: 5'-GGC ACT CCC GGC GAC CGC TCC CGC AC-3' and

5'-GTG CGG GAG CGG TCG CCG GGA GTG CC-3'

S210D: 5'-CCC GGC AGC CGC GAC CGC ACC CCG TC-3' and

5'-GAC GGG GTG CGG TCG CGG CTG CCG GG-3'

T212E: 5'-GCA GCC GCT CCC GCG AGC CGT CCC TTC CAA C-3' and

5’-GTT GGA AGG GAC GGC TCG CGG GAG CGG CTG C-3’

T231E: 5’-TGG CAG TGG TCC GTG AGC CAC CCA AGT CGC CG-3’ and

5’-CGG CGA CTT GGG TGG CTC ACG GAC CAC TGC CA-3’

S235D: 5’-CCG TAC TCC ACC CAA GGA TCC GTC TTC CGC CAA GAG-3’

and 5’-CTC TTG GCG GAA GAC GGA TCC TTG GGT GGA GTA CGG-3’

The double mutants were generated on the background of single mutants and the triple mutant on the background of the double mutant. For the 6-Phos mutant, site-directed S to E substitution at site 199/202/205 was introduced to the S396/S404E parent clone generating a 5-Phos clone, followed by the T to E substitution at site 231 on the 5 -Phos background. For the 7-Phos mutant, the S to E substitution at site 235 was introduced to the 6-Phos parent clone. All these mutants were confirmed by sequence analysis. The constructs for S202E, T205E, S202/T205E were made by Dr. Carolyn Rankin and the constructs for 5-Phos, 6-Phos and 7-Phos were made by Min He. The constructs for S396/404E and P301L were the generous gifts from Dr. Lester I. Binder. The constructs for the pseudophosphorylation mutants were transformed into BL21 (DE3) Competent Cells (Sigma, St. Louis, MO) and stored at -80ºC (*101*).

3.1.2 Purification of tau variants

BL21 (DE3) competent cells containing wild type or mutant tau cDNA-plasmid were grown in 60 ml Luria Broth (LB) overnight at 26 ºC until OD_{600} was close to 0.5 and then used to seed three flasks containing 1.8 liter LB which were

incubated at 37 ºC. IPTG was added to the culture to induce the expression of tau protein for an additional 2 hours when OD_{600} reached 0.7 - 0.8. Cells were harvested by centrifugation and resuspended in 25 ml ice cold 1x lysis buffer (500mM NaCl, 10mM Tris Base pH 8, and 5mM imidazole). Cells were lysed by passing through a French Press cell disrupter (Thermo Electron Corporation, Waltham, MA). Tau protein was purified using Nickel affinity column chromatography followed by gel filtration through a Superdex 200 column using ACTA fast protein liquid chromatography (FPLC) (Amersham Biosciences, Piscataway, NJ). The purity of the protein was determined by sodium dodecyl sulfate-polyacrylamide gel electrophoresis. Protein concentration was determined by commercial BCA assay (Pierce Chemical, Rockford, IL) using bovine serum albumin (Pierce Chemical, Rockford, IL) as a standard (*101*).

3.2 SDS – PAGE and SDS – PAGE with urea

Protein samples (wild type or pseudophosphorylation mutants, 1μg per lane) were boiled for 5 min in sample buffer containing 2% SDS and 1% β-mecaptoethanol, fractionated on 15% SDS-PAGE and stained with Commassie brilliant blue (*91, 101*). For denaturing SDS-PAGE, protein samples (1μg per lane) were boiled for 5 min in sample buffer containing 2% SDS, 1% β-mecaptoethanol and 6 M urea. Samples were fractionated on 15% SDS-PAGE containing 6 M urea and stained with Commassie brilliant blue (*91, 101*). The molecular weight of each mutant was determined from the distance on the gel.

3.3 In vitro polymerization reactions

3.3.1 Standard polymerization reactions

Two micromolar tau protein (wild type or pseudophosphorylation mutants) were incubated in polymerization buffer (10 mM HEPES pH 7.64, 100 mM NaCl, 0.1 mM EDTA and 5 mM DTT) at room temperature in the presence of 25 - 150 μM arachidonic acid (ARA) (in ethanol, final concentration of ethanol was 3.75%) for 16 – 20 hr (*194*).

3.3.2 Polymerization of pseudophosphorylation mutant tau combination

Three hundred and thirty nanomolar of each of the pseudophosphorylation mutant tau (S199E, S202/T205E, S208D, T212E, T231E/S235D, and S396/404E) were mixed and incubated in polymerization buffer (10 mM HEPES Ph 7.64, 100 mM NaCl, 0.1 mM EDTA and 5 mM DTT) with 25 or 75 μM ARA (in ethanol, final concentration of ethanol was 3.75%), 0.3 mM $MgCl_2$, 0.2 mM ATP and 20 μM Thioflavine S at 30 ºC for 20 hr.

3.4 Thioflavine S fluorescence

Thioflavine S (ThS) was added to tau polymerization reactions after 20 hr incubation at a final concentration of 20 μM. The resulting fluorescence was measured in a 96-well plate in a Cary Eclipse fluorescence spectrophotometer (Varian Analytical Instruments, Walnut Creek, CA) with excitation and emission wave lengths at 440 and 520 nm, respectively (*194*).

3.5 Right angle laser light scattering

Tau polymerization reactions were transferred into 5 x 5 mm optical glass fluorometer cuvettes (Starna Cells, Atascadero, CA) and illuminated with a 5 mW solid state laser (λ = 475 nm, B & E Tek, Inc., Newark, DE). Images were captured at a right angle to the incident light using a SONY XC-ST270 digital camera. Captured images were imported into Adobe Photoshop 7.0.1 and the intensity of the scattered light equaled the value assigned to the histogram of a 15 x 15 pixel box. The scattering at zero time point (dark current) was subtracted from all the measurements. All images were captured at an aperture of f5.6 – 8 or f8 and then normalized to the intensity corresponding to the exposure at f5.6 – 8 (*101*).

3.6 Transmission electron microscopy

3.6.1 Standard polymerization reactions

Tau polymerization reactions after 20 hr incubation were diluted 10-fold with polymerization buffer then fixed with 2% glutaraldehyde (in water) for 5 min. Ten microliters of fixed samples were placed on formvar-carbon coated grids for 1 min, washed with water, blotted, washed with 2% uranyl acetate, blotted again, stained with 2% uranyl acetate for another minute, and then blotted dry. Grids were viewed with a TECNAI G^2 20 electron microscope (FEI Company, Hillsboro, OR) and digital images were captured with the Gatan Digital Micrograph imaging system. The pictures were analyzed with Optimas image analysis program for the filament length and number of filaments (*101*).

3.6.2 Polymerization of pseudophosphorylation mutant tau combinations

Tau polymerization reaction after 20 hr incubation were diluted 5-fold with polymerization buffer, then applied to the grids for 1 min. The edge of the grid was then touched to filter paper to blot away excess liquid. One percent uranyl acetate was put on grids and stained for one minute then blotted. Grids were viewed with a JEOL 1299 EXII electron microscope and digital images were captured with the MegaViewII imaging system (Soft Imaging System, GmbH Münster, Germany) (*101*).

3.7 Kinetics of polymerization

The polymerization reaction of wild type and pseudophosphorylation tau variants at 2 μM protein concentration induced with 75 μM ARA were set up in the 5 x 5 mm optical glass fluorometer cuvettes and then monitored by LLS as described above at regular intervals for 20 hr. Images were imported into Adobe Photoshop 7. 0. 1. The intensity of laser light scattering was measured by the histogram function as described above. The data were fit to a nonlinear Gompertz equation:

$$y = ae^{-e^{-\left[\frac{(t-ti)}{b}\right]}}$$

where y is the intensity of laser light scattering measured at time t; t_i is the inflection point corresponding to the maximum increasing rate of laser light scattering; a is the maximum amount of laser light scattering at equilibrium; and b equals to $1/K_{app}$. K_{app} is proportional to the rate of filament elongation. The lag time for polymerization is equal to the value of $t_i - b$, which was defined as the time when significant amount of polymerization appears (*100, 195*).

3.8 In vitro microtubule binding assay

3.8.1 Preparation of paclitaxel stabilized microtubules

To prepare paclitaxel stabilized microtubules, 20 µl of 1.5 mg/ml tubulin was incubated with 2.5 µl cushion buffer (80 mM PIPES, pH 7.0, 2 mM $MgCl_2$, 0.5 mM EGTA in 50% (v/v) glycerol) for 20 min and then diluted into 200 µl general tubulin buffer (80 mM PIPES, pH 7.0, 2 mM $MgCl_2$, 0.5 mM EGTA) plus 2µM paclitaxel. The concentration of the stable MTs was 1.62 µM tubulin dimers. The tubulin was the generous gift from Dr. Richard H.Himes.

3.8.2 Microtubule binding assay

The microtubule binding assay was performed in general tubulin buffer (80 mM PIPES, pH 7.0, 2 mM $MgCl_2$, 0.5 mM EGTA). Tau protein ranging from 0.125 µM to 10 µM was mixed with paclitaxel stabilized microtubules (final concentration of 1.62 µM tubulin dimer) in a 50 µl reaction. Samples were incubated at room temperature for 30 min, and centrifuged in a Beckman Optima TLX ultracentrifuge at 100,000 x g for 5 min. The microtubule and tau bound to the microtubules were sedimented during centrifugation. The pellets were resuspended with 1x SDS sample buffer and tau bound to the microtubules was separated from microtubules by SDS – PAGE. Tau samples (0.06-1.0 µg per lane) were loaded on the same gel to generate the standard curve. The SDS-PAGE gels were stained with Commassie brilliant blue and scanned with a Hewlett Packard Scanjet 7400 C and imported into Adobe Photoshop 7.0.1. The intensity of standard tau samples were plot versus the amount

of tau protein and fit to a linear equation. The concentrations of tau bound to the microtubules were determined by the intensity of tau bands and the standard curve obtained from the same gel using the histogram function in Adobe Photoshop 7.0.1. The intensity of the tau bands were normalized to the intensity of the tubulin bands in each lane to take the differences in centrifugation and/or resuspension of samples into account because the concentration of tubulin should be the same in every binding sample. The amount of free tau was determined by subtracting the amount of bound tau from the amount of total tau. The concentration of bound tau was plotted versus the concentrations of free tau in GraphPad Prism and the curves were fit to a one site binding (hyperbola) equation (*101*):

$y = B_{max} * x/(Kd+x)$

where B_{max} is the maximal binding and Kd is the concentration of tau required to reach half-maximal binding.

CHAPTER 4 PSEUDOHYPERPHOSPHORYLATION OF TAU MODULATES ITS FUNCTION

Pseudophosphorylation and pseudohyperphosphorylation mutants were generated by the site-directed S/T to E/D substitution on the longest tau isoform (ht40). The changes of tau functions were assayed. We hypothesized that pseudohyperphosphorylation tau mutants will induce a greater change on tau function in microtubule binding and aggregation than the pseudophosphorylation mutants at single or double sites.

4.1. Result

4.1.1 Selection and generation of pseudophosphorylation and pseudohyperphosphorylation tau mutants

Tau is abnormally hyperphosphorylated in AD and tauopathies (*8, 53*). The molar ratio of phosphorylation is increased from 2-3 mol of phosphates per mole of tau in normal brain to 5-9 mol of phosphates per mole of tau in AD brain (*43, 53*). However, the role of hyperphosphorylation on AD and tauopathies is not clear. GSK-3β can only phosphorylate tau to a ratio of approximately 2-4 mol phosphates per mole of tau and this is sufficient to induce tau filament to coalesce into tangle-like aggregates similar to those isolated from AD (*104, 105*). Due to the low molar ratio and heterogeneous characteristics of GSK-3β phosphorylation, pseudohyperphosphorylation mutants were generated to study the role of hyperphosphorylation at specific sites on tau function. We chose to focus on the five

sites that were phosphorylated by GSK-3β when polymerized tau was used as the substrate. These five sites are S199, T205, T231, S396, and S404 (*105*). Pseudophosphorylation at S202 was added to generate the 6-Phos and pseudophosphorylation at both S202 and S235 were added to generate the 7-Phos. Phosphorylation at S202 is generally believed to happen together with phosphorylation at S199 in AD and can be recognized by antibody AT8; similarly for S235 and T231, which can be recognized by antibody TG-3 (*13, 43*). Single, double and triple mutants were also generated to determine whether similar changes induced by pseudohyperphosphorylation can be induced by pseudophosphorylation at fewer sites (Figure 4.1A). The pseudophosphorylation at T212, S208, and S210 in the proline rich region were also included in the analysis as controls. T212 has been shown to significantly increase tau aggregation in another report (*100*). S208 and S210 can be phosphorylated by a non-proline directed protein kinase, tau-tubulin kinase (TTK), and are in the same region of tau where most of GSK-3β phosphorylation sites are found (*37*). The FTDP-17 mutant, P301L, was used as a positive control because it has been shown to drastically change tau functions in previous reports (*164, 165, 173, 175, 196, 197*).

4.1.2 Pseudophosphorylation at S199/S202/T205, S396/S404, 6-Phos, and 7-Phos induced an SDS-resistant upward band shift.

Both hyperphosphorylated tau isolated from AD and tau phosphorylated by GSK-3β *in vitro* showed an SDS-resistant upward band shift (*8, 104*). This upward band shift

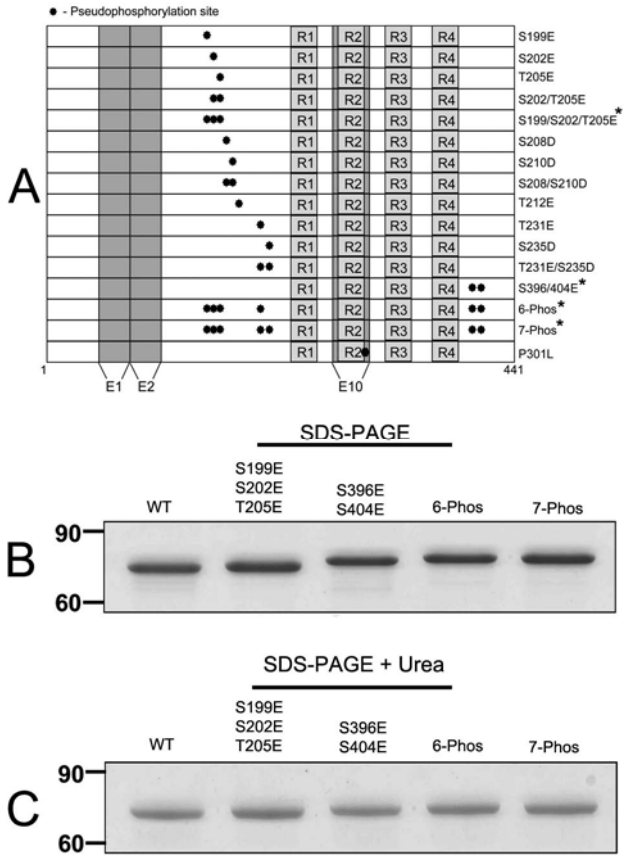
● - Pseudophosphorylation site
A
R1
R2
R3
R4
S199E
S202E
T205E
S202/T205E
S199/S202/T205E*
S208D
S210D
S208/S210D
T212E
T231E
S235D
T231E/S235D
S396/404E*
6-Phos*
7-Phos*
P301L
1
E1
E2
E10
441
SDS-PAGE
WT
S199E S202E T205E
S396E S404E
6-Phos
7-Phos
B
90
60
SDS-PAGE + Urea
C

Figure 4.1. Simulation of tau phosphorylation by glutamic acid or aspartic acid replacement. A) Schematic representation of phosphorylation sites on the longest tau isoform. Four microtubule binding repeats are indicated by light gray boxes (R1 – R4) and exon 2, 3 and 10 (E2, E3, and E10) are indicated by dark gray boxes. Pseudophosphorylation sites substituted with glutamic acid or aspartic acid are indicated by the black dots and are labeled to the right of the diagram showing their position. The mutants having "pseudohyperphosphorylation" like changes are indicated by asterisks. The exons are not drawn to scale. B) SDS-resistant conformational changes were observed in the "pseudohyperphosphorylation" like mutants (S199/S202/T205E, S396/404E, 6-Phos, and 7-Phos). One microgram of each tau protein sample was resolved by SDS-PAGE in a 15% gel. C) SDS-resistant conformational changes shown in the "pseudohyperphosphorylation" mutants were reduced by 6 M urea. One microgram of each tau protein sample (wild type, S199/S202/T205E, S396/404E, 6-Phos, and 7-Phos) was resolved by SDS-PAGE on a 15% gel containing 6 M urea.

was also observed in the pseudophosphorylation mutants with amino acid substitutions at 5 or 10 sites in the proline rich region and/or C-terminal region (*91, 198*). To determine whether the pseudophosphorylation mutants we generated have an AD-like upward band shift as well, all the pseudophosphorylation mutants were analyzed by SDS-PAGE followed by commassie stain.

Only four of these pseudophosphorylation mutants showed an SDS-resistant upward band shift (Figure 4.1B). These mutants were S199/S202/T205E, S396/404E, 6-Phos, and 7-Phos. The apparent molecular weights for wild type and these mutants determined from SDS – PAGE were 70 kDa, 72 kDa, 75 kDa, 78 kDa, and 78 kDa, respectively. All the other pseudophosphorylation mutants and P301L did not show a change in mobility. These SDS-resistant upward band shifts were drastically reduced in the presence of 6 M urea (Figure 4.1C). The apparent molecular weights for wild type, S199/S202/T205E, S396/404E, 6-Phos, and 7-Phos on the SDS-PAGE gel with 6 M urea were 70 kDa, 70 kDa, 71 kDa, 72 kDa and 72 kDa, respectively. Because these pseudophosphorylation mutants reproduced the SDS-resistant conformational change in AD, we concluded that they have the similar characteristics as hyperphosphorylated tau. Therefore, these pseudophosphorylation mutants with upward band shift (S199/S202/T205E, S396/404E, 6-Phos, and 7-Phos) are referred to pseudohyperphosphorylation mutants hereafter.

4.1.3 Pseudophosphorylation changed tau binding affinity for microtubules.

The microtubule binding of tau is negatively regulated by phosphorylation (*44-46*). A similar decrease in MT binding affinity was also observed in FTDP-17 mutants (*12, 196*) and pseudophosphorylation mutants (*101*). Therefore, we measured the microtubule binding affinity for P301L tau and fifteen pseudophosphorylation mutants by a centrifugation assay (*199*). Pellets containing microtubules and tau bound to MTs were resuspended in 1x SDS-sample buffer and resolved by SDS -PAGE (Figure 4.2A). Tau samples (0.06-1.0 μg per lane) were loaded on the same gel (lane 1-5 in Figure 4.2A) to generate a standard curve for tau concentration determination. The intensity of the standard tau samples was plotted versus the amount of tau protein and fit to a linear equation (Figure 4.2 B). The intensity of tau bands on SDS-PAGE gels were determined and normalized to the intensity of the tubulin band. The concentrations of bound tau were determined from the standard curve using the normalized intensity of the band. Normalization of the tau band to tubulin band was performed to take all the differences during centrifugation and resuspension into account. The amounts of free tau were determined by subtracting the amounts of bound tau from the total amounts of tau. The concentrations of bound tau were plotted versus the concentrations of free tau and the curves were fit to a one-site binding equation. Two representative curves are shown in Figure 4.2C (● wild type; ○ 7-Phos). The binding affinity (dissociation constant, K_d) and the maximal amount of binding (B_{max}) were calculated from the equation. The stoichiometry of binding (n) was calculated by dividing B_{max} by the final molar

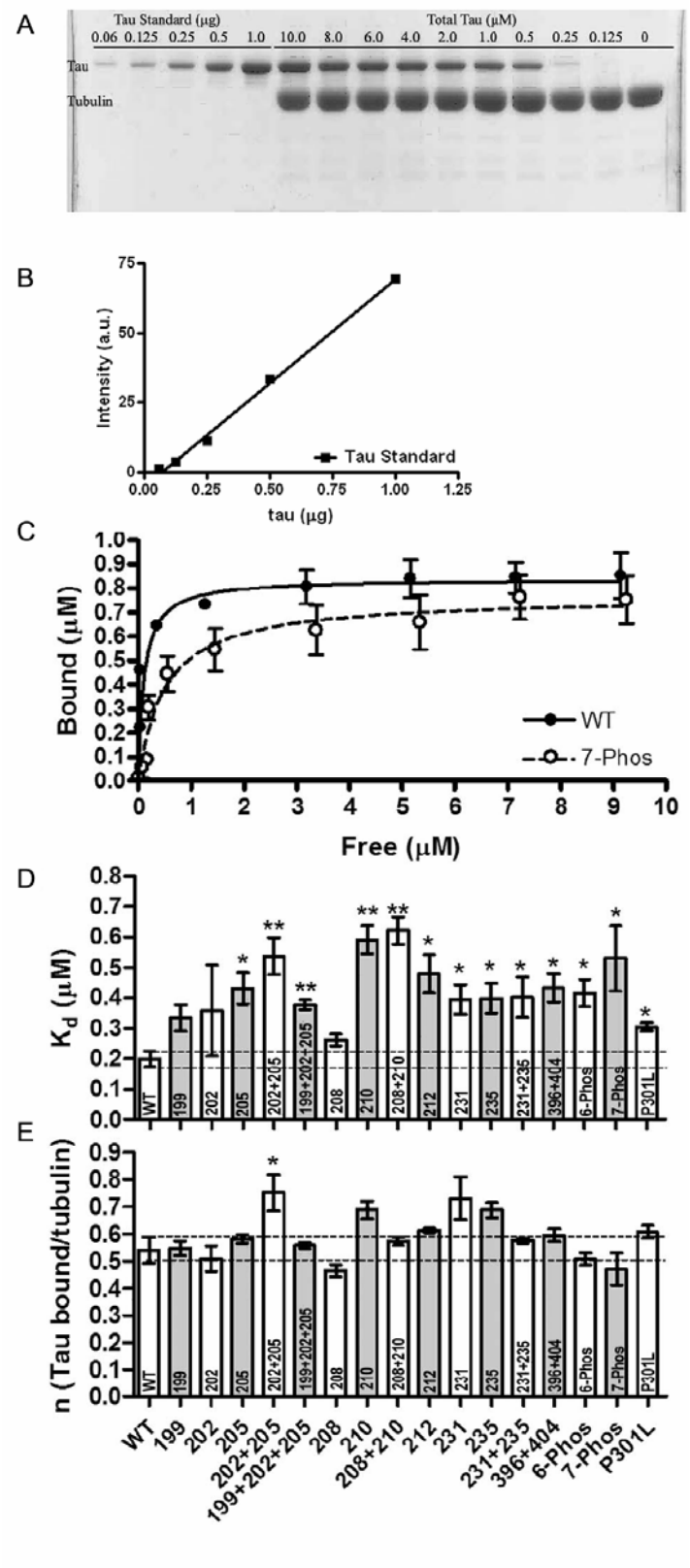
A
Tau Standard (µg)
0.06 0.125 0.25 0.5 1.0
Total Tau (µM)
10.0 8.0 6.0 4.0 2.0 1.0 0.5 0.25 0.125 0
Tau
Tubulin
B
Intensity (a.u.)
Tau Standard
tau (µg)
C
Bound (µM)
WT
7-Phos
Free (µM)
D
K_d (µM)
WT 199 202 205 202+205 199+202+205 208 210 208+210 212 231 235 231+235 396+404 6-Phos 7-Phos P301L
E
n (Tau bound/tubulin)
WT 199 202 205 202+205 199+202+205 208 210 208+210 212 231 235 231+235 396+404 6-Phos 7-Phos P301L

Figure 4.2. Pseudophosphorylation changed tau – MT binding affinity. The microtubule binding affinity of tau was determined by a centrifugation assay. A) A representative SDS-PAGE gel after centrifugation. Tau standards were loaded in lanes 1-5 with tau concentrations at 0.0625, 0.125, 0.25, 0.5, and 1.0 μg, respectively. Tau protein, concentrations varying from 0.125 to 10 μM, was incubated with taxol stabilized microtubules at a constant concentration of 1.62 μM tubulin dimers for 30 min at room temperature. The reactions were centrifuged to separate free tau from MT and tau bound to MT after incubation. The bound tau was separated from MT by SDS-PAGE and gels stained with Commassie brilliant blue. B) Representative standard curve. The intensity of tau standard bands was determined from SDS-PAGE and plotted versus the amount of tau protein in each band. The data were fit to a linear regression. C) Two representative curves of MT binding (● wild type, ○ 7-Phos). The concentrations of bound tau were determined from the intensity of tau bands on SDS-PAGE gel and standard curve. The concentrations of free tau were calculated by subtracting the concentration of bound tau from total tau concentration. The concentrations of bound tau were plotted versus that of free tau and fit to a one site binding equation. K_d and n ($n = B_{max}$ / [tubulin]) for each of three independent repetitions of the binding curves were determined from the equation and shown in panels C and D, respectively. All data were presented as the average of three independent repetitions ± s.d. ($n = 3$). Values that were significantly different from wild type values at $P < 0.05$ (*) and $P < 0.01$ (**) were determined by a student's *t* test.

concentration of tubulin dimer (1.62 μM). The values for K_d and n were plotted in Figure 4.2D and 4.2E. All of the pseudophosphorylation mutants examined, with the exception of S199E, S202E and T205E, had increased K_d values, which suggested they had significantly reduced binding affinity compared with wild type tau (Figure 4.2D). The pseudohyperphosphorylated tau mutants (S199/S202/T205E, S396/404E, 6 -Phos, and 7-Phos) did not show a larger effect compared with single or double mutants. The changes on microtubule binding were all in the 2-3 fold reduction range, which was in general agreement with the previous reports on tau phosphorylated by GSK-3β (*200, 201*) and tau phosphorylated within the proline rich region and C-terminal region by other kinases (*45*). The FTDP-17 mutant, P301L, had a lower MT binding affinity compared with wild type tau, as shown previously by another group (*12*). The stoichiometry of tau binding to microtubules was not greatly changed, with S202/T205E be the only pseudophosphorylation mutant having an elevated saturation level (Figure 4.2E). In our study, wild type and mutant tau bound to MT at a stoichiometry close to 0.5 μM tau per 1.62 μM tubulin dimers, which was roughly one tau molecule per 3 tubulin dimers.

4.1.4 Pseudophosphorylation influenced the arachidonic acid induction of tau polymerization.

4.1.4.1 Pseudophosphorylation changed the kinetics of tau polymerization induced by arachidonic acid at the optimal arachidonic acid to tau ratio.

Tau protein phosphorylated at certain sites has been shown to be prone to aggregation. A similarly increased aggregation rate was observed in the pseudophosphorylation mutant S396/404E (*76*). To determine whether pseudophosphorylation mutants of tau have an effect on the kinetics of arachidonic acid (ARA) induced tau polymerization, each protein, at a final concentration of 2 μM, was incubated with 75 μM ARA. These concentrations were chosen because this concentration of tau was close to the physiological concentration in human brain (*202*) and 75 μM ARA was shown to be the optimal inducer concentration for 2 μM tau in our previous study (*194*). The kinetics of polymerization for each mutant were followed by laser light scattering (LLS) and four representative curves are shown in Figure 4.3A. The curves were fit to a Gompertz function (*81, 100*). The maximal laser light scattering (LLS_{max}), the apparent proportional growth rate (K_{app}) and lag time for each mutant were determined from the equation and shown in Figure 4.3B - D.

None of the pseudophosphorylation mutants had an increased LLS_{max} (Figure 4.3B). Instead, seven of fifteen pseudophosphorylation mutants had a decreased amount of polymerization at apparent steady state compared with wild type tau. These mutants were S202/T205E, S199/S202/T205E, S208/S210D, T231E, S396/S404E, 6-Phos and 7- Phos. The decreased polymerization was observed in the GSK-3β phosphorylated tau in our previous report (*104*) and the phosphorylation at S262 by MARK and S214 by PKA by another group (*203*). The FTDP-17 mutant,

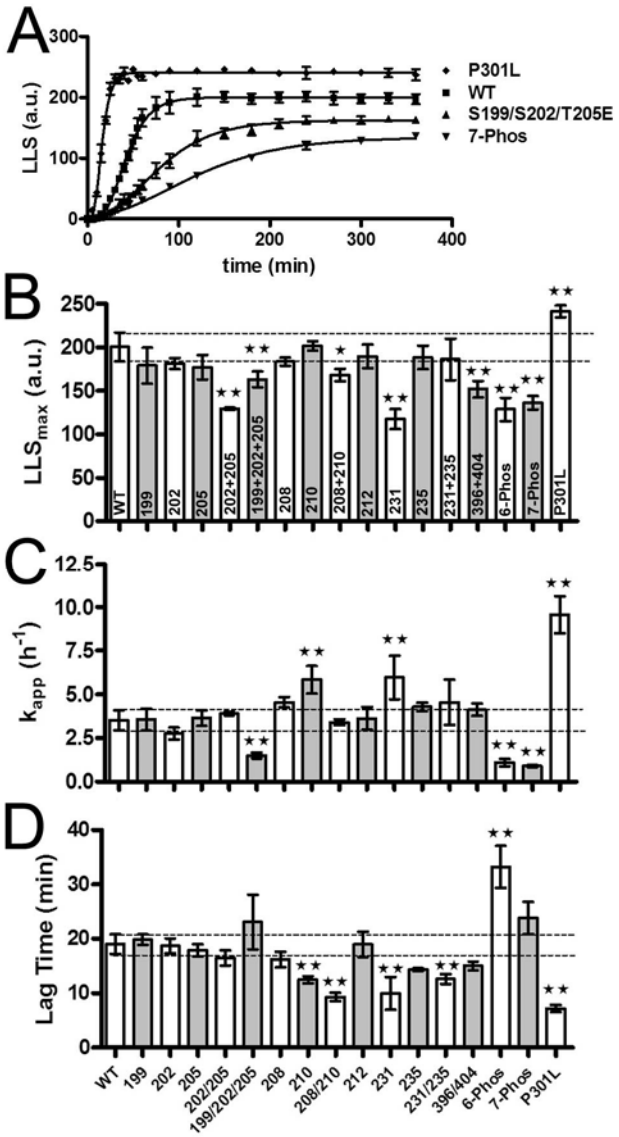
A
LLS (a.u.)
time (min)
P301L
WT
S199/S202/T205E
7-Phos
B
LLSmax (a.u.)
WT
199
202
205
202+205
199+202+205
208
210
208+210
212
231
235
231+235
396+404
6-Phos
7-Phos
P301L
C
kapp (h-1)
D
Lag Time (min)
WT
199
202
205
202/205
199/202/205
208
210
208/210
212
231
235
231/235
396/404
6-Phos
7-Phos
P301L

Figure 4.3. Pseudophosphorylation changed the kinetics of tau polymerization induced with arachidonic acid. Wild type and pseudophosphorylation tau mutants at 2 μM protein concentration were incubated with 75 μM ARA in polymerization buffer for 6 hr. The amount of polymerization at regular time intervals was monitored by laser light scattering (LLS). A) Four representative curves of laser light scattering at various time points. ■ wild type; ▲ S199/S202/T205E; ▼ 7-Phos; ♦ P301L. Each curve was fit to a Gompertz equation. Maximal laser light scattering (LLS_{max}), K_{app} and lag time were determined from the equation and shown in panels B, C and D, respectively. All data were presented as the average of three independent repetitions ± s.d. (n = 3). Values that were significantly different from wild type values at $P < 0.05$ (*) and $P < 0.01$ (**) were determined by one-way ANOVA analysis of variance with Dunnett's multiple comparison post-test using wild type as the control column.

P301L, was the only mutant that had an increased amount of polymerization compared with wild type, which was in agreement with a previous report (*67*). The apparent proportional growth rate K_{app}, which reflected the elongation rate, was not significantly changed in most of the pseudophosphorylation mutants (Figure 4.3C). P301L had a drastically increased apparent polymerization rate, K_{app}, compared with wild type, which agreed with a previous report (*67*). The K_{app} of P301L was also significantly greater than those of all the pseudophosphorylation mutants. Two of the pseudophosphorylation mutants (S210D and T231E) had an increased apparent proportional growth rate compared with wild type tau but the changes were much smaller compared with that of P301L (Figure 4.3C). The pseudohyperphosphorylated forms of tau (S199/S202/T205, 6-Phos, and 7-Phos) had a significantly lower K_{app} as shown in Figure 4.3C.

The ARA induced tau fibrillization has been shown to be a "nucleation-elongation" process (*77, 204*) which was reflected by the presence of a lag time. The nucleation rate has been suggested to be modified by phosphorylation (*205*). In our study, the decreased lag time was observed in four of the pseudophosphorylation mutants (S210D, S208/S210D, T231E, and T231E/S235D) and P301L compared to wild type tau (Figure 4.3D). However, none of these pseudophosphorylation mutants was able to reduce the time for nucleation to the same level as P301L did. A significantly increased lag time was observed in the polymerization reaction of 6-Phos, which suggested a defect in nucleation. The lag times of the S199/S202/T205E and 7 -Phos mutants were comparable to those of the wild type (Figure 4.3D).

4.1.4.2 Pseudophosphorylation changed the morphology of tau filaments induced by arachidonic acid at the optimal arachidonic acid to tau ratio.

To determine whether pseudophosphorylation changed the morphology (number and length) of the filaments, the polymerization reactions were prepared and viewed by TEM. Representative images are shown in Figure 4.4.

In general, there were fewer but longer filaments formed by pseudophosphorylation mutants compared with wild type tau. In contrast, P301L formed more and shorter filaments. This observation was confirmed by quantitative analysis of the filaments (Figure 4.5). The images were analyzed using Optimas image analysis program and the length for each filament was determined. Only particles longer than 15 nm were counted. This cutoff value is the average width of the filaments induced by arachidonic acid and particles shorter than this value are difficult to distinguish from the background. The filaments from all six images were put into one data set and plotted in Figure 4.5. The general trend of forming fewer but longer filaments was observed in most of the pseudophosphorylation mutants (Figure 4.5B and 4.5C). However, the overall filament length in all six fields of most pseudophosphorylation mutants was close to that of the wild type tau, with T231E, S202/T205E, T205E and S396/S404E being the possible exceptions (Figure 4.5D). The pseudohyperphosphorylated forms of tau (S199/S202/T205E, 6-Phos, and 7-Phos) formed the longest filaments and the one with longest average filament length was the one with the most pseudophosphorylation sites (7-Phos). The rapidly polymerizing FTDP-17 mutant, P301L, formed more, but shorter filaments than wild type, resulting

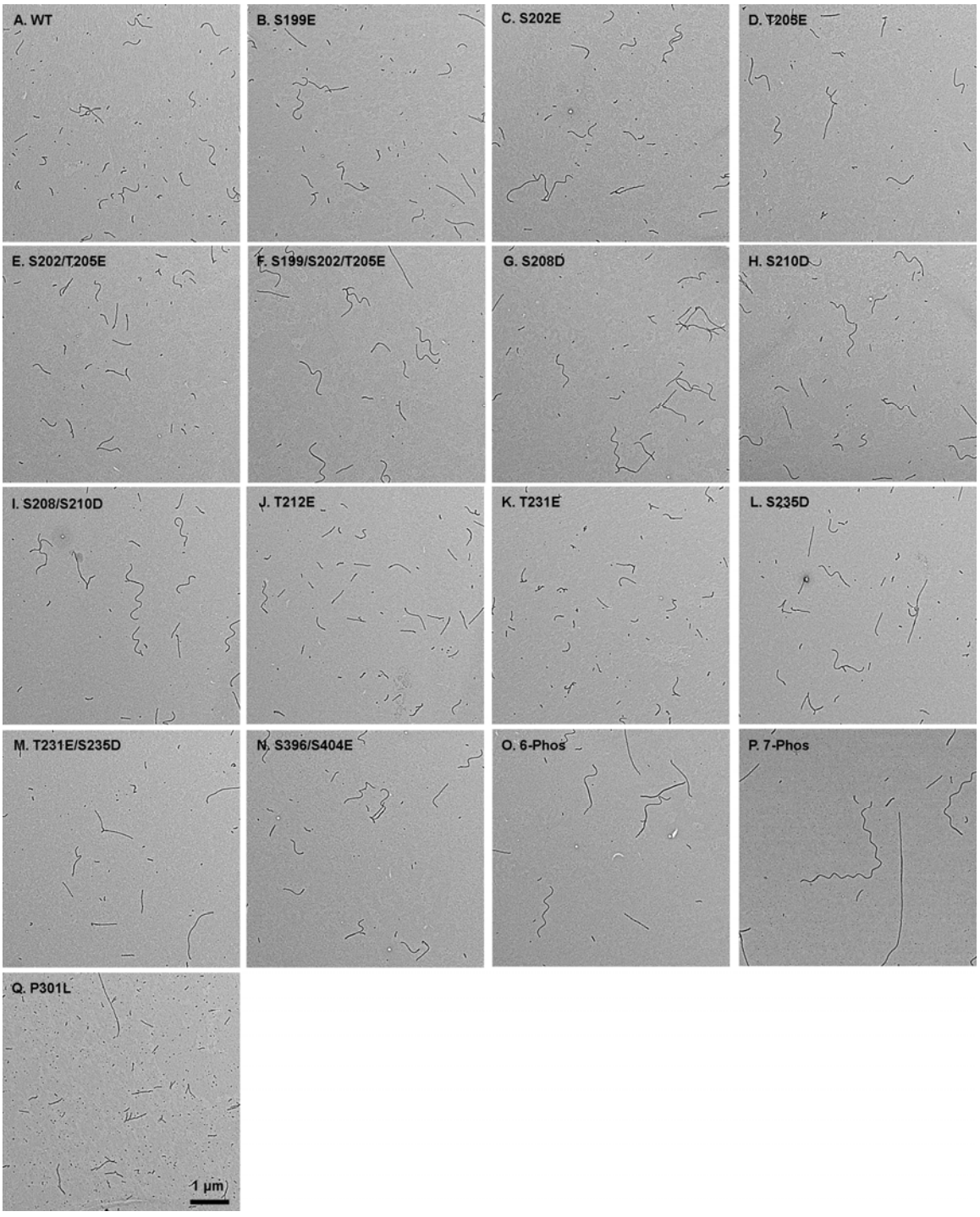
A. WT
B. S199E
C. S202E
D. T205E
E. S202/T205E
F. S199/S202/T205E
G. S208D
H. S210D
I. S208/S210D
J. T212E
K. T231E
L. S235D
M. T231E/S235D
N. S396/S404E
O. 6-Phos
P. 7-Phos
Q. P301L
1 µm

Figure 4.4. TEM analysis of polymerization at a final concentration of 2 μM tau and 75 μM arachidonic acid. The polymerization reactions of wild type or pseudophosphorylation mutant tau at a final concentration of 2 μM were incubated with 75 μM ARA inducer at room temperature for 20 hr. The reactions were viewed by TEM and representative micrographs are shown. A) wild type, B) S199E, C) S202E, D) T205E, E) S202/T205E, F) S199/S202/T205E, G) S208D, H) S210D, I) S208/S210D, J) T212E, K) T231E, L) S235D, M) T231E/S235D, N) S396/S404E, O) 6-Phos, P) 7-Phos and Q) P301L. Scale bar in Q) represents 1 μm and is applicable to all images.

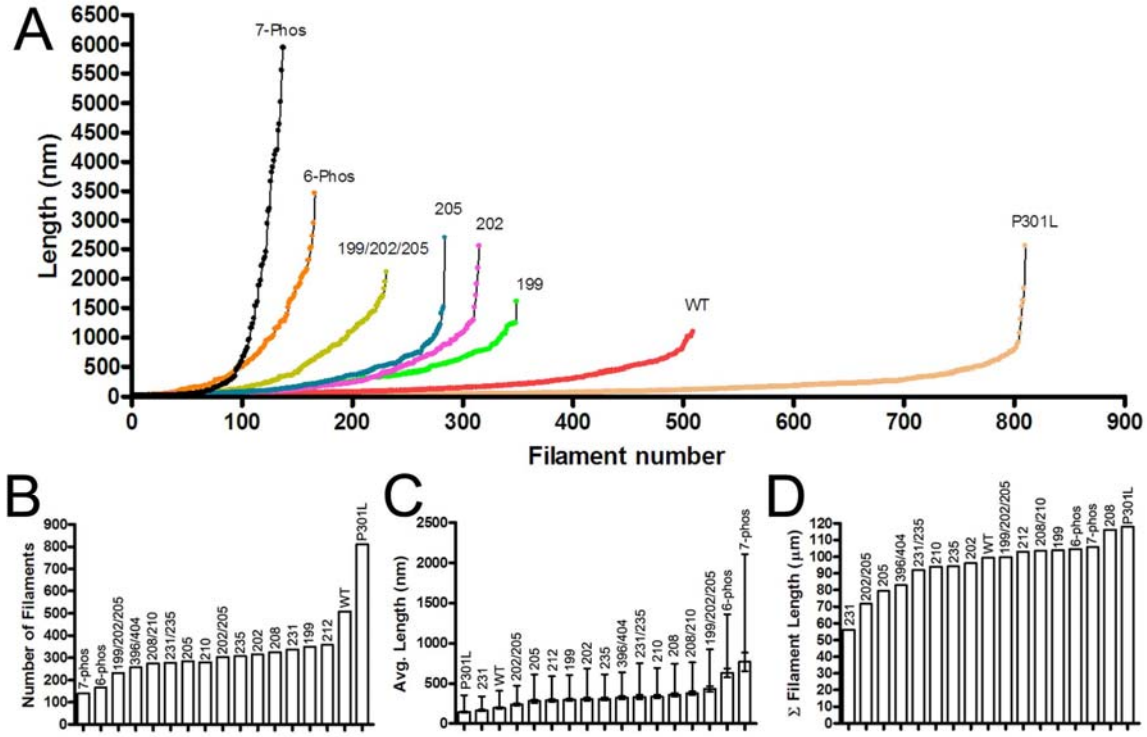
A
Length (nm)
Filament number
7-Phos
6-Phos
205
202
199/202/205
199
WT
P301L
B
Number of Filaments
C
Avg. Length (nm)
D
Σ Filament Length (μm)

Figure 4.5. Filament distribution of polymerization reactions at a final concentration of 2 μM tau protein and 75 μM arachidonic acid inducer. The polymerization reactions of 2 μM wild type tau and pseudophosphorylation mutant tau induced by 75 μM ARA were viewed by TEM after 20 hr incubation at room temperature. Resulting filament lengths were analyzed by Optimas image analysis program. Six 6 x 6 μm fields were analyzed for each protein. Only the filaments longer than 15 nm were counted. A) The filament lengths from all six fields were combined into a single data set and ranked from the shortest to the longest. Each individual filament was plotted against its corresponding rank for each protein. Eight samples were shown and each sample was individually colored and labeled on the graph. The distributions for S210D, S208/S210D, T231E/S235D and S396/S404E were similar to that of T205E. The distributions for S202T/205E, S208D and S235D were similar to that of S202E. The distributions for T212E and T231E were similar to S199E. B) The total number of filaments observed in all six fields for each protein is shown and ranked from the one with the least filaments to the one with most. Each bar was individually labeled on the graph. C) The average length of the filaments observed in all six fields for each protein is shown and ranked from the one with the shortest average filament length to the one with the longest. Each bar is individually labeled on the graph. Values are shown as average ± s.d. (error bars above only) and ± s.e.m. (bar above and below) (n=6). D) The sum of filament lengths of all the filaments observed from all six fields for each protein is shown and ranked from the one with least total filament mass to the one with greatest. Each bar is individually labeled on the graph. In general, fewer but longer filaments were observed in pseudophosphorylation mutants compared with wild type tau.

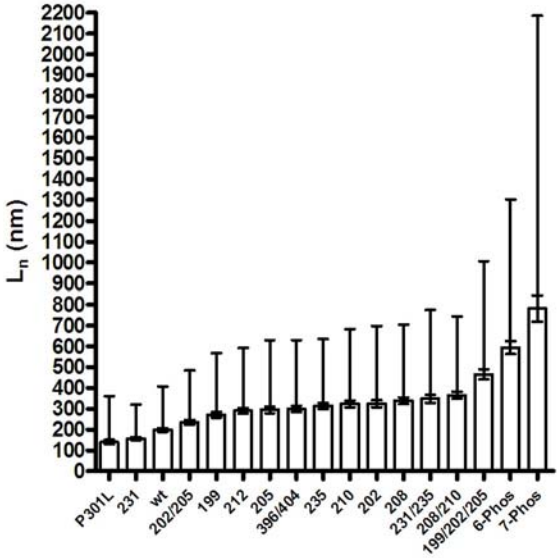

Figure 4.6. Pseudophosphorylation mutant tau forms longer filaments than wild type tau. Wild type tau and pseudophosphorylated mutant tau at 2 μM protein concentration were incubated with 75 μM ARA in polymerization buffer at room temperature for 20 hr. Resulting filament lengths of 500 filaments were measured by Optimas image analysis program. The number-average filament length ± s.d. (error bars above only) and ± s.e.m. (error bars above and below) for each protein was shown and ranked from the one with longest average filament length to the one with the shortest. Each bar was individually labeled on the x-axis.

in an overall increase in the total filament length from all six fields. Both the standard deviation and standard error of the mean for the average filament lengths are shown in Figure 4.5C. The standard deviation was approximately equal to the value of the average filament length for most proteins, suggesting the filaments were in an exponential distribution (*206*). The standard error of the mean was the estimation of the accuracy of the determination of the true mean. Due to the differences in the number of filaments, the variability in filaments distribution on the TEM grids, the biological variability in filament lengths, and the exponential distribution of filament lengths, the statistical analysis of differences between the filaments is difficult. Therefore, it is possible that the apparent differences in filament distribution shown in Figure 4.5 could come from differences in sampling. To test this possibility, we measured 500 filaments for each protein and determined the number-average length ($L_n=(\Sigma N_i L_i)/(\Sigma N_i)$, Figure 4.6) for each protein. All the pseudophosphorylation mutants formed longer filaments than wild type tau, with T231E to be the lone exception (Figure 4.6). The number-average filament length of P301L was shorter than wild type as seen in Figure 4.5C. This analysis also confirmed that pseudohyperphosphorylated forms of tau (S199/S202/T205E, 6-Phos, and 7-Phos) formed longer filaments than wild type tau.

4.1.4.3 Pseudophosphorylation mutants responded differently to the changes in tau: ARA ratios.

The maximal amount of polymerization was not significantly increased in any of the pseudophosphorylation mutants (Figure 4.3). However, in a previously published report, a 2-3 fold increase in the amount of polymerization induced by arachidonic acid was observed in some of the pseudophosphorylation mutants. These pseudophosphorylation mutants included T212E and S199/S202/T205E, which did not show a significant increase in our studies (*100*). We previously showed that the amount of polymerization induced by arachidonic acid depended both on tau concentration and the inducer concentration and there was an optimal inducer to protein ratio (*194*). Below the optimal inducer to protein ratio, the inducer limits the polymerization reactions, and above the optimal induce to protein ratio, the inducer inhibits the reaction (*194*). The concentration of tau is difficult to determine and the difference between the protein concentrations determined by different protein assays could be as high as 5-fold (*101, 207*). For this reason, we hypothesized that the difference between our study and the previous report was due to performing experiments at different inducer to protein ratios. Therefore, we kept the protein concentration of tau constant at 2 μM (determined by bicinchoninic acid (BCA) assay) and varied the concentrations of ARA from 25 μM to 150 μM. The resulting polymerization was assayed by LLS (Figure 4.7) and ThS (Figure 4.8). None of the mutants had a significantly increased polymerization at the optimal inducer to protein ratio as assayed by LLS and ThS (Figure 4.7 and 4.8). The 2-3 fold increase in polymerization was observed in some of the pseudophosphorylation mutants at the high inducer to protein ratios (ARA concentration $\geq$ 125 μM), such as

S199/S202/T205E, S210D, S208/S210D and T231E/S235D, when assayed by LLS (Figure 4.7). This result suggested that the increase of polymerization observed in some of the pseudophosphorylation mutants was due to the diminution of the inhibitory effects at high inducer concentrations on polymerization. The amount of polymerization of P301L was significantly higher than wild type tau at all these inducer to protein ratios (Figure 4.7). The results determined by ThS fluorescence generally agreed with the results determined by LLS (Figure 4.8). All of tau variants showed a biphasic dependence on inducer concentrations. The increase in ThS signal was only observed at high inducer concentrations (≥ 125 μM) for some of the pseudophosphorylation mutants, including S199/S202/T205E, S210D, S208/S210D and T231E/S235D. However, in some of the mutants, the changes on the amount of polymerization were drastically different when using different assays (LLS or ThS). These mutants were: S396/404E, 6-Phos, 7-Phos and P301L. For S396/404E, 6- Phos and 7-Phos, the significant increase in polymerization at high inducer concentrations was not observed by LLS but observed by ThS. Because S396/404E, 6-Phos and 7-Phos were the three mutants that had a mobility change on SDS-PAGE, the change induced by pseudophosphorylation may change the binding of ThS with tau filaments and result in the changes in ThS fluorescence intensity. For P301L, the significant increase was only observed at the lowest protein concentration. This could be due to the saturation of ThS by tau filaments.

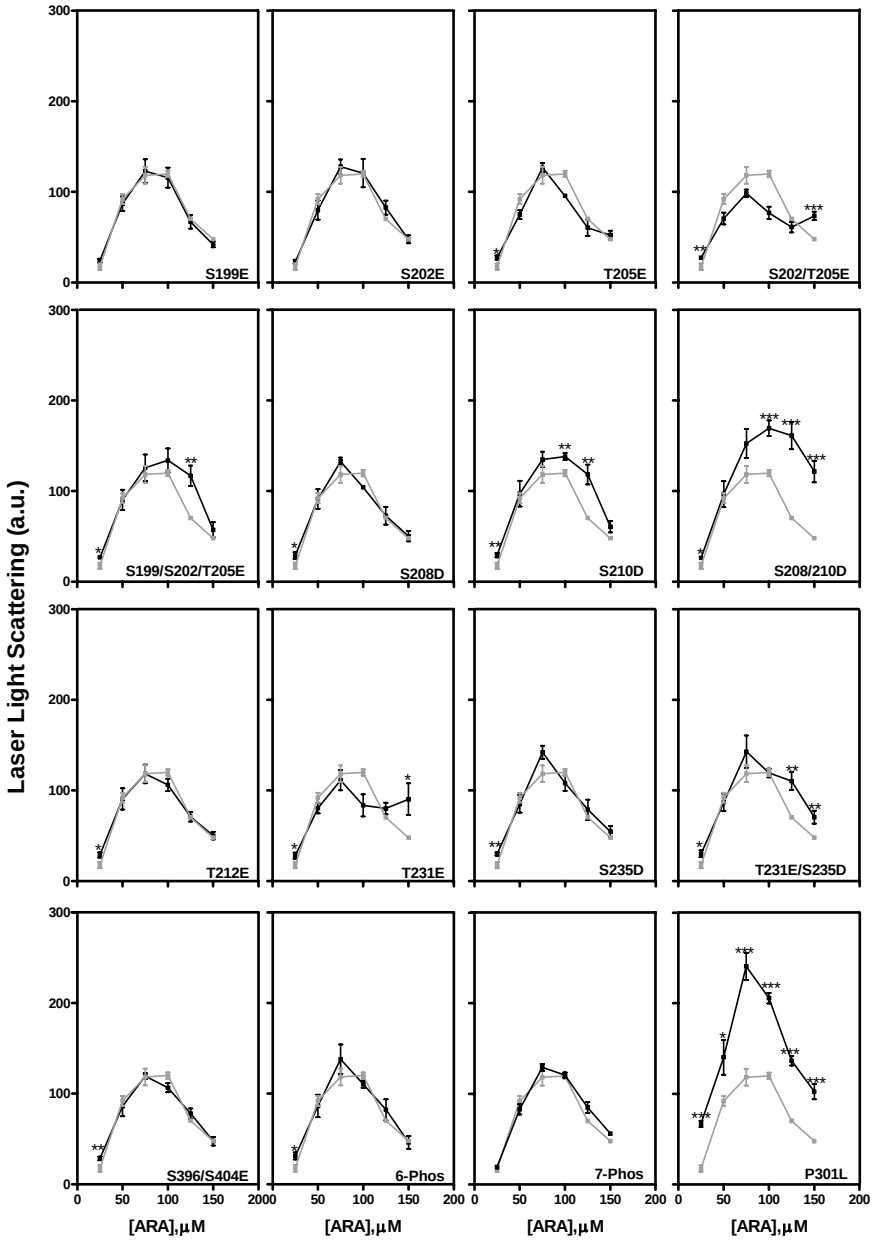
Laser Light Scattering (a.u.)
S199E
S202E
T205E
S202/T205E
S199/S202/T205E
S208D
S210D
S208/210D
T212E
T231E
S235D
T231E/S235D
S396/S404E
6-Phos
7-Phos
P301L
[ARA],µM
[ARA],µM
[ARA],µM
[ARA],µM

Figure 4.7. Polymerization reactions of pseudophosphorylation tau mutants at final concentration of 2 μM protein with various concentrations of ARA inducer were assayed by laser light scattering. Wild type and mutant tau protein (2 μM) were incubated in polymerization buffer with ARA at final concentrations varying from 25 μM to 150 μM at room temperature for 20 hr. The amount of polymerization was assayed by laser light scattering and shown. Each protein was individually labeled on each graph. For ease of comparison, the values for wild type tau were included on each graph (light gray curve). All data were presented as average values ± s.d. (n = 3). Values that were significantly greater than wild type values at $P < 0.05$ (*), $P < 0.01$ (**) and $P < 0.001$ (***) were determined by student *t* test.

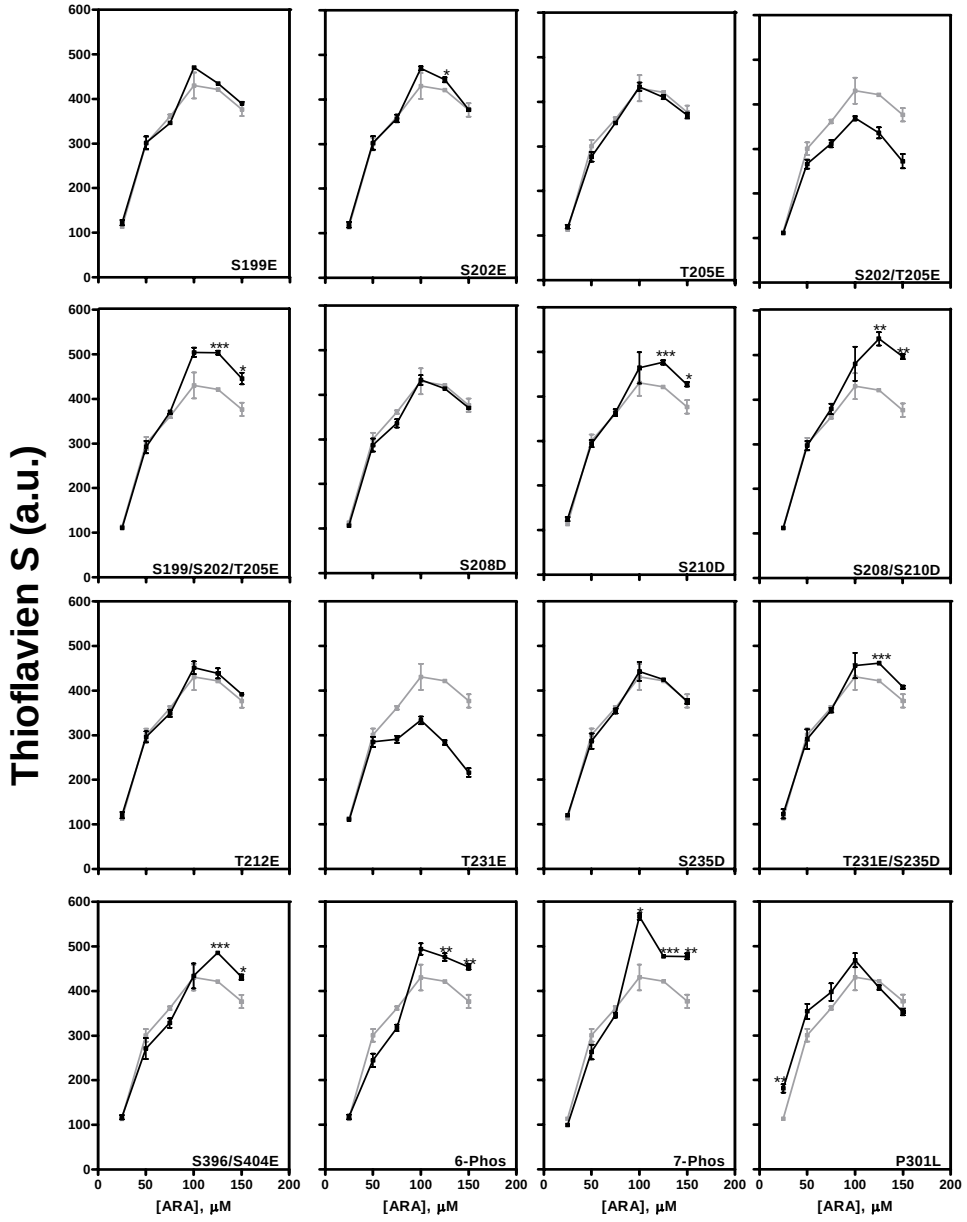
Thioflavien S (a.u.)
S199E
S202E
T205E
S202/T205E
S199/S202/T205E
S208D
S210D
S208/S210D
T212E
T231E
S235D
T231E/S235D
S396/S404E
6-Phos
7-Phos
P301L
[ARA], µM
0
50
100
150
200
100
200
300
400
500
600

Figure 4.8. Polymerization reactions of pseudophosphorylation tau mutants at final concentration of 2 μM protein with various concentrations of ARA inducer were assayed by ThS fluorescence. Wild type and mutant tau protein (2 μM) were incubated in polymerization buffer with ARA at final concentrations varying from 25 μM to 150 μM at room temperature for 20 hr. The amount of polymerization was assayed by Thioflavine S fluorescence and shown. Each protein was individually labeled on each graph. For ease of comparison, the values for wild type tau were included on each graph (light gray curve). All data are presented as average values ± s.d. (n = 3). Values significantly greater than wild type values at $P < 0.05$ (*), $P < 0.01$ (**) and $P < 0.001$ (***) were determined by a student's *t* test.

4.1.5 Pseudophosphorylation mixtures produced tangle-like aggregates similar to those induced by GSK-3β phosphorylation.

The phosphorylation of tau by GSK-3β either prior to or following polymerization promotes the formation of tangle-like aggregates from ARA induced individual filaments (*104, 105*). These tangle-like aggregates have similar morphology and density to those isolated from AD brain (*104*). However, these tangle-like aggregates were not observed in the ARA induced polymerization reactions of the pseudohyperphosphorylated forms of tau (S199/S202/T205E, 6-Phos and 7-Phos, Figure 4.4). Because there are about 2-4 mol phosphate per mole of tau after GSK-3β phosphorylation and the phosphorylation is heterogenous (*104, 201*), it is not surprising the tangle-like aggregates from homogenous pseudohyperphosphorylation were not observed. Therefore, to mimic the GSK-3β phosphorylation of tau, we mixed equal amounts (0.33 μM) of six different pseudophosphorylation mutants (S199E, S202/T205E, S208D, T212E, T231E/S235D and S396/S404E), and made the final tau concentration 2 μM. Each pseudophosphorylation mutant in the mixture had 1 or 2 mol "phosphates" per mole of tau and the stoichiometry of "phosphorylation" for the mixture was 1.5 mol "phosphates" per mole of tau. The polymerization reactions were induced with 25 μM or 75 μM ARA and viewed under TEM. We added 0.3 mM $MgCl_2$, 0.2 mM ATP and 20 μM ThS, into the polymerization buffer to mimic the polymerization conditions for GSK-3β phosphorylated tau. The representative TEM micrographs are shown in Figure 4.9. Small clusters were observed in the polymerization reactions

for both wild type tau and the pseudophosphorylation mixture (asterisks in Figure 3.9).

We also checked the polymerization reactions of wild type tau and the pseudophosphorylation mixture induced with 25 μM or 75 μM ARA without the additional buffer components and these small clusters were not formed under any of these conditions. This suggested that one or more of these buffer components could induce the clustering of filaments into these small aggregates. The large clusters similar to those found in the polymerization reactions of GSK-3β phosphorylated tau, were only observed in the polymerization reactions of pseudophosphorylation mixture induced with 75 μM ARA (arrow head in Figure 4.9D). However, even though the size of the clusters formed under this condition was close to the clusters from GSK-3β phosphorylated tau, they were significantly lower in numbers.

4.2. Discussion

4.2.1 Significance of pseudophosphorylation mutant sites

The presence of abnormally hyperphosphorylated insoluble tau in brain is a prominent characteristic of AD and other tauopathies. The phosphorylation level is at least 3 to 4 times higher in AD tau than in normal tau (*43, 208*). However, it is not clear which kinase(s) are responsible for the changes in tau phosphorylation levels. There are at least 20 kinases contributing to the phosphorylation of tau. Among these kinases, GSK - 3β is the most attractive candidate for the phosphorylation of PHF tau, which play roles in both familial and sporadic forms of AD (*53*). According to our

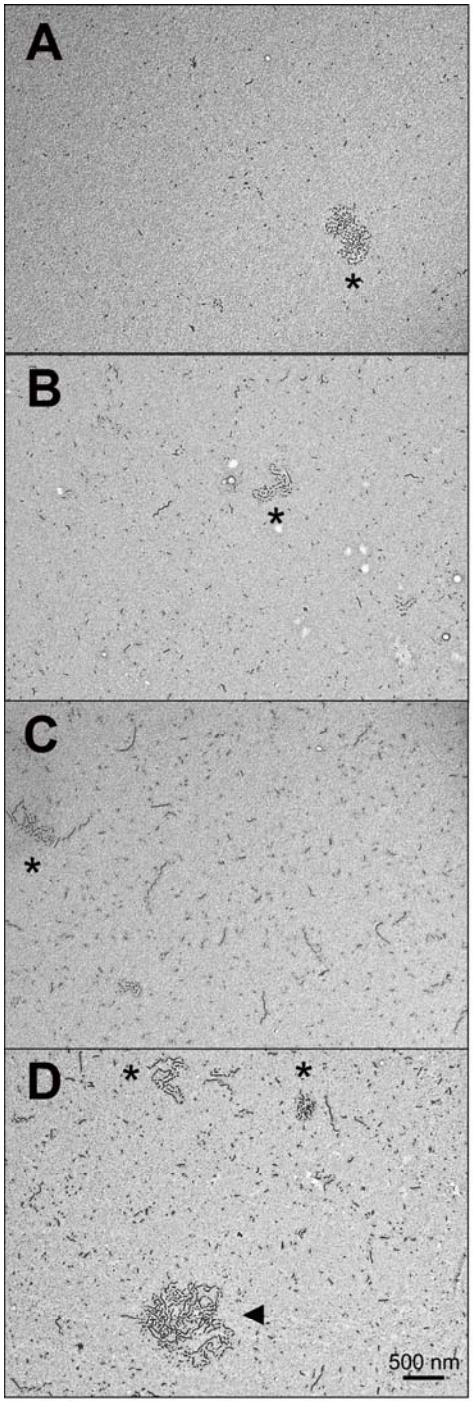
A
B
C
D
500 nm

Figure 4.9. Formation of tangle-like aggregates from the mixtures of pseudophosphorylation tau mutants. Polymerization reactions of wild type tau and the mixtures of pseudophosphorylation tau mutants were incubated with 25 or 75 μM ARA in polymerization buffer plus 0.3 mM $MgCl_2$, 0.2 mM ATP, and 20 μM ThS at 30 ºC for 20 hr and viewed by TEM. The protein concentration for wild type tau was 2 μM. The pseudophosphorylation mutant mixtures were composed of S199E, S202/T205E, S208D, T212E, T231E/S235D, and S396/404E each at a final concentration of 0.33 μM. A) wild type tau + 25 μM ARA, B) pseudophosphorylation mix + 25 μM ARA, C) wild type tau + 75 μM ARA, D) pseudophosphorylation mix + 75 μM ARA. Images were recorded at a magnification of 20,000 x. The scale bar on panel D represents 500 nm and is applicable to all images. Local aggregations of filaments were marked with asterisk (small) or arrowhead (large).

previous results, GSK-3β can phosphorylate tau at 11 sites when using monomeric tau as substrate (*104*). These phosphorylation sites are: S199, T205, T212, S214, T217, T231, S356, S396, S400, S404, and S409. Only 5 of these 11 sites can be phosphorylated by GSK-3β when using aggregated tau as substrate and phosphorylation at these five sites is sufficient to induce tau filaments to coalesce into NFT-like aggregates. These five sites are S199, T205, T231, S396 and S404 (*105*). The previous reports have suggested that all these five of these sites were important for the pathological changes of tau. S199 and T205, together with S202 are the epitopes of an AD specific antibody AT8 (*209, 210*). The pseudophosphorylation at these 3 sites has been shown to open up the hairpin conformation of tau and therefore may change its ability to aggregate and to bind microtubules and promote their assembly (*103*). The phosphorylation at T231 occurs in PHF tau and can be recognized by a phosphorylation dependent antibody AT180 (*211*) and by a conformation dependent antibody TG-3 together with the phosphorylation at S235 (*212*). T231 has been suggested to be the primary phosphorylation site for GSK-3β (*213*) and the de-phosphorylation at this position in the presence of prolyl isomerase, Pin 1, can restore its ability to bind MT (*214*). Tau phosphorylated at S396 and S404 accumulates in late-stage AD and is recognized by monocolonal antibody PHF-1 (*215*). The phosphorylation at these two sites opens up the hairpin conformation of tau (*103*) and increases the rate of tau aggregation by altering the inhibitory effect of the C-terminal region on aggregation (*76*).

4.2.2 Role of phosphorylation in tau aggregation

The findings that the pattern of tau phosphorylation correlates with the amount of NFTs and severity of neuropathology suggest that there is a direct correlation between tau phosphorylation and its aggregation (*216*). Under the optimal polymerization condition we used in our studies, the amount of polymerization was not significantly increased in these pseudophosphorylation mutants when assayed by laser light scattering. Instead, in some of the pseudophosphorylation mutants, a slightly reduced polymerization was observed. In general, the filaments formed from most of the single and double mutants were fewer in number and greater in length (Figure 4.4). Only slight changes in polymerization kinetics were observed for most of these single and double mutants. However, significantly decreased elongation rates were observed in the pseudohyperphosphorylated tau variants (S199/S202/T205E, 6-Phos, and 7-Phos). At the same time, these tau variants had longer lag time compared with wild type tau. The changes in kinetics of these pseudohyperphosphorylated tau mutants were in agreement with the changes to tau filament morphology. Longer but fewer filaments were observed in these three mutants and this suggested an impaired nucleation process.

The polymerization condition we used to assay the changes on kinetics and polymerization is the optimal condition for polymerization. Under the optimal condition, a large percentage of tau will form filaments. At lower inducer concentrations, the inducer will limit the reaction. And at higher inducer concentrations, the polymerization can be inhibited by the inducer (*194*). Although,

the pseudophosphorylation mutants did not change the amount of polymerization at the optimal inducer concentration, the amount of polymerization may be different from wild type tau at other inducer concentrations. A 2-3 fold increase in polymerization was observed at higher inducer concentrations in some of the pseudophosphorylation mutants including S199/S202/T205E, S210D, S208/S210D, S396/S404E, 6-Phos and 7-Phos by LLS and/or ThS fluorescence (Figure 4.7 and Figure 4.8). This suggested high inducer concentrations inhibited polymerization to a lesser extent than wild type tau in some pseudophosphorylation mutants.

Arachidonic acid has been known to induce tau polymerization by decreasing the energetic barrier for the nucleation of polymerization (*194*). Although no direct evidence has been shown, the induction process may involve the direct binding between tau and ARA. The decreased nucleation process suggested by kinetics and filament morphology together with the decreased inhibitor effects at higher inducer concentrations may be caused by the diminished interactions between ARA and tau. This idea was supported by the observed mobility changes on SDS-PAGE (Figure 4.1). The different results between LLS and ThS observed on S396/404E, 6-Phos, and 7-Phos may also be due to the altered interactions between tau and ThS resulting from conformational changes.

4.2.3 Role of phosphorylation in microtubule binding

The phosphorylation at the region outside of the MT binding repeats usually results in a 2-3 fold decrease in the tau-MT binding affinity (*47*). A similar 2-3 fold

decrease was observed in most of our pseudophosphorylation mutants without significantly changing the saturation levels of binding. An interesting aspect of the changes in MT binding is that these changes are not additive. For example, both T231E and S235D had a lower MT-binding affinity compared with wild type tau. However, no further decrease was observed in the MT-binding affinity of T231E/S235D double mutant. Similarly, the S202/T205E double mutant had a significantly decreased MT-binding. However, instead of causing a decrease, the additional mutation at S199 increased the MT-binding affinity (albeit still more lowly than wild type tau). This observation suggests that the effect of phosphorylation on MT-binding does not depend on the number of phosphorylation sites. Rather, the regulation of MT-binding is through a more complicated site specific manner.

4.2.4 Comparison with phosphorylation by GSK-3β

Pseudophosphorylation has been used to study the contribution of the phosphorylation at specific sites on tau functions. The results from this study showed that pseudophosphorylation reproduced the changes induced by GSK-3β in many aspects. The SDS-resistant conformational change similar to that induced by GSK-3β phosphorylation was observed in four of our pseudophosphorylation mutants (*104, 201*). The reduction of tau-MT binding affinity was approximately 2-3 fold and was similar to the mild reduction induced by GSK-3β phosphorylation (*217*). GSK-3β phosphorylation had a slightly decreased polymerization compared to wild type tau which was reproduced by our pseudophosphorylation mutants. However, the tangle-

like aggregates induced by GSK-3β were not formed in any of the pseudophosphorylation mutants, not even in the pseudohyperphosphorylation mutants. Similar aggregates, but drastically few in number, were observed in the mixture of some of these pseudophosphorylation mutants. One difference between pseudohyperphosphorylation mutants and the mixture of pseudophosphorylation mutants is the ratio of "phosphate" to tau. The ratio of 1.5 mol phosphates per mole of tau in the mixture of pseudophosphorylation mutants is closer to the 2-4 mol phosphate in the GSK-3β phosphorylated tau (*104, 201*). In addition, the mixture of pseudophosphorylation mutants reproduced the heterogenous phosphorylation induced by GSK-3β better than the homogenous pseudohyperphosphorylation. Therefore pseudophosphorylation mimics phosphorylation induced by GSK-3β to a certain degree, but does not completely model the full effects of phosphorylation.

4.2.5 Phosphorylation, polymerization, NFTs formation and neurotoxicity

NFTs are one of the diagnostic hallmarks of AD and the number of NFTs correlates with the degree of dementia (*8*). Therefore, NFTs have been considered as the toxic species in AD for a long time. However, increasing evidence from tau-expressing cultured cells, transgenic *C. elegans* models, transgenic *Drosophila* models and transgenic mouse models suggest that NFTs are not required for neurotoxicity (1.5.1). The hyperphosphorylation of tau resulting from the constitutive activation of cdk5 in primary neurons and pseudohyperphosphorylated tau expressed in PC12 cells were sufficient to promote cell death without the presence of detectable

protein aggregates (*118*). The neuronal dysfunction and neuronal loss were observed without or before the presence of NFTs in Tg *C. elegans*, Tg *Drosophila* and Tg mice (*142, 146, 160-162*). Although NFTs and tau filaments were not observed in these models, hyperphosphorylation and the resulting conformational changes are required for the toxicity. The evidence for this came from the fact that tau isolated from NFTs and these animals was hyperphosphorylated and had an SDS-resistant mobility change (*142, 146, 160-162*). In addition, the presence of soluble hyperphosphorylated tau correlates with the cognitive deficiencies in a Tg mouse model (*166*). The toxicity of hyperphosphorylated tau was due to the disruption of the cytoskeleton. The hyperphosphorylated tau with the conformational change can be released from MT and was able to sequester the normal tau, and therefore disrupted the MT network and resulted in cell death. The toxicity of hyperphosphorylated tau could be reduced by the formation of filaments and consequent formation of NFTs. Therefore, hyperphosphorylated tau monomers and/or oligmers could be the toxic species and tau filaments and NFTs may work as a result of cellular attempts to reduce toxicity.

Our results provide a possible mechanism for the potential toxicity of hyperphosphorylated tau in neurons. The hyperphosphorylated tau with lower MT binding affinity will be released from MT. Therefore, the concentration of cytosolic hyperphosphorylated tau, which is most likely to be the toxic species, will be increased. This will result in two changes: 1) the soluble hyperphosphorylated tau will sequester normal tau and further de-stabilize microtubules; 2) the soluble

hyperphosphorylated tau at high concentrations will start to coalesce into filaments. However, the hyperphosphorylated tau has slower kinetics of aggregation compared with wild type tau and the hyperphosphorylated tau will stay in the toxic soluble form for a longer time. The toxic hyperphosphorylated tau may finally be removed by the formation of less toxic filaments. These filaments can further coalesce into neurofibrillary tangles which have been observed from GSK-3β phosphorylated tau and the mix of pseudophosphorylated tau (*104, 105*).

CHAPTER 5: CONCLUSIONS AND IMPLICATIONS

My dissertation work focused on the effects of hyperphosphorylation on tau functions. This work contributes to the understanding of tau toxicity in the progression of AD and other tauopathies.

5.1 Tau toxicity

Although much progress has been made in the study of tau protein, it is still not clear how tau dysfunction contributes to toxicity and neurodegeneration in tauopathies. Both the loss of normal tau function and the gain of toxic function are believed to play a role in inducing neuronal dysfunction and dementia.

5.1.1 The loss of normal tau function

The major function of tau in neurons is to bind and stabilize microtubules and to promote microtubule assembly (reviewed in (*8*)). Both missense mutations in FTDP-17 and hyperphosphorylated tau in sporadic AD have reduced abilities for regulating microtubule stability and dynamics (reviewed in (*8, 13, 30, 32*)). Because 4R isoforms and 3R isoforms have different binding affinities for microtubules, the changes of 3R to 4R ratios in some of the mutations linked to FTDP-17 also alter tau function of binding microtubules (reviewed in (*32*)). The reduced ability of tau to regulate microtubule stability and dynamics and the missorting of tau into somatodendrites will disrupt the microtubule in axons (*205*). Therefore neurons will lose the tracks for axonal transport, resulting in synaptic damage. Axonal dysfunction

and synaptic damage were observed in early stages of AD (*218*) and were mimicked in a transgenic *Drosophila* model (*219*) and transgenic mouse models (*172, 220*).

However, the results from tau knock-out mice suggested the loss of normal function alone was subtle and was not sufficient to induce neurodegeneration. In tau knock-out mice, axonal elongation and axonal transport rates were normal and no sign of cytoskeletal collapse was observed in these mice (*157, 221*). This observation may be due to the present of redundant microtubule associated proteins such as MAP1 and MAP2 in neurons (*157*). Therefore, other mechanisms must be present and contribute to tau toxicity.

5.1.2 The gain of toxic function

The gain of toxic function of tau was first suggested by the close correlation between the number of NFTs and the severity of cognitive decline in AD (*18*). The early onset dementia in FTDP-17 further strengthens the correlation between tau dysfunction and dementia (*32*). However, the dissociation of NFTs with neurotoxicity in transgenic (Tg) *C. elegans*, Tg *Drosophila* and Tg mouse models suggests NFTs are not required for neurotoxicity (reviewed in (*222*)). Instead, hyperphosphorylated tau monomers or intermediates of tau polymerization, including oligomers and protofibrils, might be the species causing neurotoxicity (*223, 224*). The abnormally hyperphosphorylated tau can sequester normal tau from microtubules (*61*) and this can result in the disruption of microtubule networks and the loss of synapses (*205, 225*). Hyperphosphorylated tau has a reduced ability in recruiting

normal tau after it aggregates into filaments (*226*). Therefore, hyperphosphorylated monomeric tau or tau oligomers are the toxic species, and PHFs and NFTs are possibly the end products of cellular attempts to remove the toxic species (reviewed in (*227*)). Although there is no report of FTDP-17 mutations resulting in sequesteration of normal tau, these mutant taus are better substrates for kinases, and may therefore be more toxic than wild type tau due to increased phosphorylation (*64*). In support of this, Tg mice expressing FTDP-17 mutations always have more severe neurotoxic pathologies than wild-type tau, and human tau expressed in these mice is always hyperphosphorylated (reviewed in (*222*)).

Although the MT inhibitory effects can be removed when hyperphosphorylated tau forms PHFs and NFTs, NFTs can still affect the normal function of neurons. NFTs can serve as a physical barrier and compromise normal cell functions. The accumulation of NFTs takes up space in cells and pushes away the cytoplasmic organelles from their normal positions. The mislocated organelles, as well as a decreased number of cytoplasmic organelles were observed in Tg mice expressing P301L tau (*165*). In addition, NFTs can physically block the movement of organelles (such as mitochondria) along microtubules or trigger the release of cargo from kinesin (*228, 229*).

Our results contribute to the hypothesis of "the loss of normal function and the gain of toxic function" in several aspects. First, reduced MT binding affinity was observed in pseudohyperphosphorylation tau mutants. And this is in agreement with the hypothesis of the loss of normal function. Second, pseudohyperphosphorylation

tau mutants have increased lag times for polymerization which keeps these tau mutants in monomer or oligomer forms for longer periods of time. Because evidence suggests monomers and oligomers are the toxic species for cells, this could explain the higher toxicity for hyperphosphorylated tau. The toxicity can be removed by aggregating into filaments and NFTs.

5.2 What triggers the hyperphosphorylation of tau?

The abnormal hyperphosphorylation of tau is the result of an imbalance between protein phosphorylation and de-phosphorylation. Many kinases and phosphatases are believed to be involved in this process (reviewed in (*230*)). However, it is not clear what kind of changes in brain trigger the upregulation of kinases and downregulation of phosphatases. Considering the different phenotypes in different tauopathies, there must be more than one pathway involved. Therefore, the combination of these pathways in different subgroups of tauopathies results in the different disease phenotypes. Several hypotheses have been suggested based on the results from *in vivo* or *in vitro* experiments.

5.2.1 Aβ hypothesis

Aβ peptide is the proteolytic product of Aβ precursor protein (APP) (reviewed in (*231, 232*)). Because mutations in APP can cause the early onset familial AD with all the typical neuropathologies of AD (reviewed in (*231, 232*)), Aβ was believed to be the factor inducing tau phosphorylation and aggregation. Extracellular soluble Aβ was suggested to bind to receptors on the cell membrane and activate intracellular

kinases such as GSK-3β and increase the phosphorylation levels of tau (*233*). The increased amount of fibrillar Aβ can also induce oxidative stress in cells and produce reactive oxygen species (reviewed in (*231*)). Intracellular reactive oxygen species can active kinases (such as JNK and MAPK) and induce the hyperphosphorylation of tau (reviewed in (*231*)).

The effects of Aβ peptides on tau phosphorylation have been demonstrated in transgenic mouse models. NFTs composed of hyperphosphorylated tau were observed in Tg mice expressing an AD-associated APP mutation (*190*) and P301L tau, and in P301L Tg mice after microinjection of Aβ fibrils into the brain (*193*). However, the Aβ hypothesis can not explain the occurrence of tau hyperphosphorylation in other tauopathies which are free of Aβ pathology.

5.2.2 Oxidative stress hypothesis

The involvement of oxidative stress in AD and other neurodegenerative diseases have been suggested in many reports (reviewed in (*234*)). Heavy metals, as the potential sources of free radicals have been found to colocalize with NFTs in AD (reviewed in (*234*)) and Aβ filaments can promote tau phosphorylation through the generation of reactive oxygen species as mentioned above. The following aggregation of hyperphosphorylated tau can remove the free radicals and therefore this is believed to be a protective response to the toxic oxygen species.

5.2.3 Impaired glucose metabolism hypothesis

In addition to phosphorylation, tau also undergoes other posttranslational modifications, such as glycosylation. There is a different glycosylation, O-GlcN-acylation, for neuronal phosphoproteins such as tau (*235*). O-GlcN-acylation is the modification of adding a single sugar at serine or threonine residues, which are potential sites for phosphorylation. Therefore, the reduction of O-GlcN-acylation results in the increase of phosphorylation (reviewed in (*230*)). The regulation of O-GlcN-acylation is directly related to the glucose uptake/metabolism and the impaired glucose metabolism in AD brain can increase tau phosphorylation through decreased O-GlcN-acylation (reviewed in (*230*)).

5.2.4 Other factors

There are other less general factors that are involved in promoting tau phosphorylation in AD and other tauopathies. Several FTDP-17 mutants are more favorable substrates for kinases and therefore can be phosphorylated more easily than wild type tau (reviewed in (*16*)). The presence of one or two APOE4 alleles increases tau phosphorylation through indirect regulation of GSK3 in AD (reviewed in (*232*)). The wnt signaling pathway can upregulate tau phosphorylation by increasing GSK3 activity and/or increasing Aβ aggregation (reviewed in (*232*)).

The progression of AD is a complicated process. There are still many unsolved issues in this puzzle. A schematic showing the proposed major steps in the tau contribution to AD is listed in Figure 5.1.

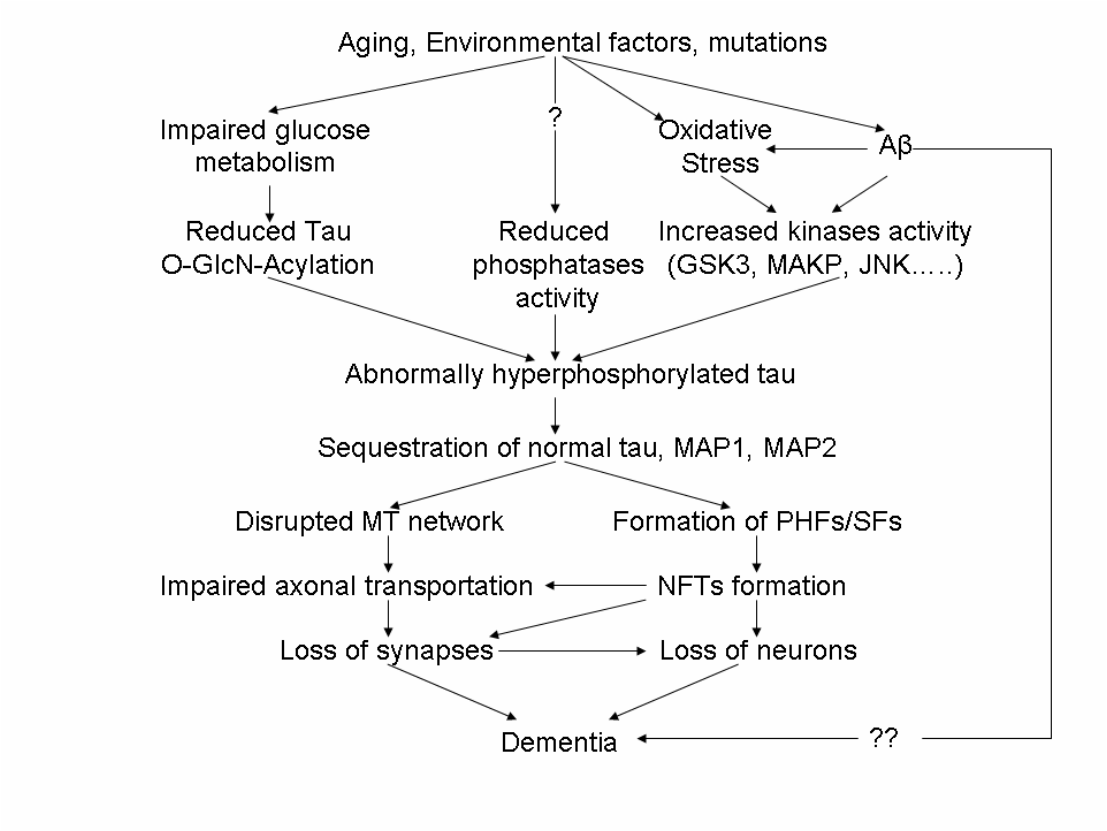

Figure 5.1. A schematic showing the proposed major steps in the progression of Alzheimer's Disease.

5.3 Future directions

To test the hypothesis about hyperphosphorylated tau toxicity, a cell model expressing pseudohyperphosphorylated tau mutant (7-Phos) will be built. The following changes could be assayed in cultured cells: kinase/phosphatase activities, the phosphorylation states of tau at other sites, the intracellular distribution of tau, the amounts of sarkosyl soluble tau and other microtubule associate proteins (MAP1 and MAP2), the amount and morphology of sarkosyl insoluble tau, and microtubule dynamics. These changes will be analyzed together with the changes in cell viability, cell morphology and cell function. The relation between the changes in tau function and cell viability/function could reveal the potential mechanism of hyperphosphorylated tau toxicity.

APPENDIX CHAPTER: IN VITRO TAU POLYMERIZATION IS INFLUENCED BY THE MOLECULAR NATURE OF THE INDUCER AND THE VOLUME OF THE REACTION.

App.1 Rationale and aims

The microtubule associated protein tau is hyperphosphorylated in AD and other tauopathies (reviewed in (*8*)). Hyperphosphorylated tau can spontaneously self-aggregate into paired helical filaments (PHFs) and straight filaments (SFs). PHFs and SFs can further coalesce into neurofibrillary tangles (NFTs), which are correlated with the type and severity of dementia in AD (reviewed in (*69, 236*)). However, recombinant human tau does not spontaneously aggregate under physiological conditions and inducer molecules are required to initiate the aggregation of tau *in vitro* (reviewed in (*75, 237*)). To date, the known inducer molecules are polyanionic compounds such as heparin (*238*), polyglutamate (*79*), RNA (*80*) and fatty acids (*81*). Arachidonic acid (ARA) is one of these inducer molecules. However, the mechanism of ARA induced tau aggregation is not understood. ARA contains a single charge at its carboxyl group and a long hydrophobic tail. It has a high tendency to form polyanionic micelles in aqueous solutions and has been suggested to promote the initiation of tau polymerization in the form of micelles (*84*). In support of this hypothesis, a decreased critical micelle concentration (CMC) of ARA was observed in the presence of tau as assayed by N-phenyl-1-napthylamine (NPN) and individual ARA molecules were not found to be associated with tau filaments (*204*). In addition,

the polymerization of tau can be induced by lipid vesicles and carboxylate-conjugated polystyrene microspheres, which are similar to ARA micelles in the aspect of structure and charge distribution (*204, 239*). All these data suggested that the formation of micelles is a prerequisite for the ARA-induced tau aggregation.

However, the results from other experiments questioned this hypothesis. First, ARA micelle formation was not observed in the presence of an assembly incompetent form of tau when assayed by laser light scattering (*240*). Meanwhile, micelle formation of an alkyl sulfate detergent was easily detected under the same condition by laser light scattering (*240*). Second, the critical micelle concentration of ARA was drastically different when determined by laser light scattering and N-phenyl-1-napthylamine (*204, 241*). The difference may come from the direct binding between tau and N-phenyl-1-napthylamine which has been suggested to bind directly to certain proteins having high affinity for aldehydes or fatty acids (*242*). Or this difference might be due to the size of micelles forming in the presence of tau being too small to be detected by laser light scattering. Third, although tau filaments were observed by the induction of carboxylate-conjugated polystyrene microspheres, the length distribution of these filaments is significantly different from these induced by ARA (*204, 239*). This evidence suggests that ARA can induce tau polymerization through different mechanisms and the molecular nature of ARA can affect the morphology of tau filaments.

The aim of this study is to determine the relationship between the molecular nature of ARA with filament morphology induced by ARA and to determine the

mechanism of ARA induced tau polymerization. To address this, divalent cations at different final concentrations were added to the reaction buffer to alter ARA micelle formation and the filaments formed under different conditions were assayed and compared with the filaments induced by carboxylate-conjugated polystyrene microspheres. The surface area : volume ratio was also found to influence tau polymerization induced by ARA. Therefore, the polymerization reactions induced by ARA in different reaction volumes were also assayed by laser light scattering and transmission electron microscopy.

App.2 Materials and methods

App.2.1 ARA induced tau polymerization

Two micromolar tau protein (wild type or cys-less mutant tau (htau40$^{C291/322A}$)) was incubated in polymerization reaction buffer (10 mM HEPES pH 7.6, 100 mM NaCl, 0.1 mM EDTA and 5 mM DTT) in the presence of 75 μM ARA (in ethanol, final concentration was 3.75%) for 20 hrs (*101*). $MgCl_2$ and $CaCl_2$ at a low (0.3 mM) or high (3 mM) concentration with or without 2 mM ATP were added to the reactions when indicated in the results section. The total volume of the polymerization reaction was 200 μl unless separately indicated.

App.2.2 Carboxylate-conjugated polystyrene microspheres induced tau polymerization

Tau protein at final concentration of 2 μM was incubated in polymerization buffer (10 mM HEPES pH 7.6, 100 mM NaCl, 0.1 mM EDTA and 5 mM DTT) in the presence of carboxylate-conjugated polystyrene microspheres (final concentrations were 0-6056 pM) at 37 ºC with constant rotation for 20 hr (*204*).

App.2.3 Right angle laser light scattering

Tau polymerization reactions after 20 hr incubation were transferred into 5 x 5 mm optical glass fluorometer cuvettes (Starna Cells, Atascadero, CA) and illuminated with a 5 mW solid state laser (λ = 475 nm, B & W Tek, Inc., Newark, DE). Images were captured at 90º to the incident light using a SONY XC-ST270 digital camera. Resulting images were imported into Adobe Photoshop 7.0.1 and the intensity of the scattered light was measured by the histogram function of Adobe Photoshop (*101*). The images were captured at four different apertures (f5.6, f8, f11 and f16) and normalized to the intensity corresponding to f5.6 or f8.

App.2.4 Transmission electron microscopy

Tau polymerization reactions after 20 hr incubation were diluted 10-fold with polymerization buffer and then fixed with glutaraldehyde (final concentration was 2%) for 5 min. Ten microliters of fixed reactions were placed on formvar-carbon coated grids for 1 min, washed with water, blotted, washed with 2% uranyl acetate, blotted again, stain with 2% uranyl acetate for 1 min, and then blotted dry. Grids were viewed with a JEOL 1200 EXII electron microscope and digital images were captured

with the MegaViewII imaging system (Soft Imaging System, GmbH Münster, Germany). The captured images were imported into Optimas analytical imaging software (Media Cybernetics, Sliver Spring, MD). The number of filaments and the average filament length were determined from the digital electron micrographs. The filament lengths measured by Optimas were exported to Prism GraphPad (San Diego) and sorted into 50 nm bins, with the center of the first bin at 25 nm. At least four images were analyzed for each reaction condition. The average length of filaments was multiplied by the total number of filaments to obtain the total filament mass for each field.

App.2.5 Critical micelle concentration (CMC) determined by laser light scattering

ARA ranging from 25 μM to 150 μM final concentrations was diluted into polymerization buffer in the presence or absence of 2 μM htau40$^{I277/308P}$ mutant tau and scattered light was measured as described above. $MgCl_2$ and $CaCl_2$ at a low (0.3 mM) or high (3 mM) concentration with or without 2 mM ATP were added to the reaction as indicated in the results section. CMC was determined from abscissa intercepts with least squares linear regression (*204*). Only data points in the linear portion of the curve were used for the calculation.

App.2.6 Critical micelle concentration (CMC) determined by NPN fluorescence

ARA ranging from 25 μM to 150 μM final concentrations was diluted into polymerization buffer containing NPN (final concentration was 10 μM) in the

presence or absence of 2 μM wild type tau or htau40$^{I277/308P}$ mutant tau. The samples were incubated for 20 min at room temperature before taking the fluorescence readings. The resulting fluorescence was measured at λ_{ex} of 346 nm and λ_{em} of 420 nm in a 96-well plate format in a Cary Eclipse fluorescence spectrophotometer (Varian Analytical Instruments, Walnut Creek, CA) (*204, 243*). $MgCl_2$ and $CaCl_2$ at a low (0.3 mM) or high (3 mM) concentration with or without 2 mM ATP were added to the reaction when indicated in the results section. CMC was estimated from abscissa intercepts with least squares linear regression (*243*). Only data points in the linear portion of the curve were used for the calculation.

App.3 Results

App.3.1 CMC determined by LLS and NPN

Because the molecular nature of arachidonic acid (ARA) depends on the solvent, the critical micelle concentration (CMC) of ARA in polymerization buffer (10 mM HEPES pH 7.6, 100 mM NaCl, 0.1 mM EDTA and 5 mM DTT) in the absence of tau was determined first with laser light scattering (LLS) and N-phenyl-1-naphthylamine (NPN) fluorescence. The CMC of ARA in polymerization buffer was assayed individually by these two methods (Figure app.1). The CMC value equals the x-axis intercept of the data fit by least squares linear regression. The CMCs determined by LLS and NPN were 54 ± 3 μM and 55 ± 15 μM, respectively. To alter the micelle formation, the divalent cations were added to the solution and the reduced CMC values were observed by both LLS and NPN fluorescence with the only

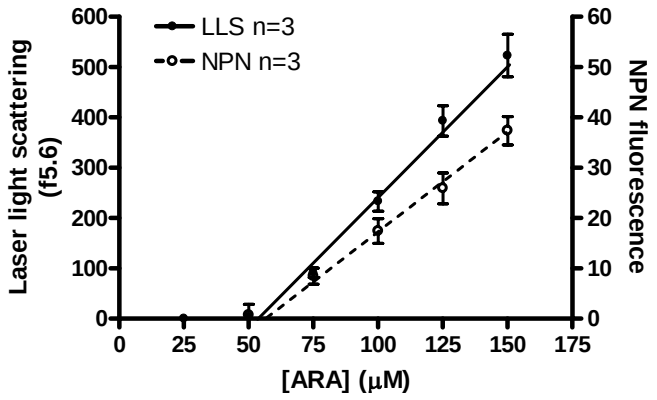

Figure app.1. Critical micelle concentration (CMC) determination. ARA at concentrations varying from 25 μM to 150 μM was diluted in polymerization buffer and then assayed by laser light scattering (LLS, ●, left axis) and NPN fluorescence (NPN, ○, right axis). The data were fit by linear regression using Prism GraphPad Software (San Diego, CA). The solid line represents the best fit to linear regression for LLS and the dotted line represents the best fit for NPN fluorescence. CMC was estimated from abscissa intercepts of the line. All data were presented as the average of at least three experiments ± s.d..

exception observed at 0.3 mM $MgCl_2$ (Table app.1). Because filaments with different morphology were observed in the concurrent phosphorylation and polymerization reactions (*105*), the CMC value under this condition (in the presence of 3 mM $MgCl_2$ and 2 mM ATP) was also determined by LLS and NPN fluorescence. The CMC values were close to the values in the presence of 3 mM $MgCl_2$ when assayed by both LLS and NPN.

Because the CMC of ARA has been shown to be depressed by tau in solution (*204*), we measured the CMC of ARA in polymerization buffer in the presence of tau by NPN fluorescence (Figure app. 2A). The CMC of ARA was reduced to 9.0 ± 3.3 μM by the addition of wild type tau (Table app.1), which is close to a previously published report (*204*). The assembly incompetent tau mutant (htau40$^{I277/308P}$) was also included as a control and a similar CMC value was observed in the presence of htau40$^{I277/308P}$ (Figure app.2A). The CMC values of ARA in the presence of different concentrations of divalent cations and 2 μM tau were also measured by NPN fluorescence (Table app.1). In general, the CMC values were further depressed by the addition of wild type tau and htau40$^{I277/308P}$ mutant tau in addition to the depression caused by divalent cations. Wild type tau usually had a larger effect than htau40$^{I277/308P}$ mutant tau (Table app. 1). The significant reduction resulting from the addition of wild type tau and/or htau40$^{I277/308P}$ mutant tau was observed under all conditions with the lone exception observed in the presence of 3 mM $MgCl_2$. Under this condition, wild type tau further reduced the CMC value of ARA compared with

the CMC value in the absence of wild type tau. However, htau40$^{I277/308P}$ mutant tau did not have the similar depression effect as wild type tau (Table app.1).

The CMCs of ARA in the presence of wild type tau and htau40$^{I277/308P}$ mutant tau with or without divalent cations were also determined by LLS. Surprisingly, the CMC values were drastically different from those determined by NPN fluorescence (Table app.1). Because the scattering of tau filaments formed from wild type tau interfered with the scattering from ARA micelles, only the CMC values in the presence of htau40$^{I277/308P}$ mutant tau could be determined by LLS. Instead of decreasing, the addition of htau40$^{I277/308P}$ mutant tau increased the CMC values about 2-fold (Table app.1). The increase of CMC resulting from the addition of htau40$^{I277/308P}$ mutant tau was also observed in the presence of 0.3 mM $MgCl_2$ and 0.3 mM $CaCl_2$ (Table app.1). In the presence of 3 mM $MgCl_2$, the CMC value is about the same with or without htau40$^{I277/308P}$ mutant tau. However, the depression effect of htau40$^{I277/308P}$ mutant tau on the CMC value was observed in the presence of 3 mM $MgCl_2$ + 2 mM ATP and 3 mM $CaCl_2$ (Table app.1). The results suggest that ATP could also induce the micelle formation in solution in the presence of htau40$^{I277/308P}$ mutant tau and $CaCl_2$ had a larger effect than $MgCl_2$ in the aspect of inducing micelle formation. In addition, by comparing the CMC values in the presence and the absence of htau40$^{I277/308P}$ mutant tau measured by laser light scattering, it appears that tau can increase the CMC of ARA even in the presence of low concentrations of divalent cations, but it cannot overcome the enhanced micelle formation at high concentrations of divalent cations.

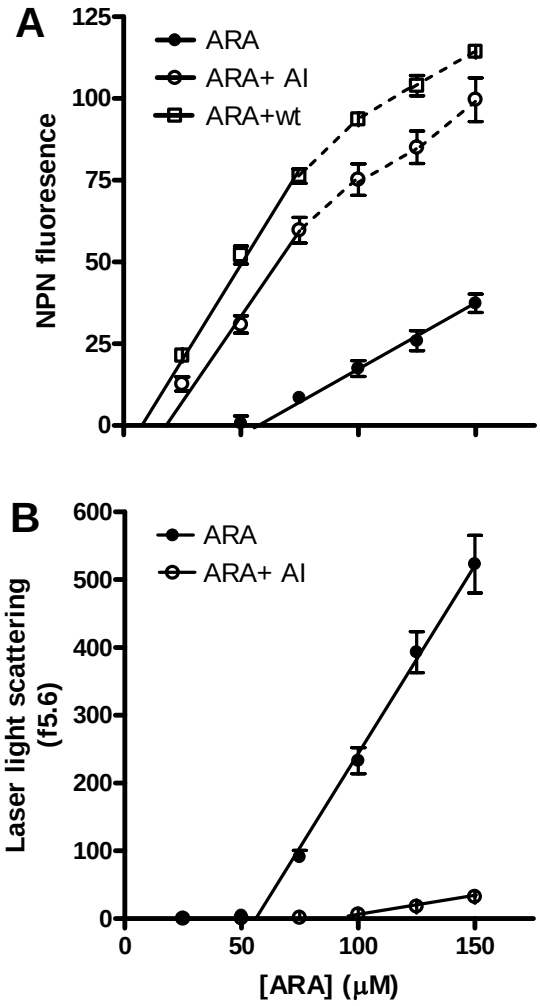
A
125
100
75
50
25
0
NPN fluoresence
ARA
ARA+ AI
ARA+wt
B
600
500
400
300
200
100
0
Laser light scattering (f5.6)
ARA
ARA+ AI
0
50
100
150
[ARA] (μM)

Figure app.2. Tau protein reduces the critical micelle concentration of ARA. A) ARA at concentrations varying from 25 μM to 150 μM was diluted in the absence (ARA,●) or the presence of 2 μM wild type tau protein (ARA+Wt, □) or assembly incompetent mutant tau (ARA+AI, ○) in polymerization buffer at room temperature and then assayed by NPN fluorescence. B) ARA at concentrations varying from 25 μM to 150 μM was diluted in the absence (ARA,●) or the presence of 2 μM assembly incompetent mutant tau (ARA+AI, ○) in polymerization buffer at room temperature and then assayed by LLS. Since the scattering from tau filaments interferes with the scattering from the micelles, the LLS readings in the presence of wild type tau were not shown in panel B. The data were fit using linear regression and only data points in the linear portion of the curves were included for the calculation. The solid lines represent the best fit of the selected data points to a linear regression. The dotted lines link the data points that are out of the linear range and were not included in the linear regression analysis. CMCs were estimated from abscissa intercepts of the lines. All data were presented as the average of at least three experiments ± s.d. ($n \geq 3$).

Table app.1. Arachidonic acid CMC values determined under different buffer conditions at room temperature

conditions	CMC (μM)				
	LLS		NPN		
	no tau	AI tau	no tau	AI tau	wt tau
ARA	54.3 ± 3.1	98.3 ± 0.2	55.3 ± 15.1	12.7 ± 6.8	9.0 ± 3.3
ARA + 0.3mM $MgCl_2$	53.9 ± 8.1	93.3 ± 12.9	46.8 ± 11.6	13.5 ± 1.3	8.68 ± 2.3
ARA + 3mM $MgCl_2$	28.7 ± 3.5	28.4 ± 4.0	13.0 ± 14.4	14.6 ± 3.9	10.7 ± 2.0
ARA + 3mM $MgCl_2$ + 2mM ATP	28.9 ± 1.1	11.0 ± 2.8	13.0 ± 3.5	4.5 ± 4.9	2.95 ± 1.9
ARA+ 0.3mM $CaCl_2$	30.5 ± 0.4	50.2 ± 3.5	17.8 ± 7.2	14.5 ± 1.5	6.92 ± 0.9
ARA + 3mM $CaCl_2$	12.8 ± 0.6	8.2 ± 1.6	13.4 ± 7.0	12.4 ± 2.4	1.09 ± 1.4

Data are presented as average ± s.d. ($n \geq 3$).

LLS, laser light scattering;

NPN, N-phenyl-1-naphthylamine;

Wt, wild type tau;

AI, htau40$^{I277/308P}$ mutant tau

The difference in results between NPN fluorescence and LLS may due to the direct interaction of NPN with tau in the presence of ARA. NPN is known to bind to certain classes of proteins that have high affinities for aldehydes and fatty acids (*242*), therefore the direct binding between tau and NPN in the presence of ARA is possible. The other possible explanation for this difference is that the size of some micelles may be too small to be detected by LLS. Therefore, the micelle formation could be underestimated by LLS. If this is the case, more but smaller micelles could form in the presence of tau protein. The addition of divalent cations at high concentrations can overcome this effect and induce the formation of more and larger ARA micelles.

App.3.2 Tau filaments have difference morphologies with different ARA status

To determine whether there are morphological differences in tau filaments under conditions of different micelle formation as determined by LLS, polymerization of 2 μM wild type tau was induced by 75 μM ARA in different conditions. These reactions were viewed by TEM and the representative images from each condition are shown in Figure 3. In the presence of ARA alone and ARA + 0.3 mM $MgCl_2$, ARA presented as free ARA or small micelles (smaller than the low limitation detectable for LLS) and filament formation was observed (Figure app.3A and app.3C). As shown in Figure 3B and 3D, many small filaments with length shorter than 0.25 μm were observed under these conditions. The average filament length was approximately equal under the conditions with or without 0.3 mM $MgCl_2$ (Figure app.4A). The number of filaments and therefore the overall

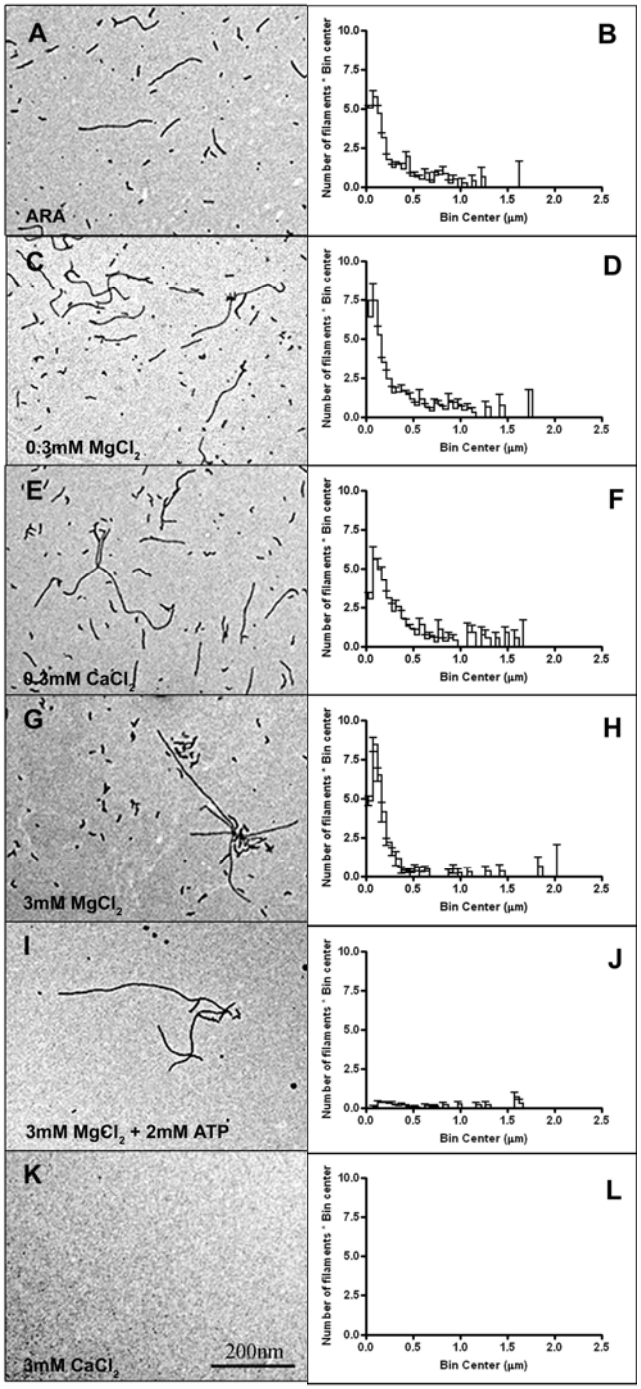
A
ARA
B
Number of filaments * Bin center
Bin Center (μm)
C
0.3mM MgCl2
D
E
0.3mM CaCl2
F
G
3mM MgCl2
H
I
3mM MgCl2 + 2mM ATP
J
K
3mM CaCl2
200nm
L

Figure app.3. The length distribution of tau filaments changes with different ARA micelle formation. Polymerization reactions with 2 μM wild type tau and 75 μM ARA in the presence of different concentrations of $MgCl_2$, $CaCl_2$ and ATP were incubated at room temperature for 20 hr. The resulting polymerizations were viewed by TEM and the representative electron micrographs taken at 20,000 x are shown. A) ARA only; C) 0.3 mM $MgCl_2$; E) 0.3 mM $CaCl_2$; G) 3 mM $MgCl_2$; I) 3 mM $MgCl_2$ + 2 mM ATP; K) 3 mM $CaCl_2$. The average mass distribution are shown for each of these condition and are plotted as the sum of lengths of the filaments in that bin (y-axis) versus the center of the bin size (x-axis) (B,D,F,H,J,L).

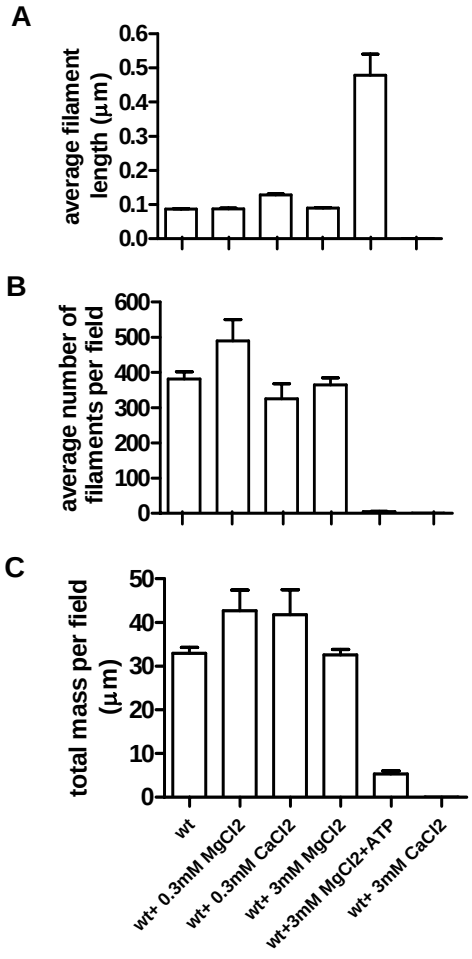

Figure app.4. The morphology of tau filaments changes according to different ARA micelle formation. Tau polymerization reactions with 2µM wild type tau and 75µM ARA in the presence or absence of divalent cations ($MgCl_2$ or $CaCl_2$) and ATP were incubated at room temperature for 20 hr and viewed with electron microscopy. A) The average filament length, B) the average number of filaments per field and C) the "total mass" or the sum total length of filaments per field was determined from at least 4 fields. All data are presented as average ± s.d..

filament mass was higher in the presence of 0.3 mM $MgCl_2$ (Figure app.4B and app.4C), but none of these increases were significant.

In the presence of 0.3 mM $CaCl_2$, the CMC values determined by LLS and NPN fluorescence were both lower than 75 μM. The CMC value suggested that under the polymerization condition with 75μM ARA + 2 μM tau + 0.3 mM $CaCl_2$, the ARA micelles detectable by LLS were formed. There was a significant increase in the number of the filaments longer than 1.0 μm (Figure app.3E and app.3F) ($p < 0.05$), and the average length of filament per field was significantly greater than those formed in the absence of LLS detectable ARA micelles (Figure app.4A). The number and total mass of filaments per field were slightly decreased compared with these formed in the absence of LLS detectable ARA micelles and none of those changes was significant (Figure app.4B and app.4C).

With the addition of 3 mM $MgCl_2$ and 2 μM wild type tau, more LLS detectable micelles were expected to form as suggested by CMC value determined by LLS. Under this condition, filaments were observed, and some of the filaments seemed to originate from a common point (Figure app.3G). The length distribution of the filaments was also changed with the addition of 3 mM $MgCl_2$, and the majority of filaments were shorter than 50 nm in length (Figure app.3H). At the same time, some very long filaments (longer than 2.0 μM) were only observed under this condition (Figure app.3H). However, the overall filament length, number of filaments and filament mass were similar to those formed in the absence of LLS detectable ARA micelles (Figure app.4). According to the CMC determined by LLS and NPN

fluorescence, the micelle formation of ARA was further increased by the combination of 3 mM $MgCl_2$ and 2 mM ATP (Table app.1). Under this condition, very few filaments were formed, and some of these filaments seemed to originate from a common site, similarly to those observed in the presence of 3 mM $MgCl_2$ (Figure app.3I and app.3J). Although the average filament length was significantly greater than that of the filaments induced by ARA alone, the decreased number of filaments resulted in an overall decrease of the total filament mass (Figure app.4).

The greatest amount of micelle formation should be observed in the presence of 3 mM $CaCl_2$ according to the CMC values (Table app.1). Under this condition, no filament formation was observed (Figure app.3K, app.3L and Figure app.4).

App.3.3 Free ARA or small ARA micelles are more efficacious in inducing tau polymerization.

Carboxylate-conjugated polystyrene microspheres are microspheres coated with COOH- groups and can mimic the negatively charged surface of ARA micelles (*239*). The anionic surface of the carboxylate-conjugated polystyrene microspheres promotes the assembly-competent conformation of tau through simple adsorption and this potency directly depends on the anionic charge density of the surface of microspheres (*239*). Most of the filaments were microsphere associated and appeared to grow out of the surface of the microsphere when viewed at 100,000-fold magnification using TEM (*239*). To compare the polymerization reaction induced by ARA with the polymerization induced by micelle-like negatively charged

microspheres, carboxylate-conjugated polystyrene microspheres at concentrations varying from 505 pM to 6056 pM were used to induce tau polymerization. Low amounts of filaments were observed at the lowest microspheres concentration (505 pM) in the form of single short filaments emanating from single beads (Figure app.5A, app.5J and Figure app.6). With the increase of microsphere concentration, the number of filaments and total filament mass increased to a maximum, and then decreased in a biphasic fashion (Figure app.5). At low microsphere concentrations (505 pM and 1009 pM), at most two filaments were observed to emanate from the surface of each microsphere (Figure app.5 and Figure app.6). When the microsphere concentration reached 2053 pM, some of microspheres served as the nucleation center for polymerization and several filaments were observed to emanate from the surface of a single microsphere (Figure app.5 and app.6C). This phenomenon is similar to that which we observed in the polymerization reaction with increasing ARA micelle concentrations (Figure app.3E, app.3G and app.3I). Also similar to ARA induction of tau polymerization was the complete diminution of tau polymerization at the highest concentration of carboxylate-conjugated polystyrene microspheres concentration (Figure app.5G – J and Figure app.6). To compare the efficacy of ARA and microspheres in inducing tau polymerization, the maximum amount of filaments in each condition were compared. The maximum amount of polymerization for ARA and microspheres induction was reached under the condition of 0.3 mM $CaCl_2$ + 75μM ARA + 2 μM tau and 1514 pM microspheres, respectively (Figure app.4 and

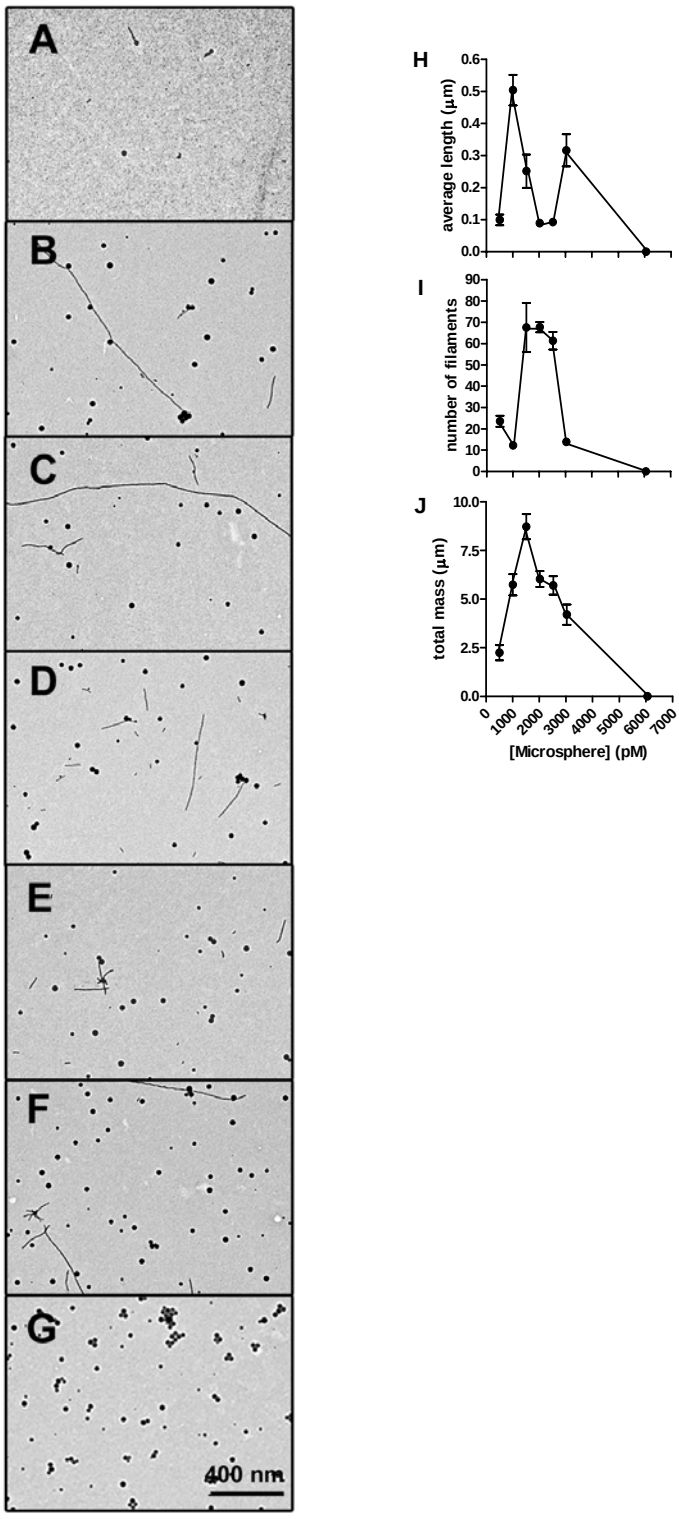
A
B
C
D
E
F
G
400 nm
H
average length (µm)
0.6
0.5
0.4
0.3
0.2
0.1
0.0
I
number of filaments
90
80
70
60
50
40
30
20
10
0
J
total mass (µm)
10.0
7.5
5.0
2.5
0.0
0
1000
2000
3000
4000
5000
6000
7000
[Microsphere] (pM)

Figure app.5. Carboxylate-conjugated polystyrene microspheres induce tau polymerization. Two micromolar tau protein was incubated with carboxylate-conjugated polystyrene microspheres at concentrations varying from 505 pM to 6056 pM at 37ºC for 20 hr with constant rotation and viewed with TEM at 20,000x. The representative images at each concentration were shown: A) 505 pM; B) 1009 pM; C) 1514 pM; D) 2019 pM; E) 2503 pM; F) 3028 pM; G) 6056 pM. The average filament length (H), the number of filaments (I) and "total mass" or the sum total length of filaments (J) from 9 micrographs under each condition were plotted against microsphere concentrations. All data are presented as average ± s.d..

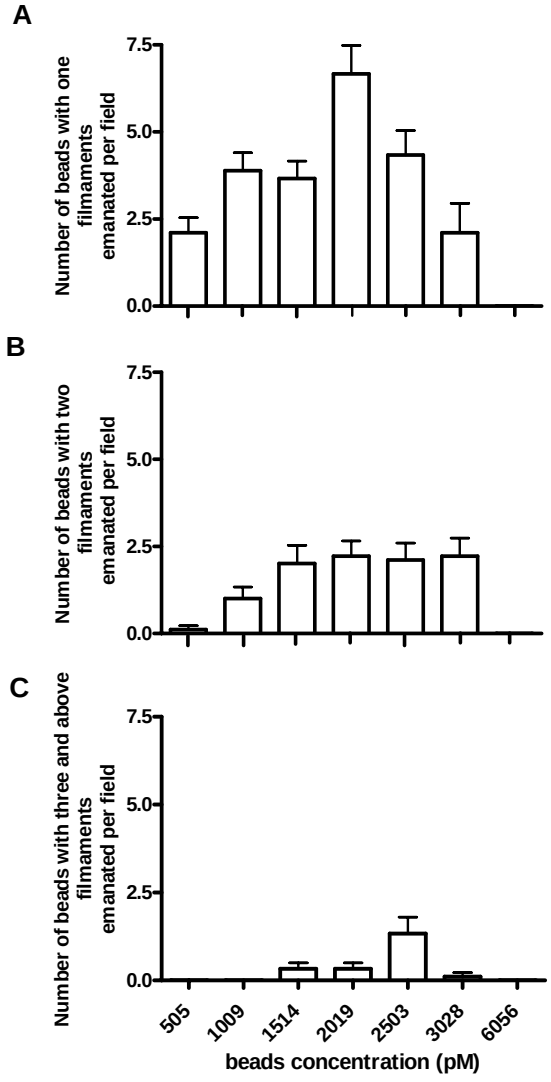
A
Number of beads with one filmaments emanated per field
7.5
5.0
2.5
0.0
B
Number of beads with two filmaments emanated per field
7.5
5.0
2.5
0.0
C
Number of beads with three and above filmaments emanated per field
7.5
5.0
2.5
0.0
505
1009
1514
2019
2503
3028
6056
beads concentration (pM)

Figure app.6. Concentration of carboxylate-conjugated polystyrene microspheres changes the number of filaments emanating from a single bead. Carboxylate-conjugated polystyrene microspheres at concentrations varying from 505 – 6056 pM were incubated with 2 μM wild type tau at 37 ºC for 20 hr with constant rotation and reactions were viewed with electron microscopy. The average number of beads with A) one, B) two, and C) three and above filaments emanating from its surface was calculated from 9 micrographs at each concentration and plotted against the concentration of carboxylate-conjugated polystyrene microspheres. All data are presented as average ± s.d..

Figure app.5). The maximum amount of polymerization induced by ARA was about 5-fold higher than the maximum amount induced by carboxylate-conjugated polystyrene microspheres (Figure app.4C and app.5J). According to the CMC values determined by LLS and NPN fluorescence, both large micelles and free ARA (and/or small micelles) were present in the presence of 0.3 mM $CaCl_2$. The higher value of filament mass, compared to anionic microspheres induced polymerization reaction, may due to the induction of free ARA or small micelles. The result also suggested that small micelles and/or free ARA had higher potency in inducing tau polymerization compared with large micelles. This is in agreement with the previously reported dependence of the amount of polymerization on the concentration of negative charges on the microspheres surface (*239*).

App.3.4 The surface area : volume ratio of the reaction influences tau polymerization and changes the length distribution of tau filaments.

In vitro results on the effect of pseudophosphorylation on tau polymerization from different groups are somehow in conflict (*100, 244*). Many factors have been shown to change the amount of tau polymerization *in vitro* (*194*), such as the inducer to ARA ratio and the status of ARA. The ratio between surface area and reaction volume was also found to influence the amount of tau polymerization *in vitro*. To make the calculation easy, the polymerization reactions were performed in glass cuvettes with constant surface area. By changing the volume of the reactions, the surface area : volume ratio was changed accordingly. The different amounts of

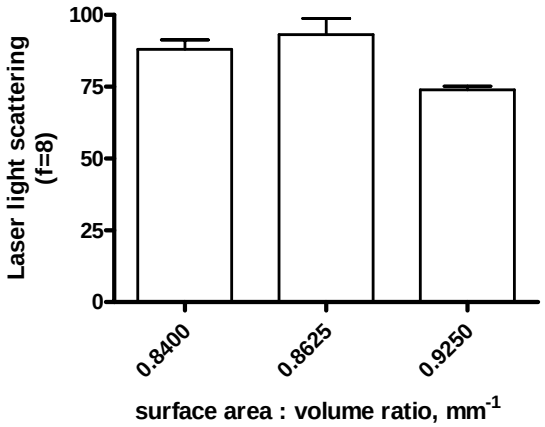

Figure app.7. The surface area : volume ratio changes the amount of tau polymerization. The polymerization reactions with 2 μM tau protein and 75 μM ARA inducer in a total volume of 200 μl, 400 μl or 600 μl were incubated in optical glass fluorometer cuvettes at room temperature for 20 hr. The surface area : volume ratios are 0.925/mm, 0.8325/mm and 0.84/mm for 200 μl, 400 μl and 600 μl reactions, respectively. The amount of polymerization was assayed by laser light scattering at f8. All data are presented as average ± s.d. (n=3).

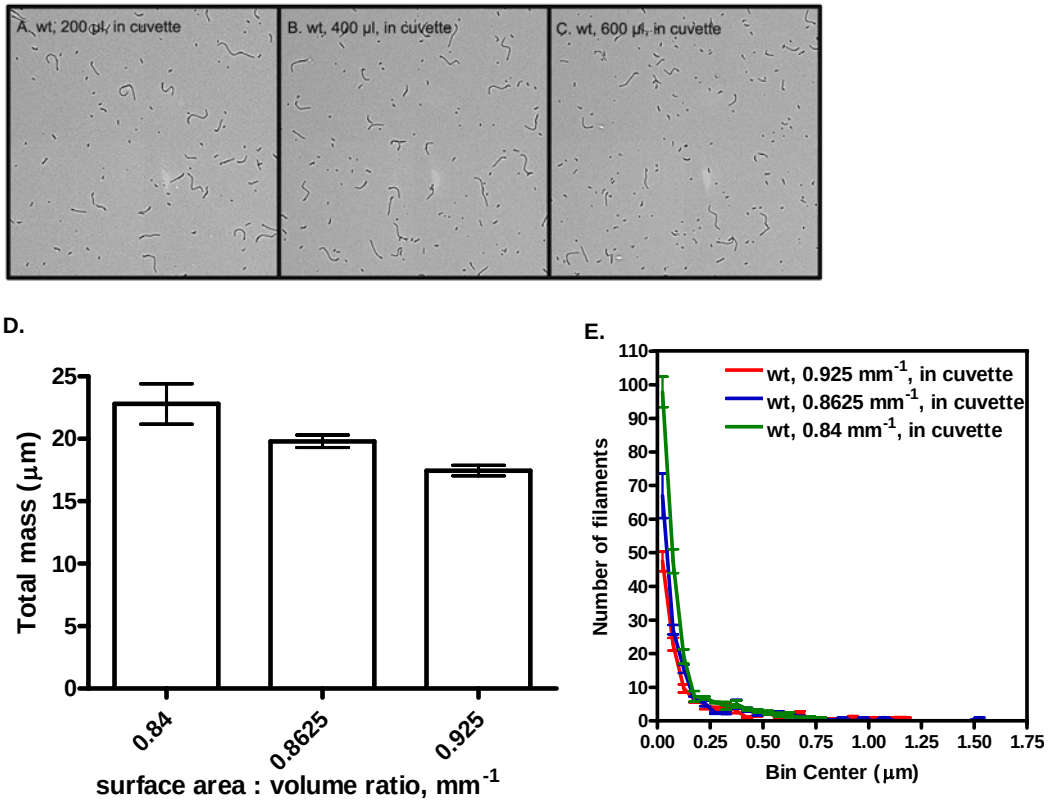

Figure app8. **The morphology and the length distribution of tau filaments are affected by the surface area : volume ratios.** The polymerization reactions with 2 µM tau protein and 75 µM ARA inducer in a total volume of 200 µl, 400 µl or 600 µl were incubated in optical glass fluorometer cuvettes at room temperature for 20 hr. The surface area : volume ratios are 0.925/mm, 0.8325/mm and 0.84/mm for 200 µl, 400 µl and 600 µl reactions, respectively. The resulting reactions were viewed by TEM. Six TEM images for each reaction were captured and the representative micrographs were shown in panel A-C (200 µl, 400 µl and 600 µl, respectively). The total filament mass were determined by using the Optimas measuring program and shown in panel D. The distribution of the filaments was shown in panel E and individually colored. All data are presented as average ± s.d. (n=6).

polymerization were observed at the different surface area : volume ratios (Figure app.7). The surface area : volume ratios are 0.925/mm, 0.8325/mm and 0.84/mm for 200 µl, 400 µl and 600 µl reactions, respectively. The LLS readings had a biphasic dependence on the surface area : volume ratio, with the maximum reading being reached at the surface area : volume ratio of 0.8625 mm^{-1}. The amount of polymerization was also assayed by TEM (Figure app.8). However, the biphasic dependence on the surface area : volume ratio was not observed. Instead, total filament mass increased with the decrease in surface area : volume ratio (Figure app.8D). There were more short filaments formed in the reactions with the decrease in surface area : volume ratio, and these short filaments were not detectable by LLS but by TEM (Figure app.8E). The presence of these short filaments likely caused the difference between LLS and TEM. In agreement with the presence of more but shorter filaments in the reaction with larger final volume, the half time of the polymerization reactions were decreased in the reactions with larger final volume (Figure app.9C). By changing the surface area : volume ratio, the oxidative condition of the reaction could be changed. Therefore, we tested the kinetics of the polymerization reaction with 2 µM cysless mutant tau at various surface area : volume ratio. The two cysteine residues (Cys291 and Cys322) were replaced with alanine in the cys-less mutant tau ($htau40^{C291/322A}$) and the polymerization of cysless mutant tau would not be affected by the oxidative condition through cysteine oxidation. However, similar biphasic dependence of the maximum laser light

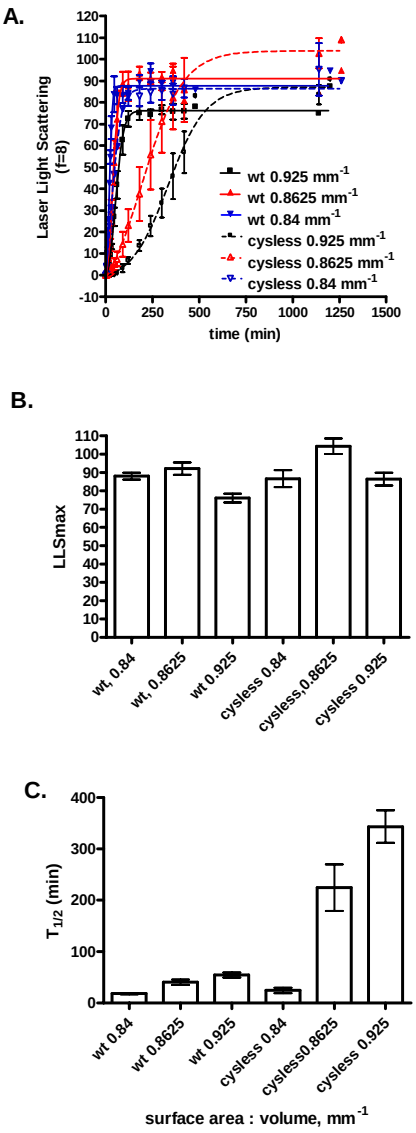
A.
Laser Light Scattering (f=8)
time (min)
wt 0.925 mm-1
wt 0.8625 mm-1
wt 0.84 mm-1
cysless 0.925 mm-1
cysless 0.8625 mm-1
cysless 0.84 mm-1
B.
LLSmax
wt, 0.84
wt, 0.8625
wt 0.925
cysless 0.84
cysless,0.8625
cysless 0.925
C.
T1/2 (min)
wt 0.84
wt 0.8625
wt 0.925
cysless 0.84
cysless0.8625
cysless 0.925
surface area : volume, mm-1

Figure app.9. **The kinetics of tau filaments are affected by the surface area : volume ratios.** The polymerization reactions of 2 μM tau (wild type or cysless mutant) and 75 μM ARA inducer in a total volume of 200 μl, 400 μl and 600 μl were incubated in optical glass fluorometer cuvettes at room temperature for 20 hr. The surface area : volume ratios are 0.925/mm, 0.8325/mm and 0.84/mm for 200 μl, 400 μl and 600 μl reactions, respectively. The kinetics of the reactions were monitored by LLS at regular intervals. The amount of polymerization was plotted versus time and shown in panel A. The data were fit to a non-linear Boltzmann sigmoidal equation and the maximal laser light scattering (LLSmax) and half time of the reaction ($T_{1/2}$) were determined from the equation and plotted in Panel B and Panel C. All data are presented as average value ± s.d. (n=3).

scattering on the surface area : volume ratio and the decreased half time were observed in the cys-less mutant tau (Figure app.9). This result suggested that the changes on the amount of polymerization with the changes of surface area : volume ratio was not through changing the oxidation of cysteines in the reaction.

App.4 Discussion

App.4.1 Comparison between laser light scattering (LLS) and N-phenyl-1-naphthylamine (NPN) fluorescence in determining the critical micelle concentration (CMC) in the presence of tau protein

The formation of micelles from free fatty acid in solution depends on both the structure of the fatty acid and the medium composition (pH, temperature, ionic strength) (*245*). NPN fluorescence and LLS are two methods currently used to determine the critical micelle concentrations (CMCs) of arachidonic acid (ARA). The CMC determined by LLS is based on the size difference between large particles (micelles) that can scatter light and small particles and/or free ARA that can not scatter light. The CMC determined by NPN comes from the increase in the fluorescence intensity and a blue shift on the maximum fluorescence emission after NPN molecules partition into the core of micelles (*243*). In our buffer system, the CMC values determined by NPN fluorescence and LLS are similar in the absence of tau protein. However, in the presence of tau, the CMC value determined by NPN fluorescence is significantly lower than that determined by LLS (Table 1). There are two possible explanations for the difference between these two methods. The first

possibility comes from the direct binding between tau and NPN in the presence of ARA. NPN has been shown to bind certain classes of proteins that have high affinities for aldehydes and fatty acids (*242*). In addition, NPN is structurally similar to 8-anilino-1-napthalene sulfonic acid, which is a planar aromatic dye and binds to an intermediate in the tau polymerization pathway (*246*). The second possibility is that micelles formed in the presence of tau are too small to be detected by LLS. Because of this technical limitation, it is impossible to differentiate small micelles from free ARA. However, the results from this study suggested that free ARA and/or small micelles may induce tau polymerization through a different mechanism than large micelles. This is supported by the observation that the morphologies of tau filaments are significantly different in the presence of 0.3 mM $CaCl_2$ and 3 mM $MgCl_2$, although the CMC values are similar as determined by NPN fluorescence (Table app.1 and Figure app.4).

App.4.2 ARA can induce tau polymerization through two different mechanisms.

Tau protein has been shown to adopt local beta strand conformation with several hydrophobic residues on one face and a relatively polar face on the opposite side (reviewed in (*65, 247*)). The presence of a positively charged proline rich region would prevent the self aggregation of wild type tau (*248*). Therefore, polyanionic compounds are required for *in vitro* tau aggregation. ARA has been hypothesized to induce tau polymerization by two mechanisms. As a monomer, the negative charges on ARA can neutralize the positively charged proline rich region and offset the

electrostatic repulsion between proline rich regions. The hydrophobic tail of ARA monomer can also interact with the hydrophobic side chains and further facilitate the polymerization. The double effects of ARA monomer on tau polymerization could make it a more efficient inducer than ARA micelle. As large micelles, ARA may induce tau polymerization by binding to tau and inducing beta strand conformation on the negatively charged micelle surface. Tau concentrated on the micelle surface produces a localized high concentration of tau protein and therefore overcomes the energy barriers for the nucleation (*249*). It is not clear whether small micelles exist. If they exist, small micelles might work through a similar mechanism as ARA monomer but with a different efficiency. Because the size of small micelles might not be large enough to produce a localized high concentration, they could neutralize the positive charges in the proline rich region after binding. Therefore, the filaments with different morphology than those induced with large micelles should be observed.

The data from our study provided evidence for both of these two mechanisms. The CMC of ARA was about 100 μM in the presence of tau as determined by LLS. This suggests at the ARA concentration we used (75 μM), ARA in present as monomers or small micelles. ARA may be present in similar states in the presence of 0.3 mM $MgCl_2$ because both the CMC value and the polymerization of tau were largely unaffected by the addition of low concentrations of $MgCl_2$. In the presence of a low concentration of $CaCl_2$, the CMC value was lower than 75 μM, which suggested ARA was in the state of the combination of large micelles and free ARA (or small micelles). The polymerization under this condition was slightly changed.

In the presence of a high concentration of $MgCl_2$, a high concentration of $MgCl_2$ plus ATP and a high concentration of $CaCl_2$, a drastically increased micelle formation was detected by both NPN fluorescence and LLS. The morphology of filaments also changed accordingly. There were less but longer filaments formed and some of the filaments appeared to nucleate from a single center. These results also suggested that large ARA micelles induced tau polymerization with lower efficiency. The polymerization induced by carboxylate-conjugated polystyrene microspheres was similar to that induced by large ARA micelles and gave the direct evidence for the micelle induction hypothesis. When the concentration of micelles or carboxylated-conjugated polystyrene microspheres is too high, localized high concentration of tau can no longer be produced, therefore tau polymerization could not be observed under these conditions.

App.4.3 The surface area : volume ratio affects tau polymerization.

In vitro tau polymerization can be affected by many factors, such as the ARA to tau ratio (*194*) and the molecular nature of ARA as shown in this study. The surface area : volume ratio was also found to change the polymerization of tau and the morphology of tau filaments. More but shorter filaments were observed with the decrease of surface area : volume ratio (Figure app.8). Also an increased half time was associated with the changes in the tau morphology (Figure app.9). This change was not through changing the oxidation of cysteines in the reaction. The CMC of ARA was not changed with the changes of the surface area : volume ratio as assayed

by LLS (data not shown). However, due to a technical limitation, small micelles can not be differentiated from ARA monomers. It is possible that the ratio between micelles (large or small) and ARA monomer was changed although no detectable change was observed on the CMC values as determined by LLS.

References:

(1) Weingarten, M. D., Lockwood, A. H., Hwo, S. Y., and Kirschner, M. W. (1975) A protein factor essential for microtubule assembly. *Proc Natl Acad Sci U S A 72*, 1858-62.

(2) Cleveland, D. W., Hwo, S. Y., and Kirschner, M. W. (1977) Purification of tau, a microtubule-associated protein that induces assembly of microtubules from purified tubulin. *J Mol Biol 116*, 207-25.

(3) Grundke-Iqbal, I., Iqbal, K., Quinlan, M., Tung, Y. C., Zaidi, M. S., and Wisniewski, H. M. (1986) Microtubule-associated protein tau. A component of Alzheimer paired helical filaments. *J Biol Chem 261*, 6084-9.

(4) Grundke-Iqbal, I., Iqbal, K., Tung, Y. C., Quinlan, M., Wisniewski, H. M., and Binder, L. I. (1986) Abnormal phosphorylation of the microtubule-associated protein tau (tau) in Alzheimer cytoskeletal pathology. *Proc Natl Acad Sci U S A 83*, 4913-7.

(5) Ihara, Y., Nukina, N., Miura, R., and Ogawara, M. (1986) Phosphorylated tau protein is integrated into paired helical filaments in Alzheimer's disease. *J Biochem (Tokyo) 99*, 1807-10.

(6) Kosik, K. S., Joachim, C. L., and Selkoe, D. J. (1986) Microtubule-associated protein tau (tau) is a major antigenic component of paired helical filaments in Alzheimer disease. *Proc Natl Acad Sci U S A 83*, 4044-8.

(7) Wood, J. G., Mirra, S. S., Pollock, N. J., and Binder, L. I. (1986) Neurofibrillary tangles of Alzheimer disease share antigenic determinants with the axonal microtubule-associated protein tau (tau) [published erratum appears in Proc Natl Acad Sci U S A 1986 Dec;83(24):9773]. *Proc Natl Acad Sci U S A 83*, 4040-3.

(8) Buee, L., Bussiere, T., Buee-Scherrer, V., Delacourte, A., and Hof, P. R. (2000) Tau protein isoforms, phosphorylation and the role in neurodegenerative disorders. *Brain Res Brain Res Rev 33*, 95-130.

(9) Neve, R. L., Harris, P., Kosik, K. S., Kurnit, D. M., and Donlon, T. A. (1986) Identification of cDNA clones for the human microtubule-associated protein tau and chromosomal localization of the genes for tau and microtubule-associated protein 2. *Brain Res 387*, 271-80.

(10) Goedert, M., Spillantini, M. G., Jakes, R., Rutherford, D., and Crowther, R. A. (1989) Multiple isoforms of human microtubule-associated protein tau: sequences and localization in neurofibrillary tangles of Alzheimer's disease. *Neuron 3*, 519-26.

(11) Gibb, G. M., de Silva, R., Revesz, T., Lees, A. J., Anderton, B. H., and Hanger, D. P. (2004) Differential involvement and heterogeneous phosphorylation of tau isoforms in progressive supranuclear palsy. *Brain Res Mol Brain Res 121*, 95-101.

(12) Hong, M., Zhukareva, V., Vogelsberg-Ragaglia, V., Wszolek, Z., Reed, L., Miller, B. I., Geschwind, D. H., Bird, T. D., McKeel, D., Goate, A., Morris, J. C., Wilhelmsen, K. C., Schellenberg, G. D., Trojanowski, J. Q., and Lee, V.

M. (1998) Mutation-specific functional impairments in distinct tau isoforms of hereditary FTDP-17. *Science 282*, 1914-7.
(13) Lee, V. M., Goedert, M., and Trojanowski, J. Q. (2001) Neurodegenerative tauopathies. *Annu Rev Neurosci 24*, 1121-59.
(14) Goode, B. L., Denis, P. E., Panda, D., Radeke, M. J., Miller, H. P., Wilson, L., and Feinstein, S. C. (1997) Functional interactions between the proline-rich and repeat regions of tau enhance microtubule binding and assembly. *Mol Biol Cell 8*, 353-65.
(15) Chen, J., Kanai, Y., Cowan, N. J., and Hirokawa, N. (1992) Projection domains of MAP2 and tau determine spacings between microtubules in dendrites and axons. *Nature 360*, 674-7.
(16) Gendron, T. F., and Petrucelli, L. (2009) The role of tau in neurodegeneration. *Mol Neurodegener 4*, 13.
(17) (2007) *Neurobiology of Alzheimer's Disease*, Third ed., Oxford University Press Inc.
(18) Arriagada, P. V., Growdon, J. H., Hedley-Whyte, E. T., and Hyman, B. T. (1992) Neurofibrillary tangles but not senile plaques parallel duration and severity of Alzheimer's disease. *Neurology 42*, 631-9.
(19) Braak, H., and Braak, E. (1991) Neuropathological stageing of Alzheimer-related changes. *Acta Neuropathol 82*, 239-59.
(20) Terry, R. D. (1963) The Fine Structure of Neurofibrillary Tangles in Alzheimer's Disease. *J Neuropathol Exp Neurol 22*, 629-42.
(21) Gibson, P. H., Stones, M., and Tomlinson, B. E. (1976) Senile changes in the human neocortex and hippocampus compared by the use of the electron and light microscopes. *J Neurol Sci 27*, 389-405.
(22) Manetto, V., Perry, G., Tabaton, M., Mulvihill, P., Fried, V. A., Smith, H. T., Gambetti, P., and Autilio-Gambetti, L. (1988) Ubiquitin is associated with abnormal cytoplasmic filaments characteristic of neurodegenerative diseases. *Proc Natl Acad Sci U S A 85*, 4501-5.
(23) Ginsberg, S. D., Crino, P. B., Lee, V. M., Eberwine, J. H., and Trojanowski, J. Q. (1997) Sequestration of RNA in Alzheimer's disease neurofibrillary tangles and senile plaques. *Ann Neurol 41*, 200-9.
(24) Marui, W., Iseki, E., Ueda, K., and Kosaka, K. (2000) Occurrence of human alpha-synuclein immunoreactive neurons with neurofibrillary tangle formation in the limbic areas of patients with Alzheimer's disease. *J Neurol Sci 174*, 81-4.
(25) Leroy, K., Yilmaz, Z., and Brion, J. P. (2007) Increased level of active GSK-3beta in Alzheimer's disease and accumulation in argyrophilic grains and in neurones at different stages of neurofibrillary degeneration. *Neuropathol Appl Neurobiol 33*, 43-55.
(26) Huang, Y., Liu, X. Q., Wyss-Coray, T., Brecht, W. J., Sanan, D. A., and Mahley, R. W. (2001) Apolipoprotein E fragments present in Alzheimer's disease brains induce neurofibrillary tangle-like intracellular inclusions in neurons. *Proc Natl Acad Sci U S A 98*, 8838-43.

(27) Joachim, C. L., Morris, J. H., and Selkoe, D. J. (1989) Diffuse senile plaques occur commonly in the cerebellum in Alzheimer's disease. *Am J Pathol 135*, 309-19.
(28) Arendt, A., Bottger, G., and Lehmann, J. (1983) [Loss of neurons in the granular layer of the cerebellum in epilepsy]. *Zentralbl Allg Pathol 128*, 351-5.
(29) Terry, R. D., Peck, A., DeTeresa, R., Schechter, R., and Horoupian, D. S. (1981) Some morphometric aspects of the brain in senile dementia of the Alzheimer type. *Ann Neurol 10*, 184-92.
(30) Tolnay, M., and Probst, A. (1999) REVIEW: tau protein pathology in Alzheimer's disease and related disorders. *Neuropathol Appl Neurobiol 25*, 171-87.
(31) Dickson, D. W. (1998) Pick's disease: a modern approach. *Brain Pathol 8*, 339-54.
(32) Gasparini, L., Terni, B., and Spillantini, M. G. (2007) Frontotemporal dementia with tau pathology. *Neurodegener Dis 4*, 236-53.
(33) Tsuboi, Y. (2006) Neuropathology of familial tauopathy. *Neuropathology 26*, 471-4.
(34) Wszolek, Z. K., Tsuboi, Y., Ghetti, B., Pickering-Brown, S., Baba, Y., and Cheshire, W. P. (2006) Frontotemporal dementia and parkinsonism linked to chromosome 17 (FTDP-17). *Orphanet J Rare Dis 1*, 30.
(35) Goedert, M., Jakes, R., Spillantini, M. G., Hasegawa, M., Smith, M. J., and Crowther, R. A. (1996) Assembly of microtubule-associated protein tau into Alzheimer-like filaments induced by sulphated glycosaminoglycans [see comments]. *Nature 383*, 550-3.
(36) Stanford, P. M., Shepherd, C. E., Halliday, G. M., Brooks, W. S., Schofield, P. W., Brodaty, H., Martins, R. N., Kwok, J. B., and Schofield, P. R. (2003) Mutations in the tau gene that cause an increase in three repeat tau and frontotemporal dementia. *Brain 126*, 814-26.
(37) Tomizawa, K., Omori, A., Ohtake, A., Sato, K., and Takahashi, M. (2001) Tau-tubulin kinase phosphorylates tau at Ser-208 and Ser-210, sites found in paired helical filament-tau. *FEBS Lett 492*, 221-7.
(38) Jakes, R., Novak, M., Davison, M., and Wischik, C. M. (1991) Identification of 3- and 4-repeat tau isoforms within the PHF in Alzheimer's disease. *Embo J 10*, 2725-9.
(39) Lee, V. M., Balin, B. J., Otvos, L., Jr., and Trojanowski, J. Q. (1991) A68: a major subunit of paired helical filaments and derivatized forms of normal tau. *Science 251*, 675-8.
(40) Goedert, M., Wischik, C. M., Crowther, R. A., Walker, J. E., and Klug, A. (1988) Cloning and sequencing of the cDNA encoding a core protein of the paired helical filament of Alzheimer disease: identification as the microtubule-associated protein tau. *Proc Natl Acad Sci U S A 85*, 4051-5.
(41) Goedert, M., Spillantini, M. G., Cairns, N. J., and Crowther, R. A. (1992) Tau proteins of Alzheimer paired helical filaments: abnormal phosphorylation of all six brain isoforms. *Neuron 8*, 159-68.

(42) Greenberg, S. G., Davies, P., Schein, J. D., and Binder, L. I. (1992) Hydrofluoric acid-treated tau PHF proteins display the same biochemical properties as normal tau. *J Biol Chem 267*, 564-9.
(43) Kopke, E., Tung, Y. C., Shaikh, S., Alonso, A. C., Iqbal, K., and Grundke-Iqbal, I. (1993) Microtubule-associated protein tau. Abnormal phosphorylation of a non-paired helical filament pool in Alzheimer disease. *J Biol Chem 268*, 24374-84.
(44) Biernat, J., Gustke, N., Drewes, G., Mandelkow, E. M., and Mandelkow, E. (1993) Phosphorylation of Ser262 strongly reduces binding of tau to microtubules: distinction between PHF-like immunoreactivity and microtubule binding. *Neuron 11*, 153-63.
(45) Bramblett, G. T., Goedert, M., Jakes, R., Merrick, S. E., Trojanowski, J. Q., and Lee, V. M. (1993) Abnormal tau phosphorylation at Ser396 in Alzheimer's disease recapitulates development and contributes to reduced microtubule binding. *Neuron 10*, 1089-99.
(46) Goedert, M., Jakes, R., Crowther, R. A., Six, J., Lubke, U., Vandermeeren, M., Cras, P., Trojanowski, J. Q., and Lee, V. M. (1993) The abnormal phosphorylation of tau protein at Ser-202 in Alzheimer disease recapitulates phosphorylation during development. *Proc Natl Acad Sci U S A 90*, 5066-70.
(47) Mandelkow, E. M., Schweers, O., Drewes, G., Biernat, J., Gustke, N., Trinczek, B., and Mandelkow, E. (1996) Structure, microtubule interactions, and phosphorylation of tau protein. *Ann N Y Acad Sci 777*, 96-106.
(48) Seubert, P., Mawal-Dewan, M., Barbour, R., Jakes, R., Goedert, M., Johnson, G. V., Litersky, J. M., Schenk, D., Lieberburg, I., Trojanowski, J. Q., and et al. (1995) Detection of phosphorylated Ser262 in fetal tau, adult tau, and paired helical filament tau. *J Biol Chem 270*, 18917-22.
(49) Evans, D. B., Rank, K. B., Bhattacharya, K., Thomsen, D. R., Gurney, M. E., and Sharma, S. K. (2000) Tau phosphorylation at serine 396 and serine 404 by human recombinant tau protein kinase II inhibits tau's ability to promote microtubule assembly. *J Biol Chem 275*, 24977-83.
(50) Liu, F., Li, B., Tung, E. J., Grundke-Iqbal, I., Iqbal, K., and Gong, C. X. (2007) Site-specific effects of tau phosphorylation on its microtubule assembly activity and self-aggregation. *Eur J Neurosci 26*, 3429-36.
(51) Amniai, L., Barbier, P., Sillen, A., Wieruszeski, J. M., Peyrot, V., Lippens, G., and Landrieu, I. (2008) Alzheimer disease specific phosphoepitopes of Tau interfere with assembly of tubulin but not binding to microtubules. *Faseb J*.
(52) Rosner, H., Rebhan, M., Vacun, G., and Vanmechelen, E. (1995) Developmental expression of tau proteins in the chicken and rat brain: rapid down-regulation of a paired helical filament epitope in the rat cerebral cortex coincides with the transition from immature to adult tau isoforms. *Int J Dev Neurosci 13*, 607-17.
(53) Iqbal, K., Liu, F., Gong, C. X., Alonso, A. D., and Grundke-Iqbal, I. (2009) Mechanisms of tau-induced neurodegeneration. *Acta Neuropathol*.

(54) Goode, B. L., and Feinstein, S. C. (1994) Identification of a novel microtubule binding and assembly domain in the developmentally regulated inter-repeat region of tau. *J Cell Biol 124*, 769-82.
(55) Khatoon, S., Grundke-Iqbal, I., and Iqbal, K. (1994) Levels of normal and abnormally phosphorylated tau in different cellular and regional compartments of Alzheimer disease and control brains. *FEBS Lett 351*, 80-4.
(56) Mah, V. H., Eskin, T. A., Kazee, A. M., Lapham, L., and Higgins, G. A. (1992) In situ hybridization of calcium/calmodulin dependent protein kinase II and tau mRNAs; species differences and relative preservation in Alzheimer's disease. *Brain Res Mol Brain Res 12*, 85-94.
(57) Sergeant, N., Bretteville, A., Hamdane, M., Caillet-Boudin, M. L., Grognet, P., Bombois, S., Blum, D., Delacourte, A., Pasquier, F., Vanmechelen, E., Schraen-Maschke, S., and Buee, L. (2008) Biochemistry of Tau in Alzheimer's disease and related neurological disorders. *Expert Rev Proteomics 5*, 207-24.
(58) Ksiezak-Reding, H., Binder, L. I., and Yen, S. H. (1988) Immunochemical and biochemical characterization of tau proteins in normal and Alzheimer's disease brains with Alz 50 and Tau-1. *J Biol Chem 263*, 7948-53.
(59) Biernat, J., Mandelkow, E. M., Schroter, C., Lichtenberg-Kraag, B., Steiner, B., Berling, B., Meyer, H., Mercken, M., Vandermeeren, A., Goedert, M., and et al. (1992) The switch of tau protein to an Alzheimer-like state includes the phosphorylation of two serine-proline motifs upstream of the microtubule binding region. *Embo J 11*, 1593-7.
(60) Jicha, G. A., Lane, E., Vincent, I., Otvos, L., Jr., Hoffmann, R., and Davies, P. (1997) A conformation- and phosphorylation-dependent antibody recognizing the paired helical filaments of Alzheimer's disease. *J Neurochem 69*, 2087-95.
(61) Alonso, A., Zaidi, T., Novak, M., Grundke-Iqbal, I., and Iqbal, K. (2001) Hyperphosphorylation induces self-assembly of tau into tangles of paired helical filaments/straight filaments. *Proc Natl Acad Sci U S A 98*, 6923-8.
(62) Wang, J. Z., Grundke-Iqbal, I., and Iqbal, K. (1996) Restoration of biological activity of Alzheimer abnormally phosphorylated tau by dephosphorylation with protein phosphatase-2A, -2B and -1. *Brain Res Mol Brain Res 38*, 200-8.
(63) Wang, J. Z., Grundke-Iqbal, I., and Iqbal, K. (2007) Kinases and phosphatases and tau sites involved in Alzheimer neurofibrillary degeneration. *Eur J Neurosci 25*, 59-68.
(64) Alonso Adel, C., Mederlyova, A., Novak, M., Grundke-Iqbal, I., and Iqbal, K. (2004) Promotion of hyperphosphorylation by frontotemporal dementia tau mutations. *J Biol Chem 279*, 34873-81.
(65) Gamblin, T. C. (2005) Potential structure/function relationships of predicted secondary structural elements of tau. *Biochim Biophys Acta 1739*, 140-9.
(66) Binder, L. I., Guillozet-Bongaarts, A. L., Garcia-Sierra, F., and Berry, R. W. (2005) Tau, tangles, and Alzheimer's disease. *Biochim Biophys Acta 1739*, 216-23.

(67) Gamblin, T. C., King, M. E., Dawson, H., Vitek, M. P., Kuret, J., Berry, R. W., and Binder, L. I. (2000) In vitro polymerization of tau protein monitored by laser light scattering: method and application to the study of FTDP-17 mutants. *Biochemistry 39*, 6136-44.
(68) Hanger, D. P., Hughes, K., Woodgett, J. R., Brion, J. P., and Anderton, B. H. (1992) Glycogen synthase kinase-3 induces Alzheimer's disease-like phosphorylation of tau: generation of paired helical filament epitopes and neuronal localisation of the kinase. *Neurosci Lett 147*, 58-62.
(69) Sergeant, N., Delacourte, A., and Buee, L. (2005) Tau protein as a differential biomarker of tauopathies. *Biochim Biophys Acta 1739*, 179-97.
(70) Sato, S., Cerny, R. L., Buescher, J. L., and Ikezu, T. (2006) Tau-tubulin kinase 1 (TTBK1), a neuron-specific tau kinase candidate, is involved in tau phosphorylation and aggregation. *J Neurochem 98*, 1573-84.
(71) Liu, F., Grundke-Iqbal, I., Iqbal, K., and Gong, C. X. (2005) Contributions of protein phosphatases PP1, PP2A, PP2B and PP5 to the regulation of tau phosphorylation. *Eur J Neurosci 22*, 1942-50.
(72) Friedhoff, P., von Bergen, M., Mandelkow, E. M., and Mandelkow, E. (2000) Structure of tau protein and assembly into paired helical filaments. *Biochim Biophys Acta 1502*, 122-32.
(73) von Bergen, M., Barghorn, S., Biernat, J., Mandelkow, E. M., and Mandelkow, E. (2005) Tau aggregation is driven by a transition from random coil to beta sheet structure. *Biochim Biophys Acta 1739*, 158-66.
(74) Mandelkow, E., von Bergen, M., Biernat, J., and Mandelkow, E. M. (2007) Structural principles of tau and the paired helical filaments of Alzheimer's disease. *Brain Pathol 17*, 83-90.
(75) Gamblin, T. C., Berry, R. W., and Binder, L. I. (2003) Tau polymerization: role of the amino terminus. *Biochemistry 42*, 2252-7.
(76) Abraha, A., Ghoshal, N., Gamblin, T. C., Cryns, V., Berry, R. W., Kuret, J., and Binder, L. I. (2000) C-terminal inhibition of tau assembly in vitro and in Alzheimer's disease. *J Cell Sci 113 Pt 21*, 3737-45.
(77) Kuret, J., Chirita, C. N., Congdon, E. E., Kannanayakal, T., Li, G., Necula, M., Yin, H., and Zhong, Q. (2005) Pathways of tau fibrillization. *Biochim Biophys Acta 1739*, 167-78.
(78) Goedert, M., Spillantini, M. G., Hasegawa, M., Jakes, R., Crowther, R. A., and Klug, A. (1996) Molecular dissection of the neurofibrillary lesions of Alzheimer's disease. *Cold Spring Harb Symp Quant Biol 61*, 565-73.
(79) Friedhoff, P., von Bergen, M., Mandelkow, E., and Davies, P. (1998) A nucleated assembly mechanism of alzheimer paired helical filaments. *Proc Natl Acad Sci U S A 95*, 15712-7.
(80) Kampers, T., Friedhoff, P., Biernat, J., Mandelkow, E. M., and Mandelkow, E. (1996) RNA stimulates aggregation of microtubule-associated protein tau into Alzheimer-like paired helical filaments. *FEBS Lett 399*, 344-9.
(81) Wilson, D. M., and Binder, L. I. (1997) Free fatty acids stimulate the polymerization of tau and amyloid beta peptides. In vitro evidence for a

common effector of pathogenesis in Alzheimer's disease. *Am J Pathol 150*, 2181-95.
(82) Sahara, N., Maeda, S., and Takashima, A. (2008) Tau oligomerization: a role for tau aggregation intermediates linked to neurodegeneration. *Curr Alzheimer Res 5*, 591-8.
(83) Gamblin, T. C., King, M. E., Kuret, J., Berry, R. W., and Binder, L. I. (2000) Oxidative regulation of fatty acid-induced tau polymerization. *Biochemistry 39*, 14203-10.
(84) Barghorn, S., and Mandelkow, E. (2002) Toward a unified scheme for the aggregation of tau into Alzheimer paired helical filaments. *Biochemistry 41*, 14885-96.
(85) Sahara, N., Maeda, S., Murayama, M., Suzuki, T., Dohmae, N., Yen, S. H., and Takashima, A. (2007) Assembly of two distinct dimers and higher-order oligomers from full-length tau. *Eur J Neurosci 25*, 3020-9.
(86) Egelhoff, T. T., Lee, R. J., and Spudich, J. A. (1993) Dictyostelium myosin heavy chain phosphorylation sites regulate myosin filament assembly and localization in vivo. *Cell 75*, 363-71.
(87) Huang, W., and Erikson, R. L. (1994) Constitutive activation of Mek1 by mutation of serine phosphorylation sites. *Proc Natl Acad Sci U S A 91*, 8960-3.
(88) Leger, J., Kempf, M., Lee, G., and Brandt, R. (1997) Conversion of serine to aspartate imitates phosphorylation-induced changes in the structure and function of microtubule-associated protein tau. *J Biol Chem 272*, 8441-6.
(89) Maas, T., Eidenmuller, J., and Brandt, R. (2000) Interaction of tau with the neural membrane cortex is regulated by phosphorylation at sites that are modified in paired helical filaments. *J Biol Chem 275*, 15733-40.
(90) Eidenmuller, J., Fath, T., Hellwig, A., Reed, J., Sontag, E., and Brandt, R. (2000) Structural and functional implications of tau hyperphosphorylation: information from phosphorylation-mimicking mutated tau proteins. *Biochemistry 39*, 13166-75.
(91) Eidenmuller, J., Fath, T., Maas, T., Pool, M., Sontag, E., and Brandt, R. (2001) Phosphorylation-mimicking glutamate clusters in the proline-rich region are sufficient to simulate the functional deficiencies of hyperphosphorylated tau protein. *Biochem J 357*, 759-67.
(92) Haase, C., Stieler, J. T., Arendt, T., and Holzer, M. (2004) Pseudophosphorylation of tau protein alters its ability for self-aggregation. *J Neurochem 88*, 1509-20.
(93) Ding, H., Matthews, T. A., and Johnson, G. V. (2006) Site-specific phosphorylation and caspase cleavage differentially impact tau-microtubule interactions and tau aggregation. *J Biol Chem 281*, 19107-14.
(94) Fath, T., Eidenmuller, J., and Brandt, R. (2002) Tau-mediated cytotoxicity in a pseudohyperphosphorylation model of Alzheimer's disease. *J Neurosci 22*, 9733-41.
(95) Guillozet-Bongaarts, A. L., Garcia-Sierra, F., Reynolds, M. R., Horowitz, P. M., Fu, Y., Wang, T., Cahill, M. E., Bigio, E. H., Berry, R. W., and Binder, L.

I. (2005) Tau truncation during neurofibrillary tangle evolution in Alzheimer's disease. *Neurobiol Aging 26*, 1015-22.

(96) Gohar, M., Yang, W., Strong, W., Volkening, K., Leystra-Lantz, C., and Strong, M. J. (2009) Tau phosphorylation at threonine-175 leads to fibril formation and enhanced cell death: implications for amyotrophic lateral sclerosis with cognitive impairment. *J Neurochem 108*, 634-43.

(97) Hooper, C., Killick, R., and Lovestone, S. (2008) The GSK3 hypothesis of Alzheimer's disease. *J Neurochem 104*, 1433-9.

(98) Pei, J. J., Tanaka, T., Tung, Y. C., Braak, E., Iqbal, K., and Grundke-Iqbal, I. (1997) Distribution, levels, and activity of glycogen synthase kinase-3 in the Alzheimer disease brain. *J Neuropathol Exp Neurol 56*, 70-8.

(99) Hanger, D. P., Anderton, B. H., and Noble, W. (2009) Tau phosphorylation: the therapeutic challenge for neurodegenerative disease. *Trends Mol Med 15*, 112-9.

(100) Necula, M., and Kuret, J. (2004) Pseudophosphorylation and glycation of tau protein enhance but do not trigger fibrillization in vitro. *J Biol Chem 279*, 49694-703.

(101) Rankin, C. A., Sun, Q., and Gamblin, T. C. (2005) Pseudo-phosphorylation of tau at Ser202 and Thr205 affects tau filament formation. *Brain Res Mol Brain Res*.

(102) Kuhla, B., Haase, C., Flach, K., Luth, H. J., Arendt, T., and Munch, G. (2007) Effect of pseudophosphorylation and cross-linking by lipid peroxidation and advanced glycation end product precursors on tau aggregation and filament formation. *J Biol Chem 282*, 6984-91.

(103) Jeganathan, S., Hascher, A., Chinnathambi, S., Biernat, J., Mandelkow, E. M., and Mandelkow, E. (2008) Proline-directed pseudo-phosphorylation at AT8 and PHF1 epitopes induces a compaction of the paperclip folding of Tau and generates a pathological (MC-1) conformation. *J Biol Chem 283*, 32066-76.

(104) Rankin, C. A., Sun, Q., and Gamblin, T. C. (2007) Tau phosphorylation by GSK-3beta promotes tangle-like filament morphology. *Mol Neurodegener 2*, 12.

(105) Rankin, C. A., Sun, Q., and Gamblin, T. C. (2008) Pre-assembled tau filaments phosphorylated by GSK-3b form large tangle-like structures. *Neurobiol Dis 31*, 368-77.

(106) Lovestone, S., Hartley, C. L., Pearce, J., and Anderton, B. H. (1996) Phosphorylation of tau by glycogen synthase kinase-3 beta in intact mammalian cells: the effects on the organization and stability of microtubules. *Neuroscience 73*, 1145-57.

(107) Wagner, U., Utton, M., Gallo, J. M., and Miller, C. C. (1996) Cellular phosphorylation of tau by GSK-3 beta influences tau binding to microtubules and microtubule organisation. *J Cell Sci 109 (Pt 6)*, 1537-43.

(108) Hong, M., Chen, D. C., Klein, P. S., and Lee, V. M. (1997) Lithium reduces tau phosphorylation by inhibition of glycogen synthase kinase-3. *J Biol Chem 272*, 25326-32.

(109) Dhavan, R., and Tsai, L. H. (2001) A decade of CDK5. *Nat Rev Mol Cell Biol 2*, 749-59.
(110) Tsai, L. H., Takahashi, T., Caviness, V. S., Jr., and Harlow, E. (1993) Activity and expression pattern of cyclin-dependent kinase 5 in the embryonic mouse nervous system. *Development 119*, 1029-40.
(111) Kesavapany, S., Li, B. S., Amin, N., Zheng, Y. L., Grant, P., and Pant, H. C. (2004) Neuronal cyclin-dependent kinase 5: role in nervous system function and its specific inhibition by the Cdk5 inhibitory peptide. *Biochim Biophys Acta 1697*, 143-53.
(112) Lew, J., Huang, Q. Q., Qi, Z., Winkfein, R. J., Aebersold, R., Hunt, T., and Wang, J. H. (1994) A brain-specific activator of cyclin-dependent kinase 5. *Nature 371*, 423-6.
(113) Baumann, K., Mandelkow, E. M., Biernat, J., Piwnica-Worms, H., and Mandelkow, E. (1993) Abnormal Alzheimer-like phosphorylation of tau-protein by cyclin-dependent kinases cdk2 and cdk5. *FEBS Lett 336*, 417-24.
(114) Lew, J., Winkfein, R. J., Paudel, H. K., and Wang, J. H. (1992) Brain proline-directed protein kinase is a neurofilament kinase which displays high sequence homology to p34cdc2. *J Biol Chem 267*, 25922-6.
(115) Scott, C. W., Vulliet, P. R., and Caputo, C. B. (1993) Phosphorylation of tau by proline-directed protein kinase (p34cdc2/p58cyclin A) decreases tau-induced microtubule assembly and antibody SMI33 reactivity. *Brain Res 611*, 237-42.
(116) Pei, J. J., Grundke-Iqbal, I., Iqbal, K., Bogdanovic, N., Winblad, B., and Cowburn, R. F. (1998) Accumulation of cyclin-dependent kinase 5 (cdk5) in neurons with early stages of Alzheimer's disease neurofibrillary degeneration. *Brain Res 797*, 267-77.
(117) Sengupta, A., Wu, Q., Grundke-Iqbal, I., Iqbal, K., and Singh, T. J. (1997) Potentiation of GSK-3-catalyzed Alzheimer-like phosphorylation of human tau by cdk5. *Mol Cell Biochem 167*, 99-105.
(118) Lee, M. S., Kwon, Y. T., Li, M., Peng, J., Friedlander, R. M., and Tsai, L. H. (2000) Neurotoxicity induces cleavage of p35 to p25 by calpain. *Nature 405*, 360-4.
(119) Patrick, G. N., Zukerberg, L., Nikolic, M., de la Monte, S., Dikkes, P., and Tsai, L. H. (1999) Conversion of p35 to p25 deregulates Cdk5 activity and promotes neurodegeneration. *Nature 402*, 615-22.
(120) Drewes, G., Mandelkow, E. M., Baumann, K., Goris, J., Merlevede, W., and Mandelkow, E. (1993) Dephosphorylation of tau protein and Alzheimer paired helical filaments by calcineurin and phosphatase-2A. *FEBS Lett 336*, 425-32.
(121) Virshup, D. M., and Shenolikar, S. (2009) From promiscuity to precision: protein phosphatases get a makeover. *Mol Cell 33*, 537-45.
(122) Sontag, E., Nunbhakdi-Craig, V., Lee, G., Brandt, R., Kamibayashi, C., Kuret, J., White, C. L., 3rd, Mumby, M. C., and Bloom, G. S. (1999) Molecular interactions among protein phosphatase 2A, tau, and microtubules.

Implications for the regulation of tau phosphorylation and the development of tauopathies. *J Biol Chem 274*, 25490-8.
(123) Billingsley, M. L., and Kincaid, R. L. (1997) Regulated phosphorylation and dephosphorylation of tau protein: effects on microtubule interaction, intracellular trafficking and neurodegeneration. *Biochem J 323*, 577-91.
(124) Gong, C. X., Singh, T. J., Grundke-Iqbal, I., and Iqbal, K. (1993) Phosphoprotein phosphatase activities in Alzheimer disease brain. *J Neurochem 61*, 921-7.
(125) Gong, C. X., Shaikh, S., Wang, J. Z., Zaidi, T., Grundke-Iqbal, I., and Iqbal, K. (1995) Phosphatase activity toward abnormally phosphorylated tau: decrease in Alzheimer disease brain. *J Neurochem 65*, 732-8.
(126) Sontag, E., Luangpirom, A., Hladik, C., Mudrak, I., Ogris, E., Speciale, S., and White, C. L., 3rd. (2004) Altered expression levels of the protein phosphatase 2A ABalphaC enzyme are associated with Alzheimer disease pathology. *J Neuropathol Exp Neurol 63*, 287-301.
(127) Pei, J. J., Sersen, E., Iqbal, K., and Grundke-Iqbal, I. (1994) Expression of protein phosphatases (PP-1, PP-2A, PP-2B and PTP-1B) and protein kinases (MAP kinase and P34cdc2) in the hippocampus of patients with Alzheimer disease and normal aged individuals. *Brain Res 655*, 70-6.
(128) Vogelsberg-Ragaglia, V., Schuck, T., Trojanowski, J. Q., and Lee, V. M. (2001) PP2A mRNA expression is quantitatively decreased in Alzheimer's disease hippocampus. *Exp Neurol 168*, 402-12.
(129) Sontag, E., Hladik, C., Montgomery, L., Luangpirom, A., Mudrak, I., Ogris, E., and White, C. L., 3rd. (2004) Downregulation of protein phosphatase 2A carboxyl methylation and methyltransferase may contribute to Alzheimer disease pathogenesis. *J Neuropathol Exp Neurol 63*, 1080-91.
(130) Wang, J. Z., Gong, C. X., Zaidi, T., Grundke-Iqbal, I., and Iqbal, K. (1995) Dephosphorylation of Alzheimer paired helical filaments by protein phosphatase-2A and -2B. *J Biol Chem 270*, 4854-60.
(131) Liu, R., Zhou, X. W., Tanila, H., Bjorkdahl, C., Wang, J. Z., Guan, Z. Z., Cao, Y., Gustafsson, J. A., Winblad, B., and Pei, J. J. (2008) Phosphorylated PP2A (tyrosine 307) is associated with Alzheimer neurofibrillary pathology. *J Cell Mol Med 12*, 241-57.
(132) Bennecib, M., Gong, C. X., Grundke-Iqbal, I., and Iqbal, K. (2001) Inhibition of PP-2A upregulates CaMKII in rat forebrain and induces hyperphosphorylation of tau at Ser 262/356. *FEBS Lett 490*, 15-22.
(133) Bennecib, M., Gong, C. X., Grundke-Iqbal, I., and Iqbal, K. (2000) Role of protein phosphatase-2A and -1 in the regulation of GSK-3, cdk5 and cdc2 and the phosphorylation of tau in rat forebrain. *FEBS Lett 485*, 87-93.
(134) Gong, C. X., Lidsky, T., Wegiel, J., Zuck, L., Grundke-Iqbal, I., and Iqbal, K. (2000) Phosphorylation of microtubule-associated protein tau is regulated by protein phosphatase 2A in mammalian brain. Implications for neurofibrillary degeneration in Alzheimer's disease. *J Biol Chem 275*, 5535-44.

(135) Pei, J. J., Gong, C. X., An, W. L., Winblad, B., Cowburn, R. F., Grundke-Iqbal, I., and Iqbal, K. (2003) Okadaic-acid-induced inhibition of protein phosphatase 2A produces activation of mitogen-activated protein kinases ERK1/2, MEK1/2, and p70 S6, similar to that in Alzheimer's disease. *Am J Pathol 163*, 845-58.
(136) Tanimukai, H., Grundke-Iqbal, I., and Iqbal, K. (2005) Up-regulation of inhibitors of protein phosphatase-2A in Alzheimer's disease. *Am J Pathol 166*, 1761-71.
(137) Tsujio, I., Zaidi, T., Xu, J., Kotula, L., Grundke-Iqbal, I., and Iqbal, K. (2005) Inhibitors of protein phosphatase-2A from human brain structures, immunocytological localization and activities towards dephosphorylation of the Alzheimer type hyperphosphorylated tau. *FEBS Lett 579*, 363-72.
(138) Chen, S., Li, B., Grundke-Iqbal, I., and Iqbal, K. (2008) I1PP2A affects tau phosphorylation via association with the catalytic subunit of protein phosphatase 2A. *J Biol Chem 283*, 10513-21.
(139) Chohan, M. O., Khatoon, S., Iqbal, I. G., and Iqbal, K. (2006) Involvement of I2PP2A in the abnormal hyperphosphorylation of tau and its reversal by Memantine. *FEBS Lett 580*, 3973-9.
(140) Brandt, R., Gergou, A., Wacker, I., Fath, T., and Hutter, H. (2009) A Caenorhabditis elegans model of tau hyperphosphorylation: induction of developmental defects by transgenic overexpression of Alzheimer's disease-like modified tau. *Neurobiol Aging 30*, 22-33.
(141) Miyasaka, T., Ding, Z., Gengyo-Ando, K., Oue, M., Yamaguchi, H., Mitani, S., and Ihara, Y. (2005) Progressive neurodegeneration in C. elegans model of tauopathy. *Neurobiol Dis 20*, 372-83.
(142) Kraemer, B. C., Zhang, B., Leverenz, J. B., Thomas, J. H., Trojanowski, J. Q., and Schellenberg, G. D. (2003) Neurodegeneration and defective neurotransmission in a Caenorhabditis elegans model of tauopathy. *Proc Natl Acad Sci U S A 100*, 9980-5.
(143) Heidary, G., and Fortini, M. E. (2001) Identification and characterization of the Drosophila tau homolog. *Mech Dev 108*, 171-8.
(144) Frank, S., Clavaguera, F., and Tolnay, M. (2008) Tauopathy models and human neuropathology: similarities and differences. *Acta Neuropathol 115*, 39-53.
(145) Khurana, V. (2008) Modeling Tauopathy in the fruit fly Drosophila melanogaster. *J Alzheimers Dis 15*, 541-53.
(146) Wittmann, C. W., Wszolek, M. F., Shulman, J. M., Salvaterra, P. M., Lewis, J., Hutton, M., and Feany, M. B. (2001) Tauopathy in Drosophila: neurodegeneration without neurofibrillary tangles. *Science 293*, 711-4.
(147) Jackson, G. R., Wiedau-Pazos, M., Sang, T. K., Wagle, N., Brown, C. A., Massachi, S., and Geschwind, D. H. (2002) Human wild-type tau interacts with wingless pathway components and produces neurofibrillary pathology in Drosophila. *Neuron 34*, 509-19.

(148) Williams, D. W., Tyrer, M., and Shepherd, D. (2000) Tau and tau reporters disrupt central projections of sensory neurons in Drosophila. *J Comp Neurol 428*, 630-40.
(149) Mudher, A., Shepherd, D., Newman, T. A., Mildren, P., Jukes, J. P., Squire, A., Mears, A., Drummond, J. A., Berg, S., MacKay, D., Asuni, A. A., Bhat, R., and Lovestone, S. (2004) GSK-3beta inhibition reverses axonal transport defects and behavioural phenotypes in Drosophila. *Mol Psychiatry 9*, 522-30.
(150) Khurana, V., Lu, Y., Steinhilb, M. L., Oldham, S., Shulman, J. M., and Feany, M. B. (2006) TOR-mediated cell-cycle activation causes neurodegeneration in a Drosophila tauopathy model. *Curr Biol 16*, 230-41.
(151) Steinhilb, M. L., Dias-Santagata, D., Fulga, T. A., Felch, D. L., and Feany, M. B. (2007) Tau phosphorylation sites work in concert to promote neurotoxicity in vivo. *Mol Biol Cell 18*, 5060-8.
(152) Steinhilb, M. L., Dias-Santagata, D., Mulkearns, E. E., Shulman, J. M., Biernat, J., Mandelkow, E. M., and Feany, M. B. (2007) S/P and T/P phosphorylation is critical for tau neurotoxicity in Drosophila. *J Neurosci Res 85*, 1271-8.
(153) Shulman, J. M., and Feany, M. B. (2003) Genetic modifiers of tauopathy in Drosophila. *Genetics 165*, 1233-42.
(154) Nishimura, I., Yang, Y., and Lu, B. (2004) PAR-1 kinase plays an initiator role in a temporally ordered phosphorylation process that confers tau toxicity in Drosophila. *Cell 116*, 671-82.
(155) Duff, K., Knight, H., Refolo, L. M., Sanders, S., Yu, X., Picciano, M., Malester, B., Hutton, M., Adamson, J., Goedert, M., Burki, K., and Davies, P. (2000) Characterization of pathology in transgenic mice over-expressing human genomic and cDNA tau transgenes. *Neurobiol Dis 7*, 87-98.
(156) Andorfer, C., Kress, Y., Espinoza, M., de Silva, R., Tucker, K. L., Barde, Y. A., Duff, K., and Davies, P. (2003) Hyperphosphorylation and aggregation of tau in mice expressing normal human tau isoforms. *J Neurochem 86*, 582-90.
(157) Harada, A., Oguchi, K., Okabe, S., Kuno, J., Terada, S., Ohshima, T., Sato-Yoshitake, R., Takei, Y., Noda, T., and Hirokawa, N. (1994) Altered microtubule organization in small-calibre axons of mice lacking tau protein. *Nature 369*, 488-91.
(158) Gotz, J., Probst, A., Spillantini, M. G., Schafer, T., Jakes, R., Burki, K., and Goedert, M. (1995) Somatodendritic localization and hyperphosphorylation of tau protein in transgenic mice expressing the longest human brain tau isoform. *Embo J 14*, 1304-13.
(159) Ishihara, T., Hong, M., Zhang, B., Nakagawa, Y., Lee, M. K., Trojanowski, J. Q., and Lee, V. M. (1999) Age-dependent emergence and progression of a tauopathy in transgenic mice overexpressing the shortest human tau isoform. *Neuron 24*, 751-62.
(160) Spittaels, K., Van Den Haute, C., Van Dorpe, J., Bruynseels, K., Vandezande, K., Laenen, I., Geerts, H., Mercken, M., Sciot, R., Van Lommel, A., Loos, R., and Van Leuven, F. (1999) Prominent axonopathy in the brain and spinal cord

of transgenic mice overexpressing four-repeat human tau protein. *Am J Pathol 155*, 2153-2165.

(161) Brion, J. P., Tremp, G., and Octave, J. N. (1999) Transgenic expression of the shortest human tau affects its compartmentalization and its phosphorylation as in the pretangle stage of Alzheimer's disease [see comments]. *Am J Pathol 154*, 255-70.

(162) Probst, A., Gotz, J., Wiederhold, K. H., Tolnay, M., Mistl, C., Jaton, A. L., Hong, M., Ishihara, T., Lee, V. M., Trojanowski, J. Q., Jakes, R., Crowther, R. A., Spillantini, M. G., Burki, K., and Goedert, M. (2000) Axonopathy and amyotrophy in mice transgenic for human four-repeat tau protein. *Acta Neuropathol 99*, 469-81.

(163) Ishihara, T., Zhang, B., Higuchi, M., Yoshiyama, Y., Trojanowski, J. Q., and Lee, V. M. (2001) Age-dependent induction of congophilic neurofibrillary tau inclusions in tau transgenic mice. *Am J Pathol 158*, 555-62.

(164) Lewis, J., McGowan, E., Rockwood, J., Melrose, H., Nacharaju, P., Van Slegtenhorst, M., Gwinn-Hardy, K., Paul Murphy, M., Baker, M., Yu, X., Duff, K., Hardy, J., Corral, A., Lin, W. L., Yen, S. H., Dickson, D. W., Davies, P., and Hutton, M. (2000) Neurofibrillary tangles, amyotrophy and progressive motor disturbance in mice expressing mutant (P301L) tau protein. *Nat Genet 25*, 402-5.

(165) Lin, W. L., Lewis, J., Yen, S. H., Hutton, M., and Dickson, D. W. (2003) Ultrastructural neuronal pathology in transgenic mice expressing mutant (P301L) human tau. *J Neurocytol 32*, 1091-105.

(166) Santacruz, K., Lewis, J., Spires, T., Paulson, J., Kotilinek, L., Ingelsson, M., Guimaraes, A., DeTure, M., Ramsden, M., McGowan, E., Forster, C., Yue, M., Orne, J., Janus, C., Mariash, A., Kuskowski, M., Hyman, B., Hutton, M., and Ashe, K. H. (2005) Tau suppression in a neurodegenerative mouse model improves memory function. *Science 309*, 476-81.

(167) Ramsden, M., Kotilinek, L., Forster, C., Paulson, J., McGowan, E., SantaCruz, K., Guimaraes, A., Yue, M., Lewis, J., Carlson, G., Hutton, M., and Ashe, K. H. (2005) Age-dependent neurofibrillary tangle formation, neuron loss, and memory impairment in a mouse model of human tauopathy (P301L). *J Neurosci 25*, 10637-47.

(168) Spires, T. L., Orne, J. D., SantaCruz, K., Pitstick, R., Carlson, G. A., Ashe, K. H., and Hyman, B. T. (2006) Region-specific dissociation of neuronal loss and neurofibrillary pathology in a mouse model of tauopathy. *Am J Pathol 168*, 1598-607.

(169) Bellucci, A., Westwood, A. J., Ingram, E., Casamenti, F., Goedert, M., and Spillantini, M. G. (2004) Induction of inflammatory mediators and microglial activation in mice transgenic for mutant human P301S tau protein. *Am J Pathol 165*, 1643-52.

(170) Gotz, J., Chen, F., Barmettler, R., and Nitsch, R. M. (2001) Tau filament formation in transgenic mice expressing P301L tau. *J Biol Chem 276*, 529-534.

(171) Yilmazer-Hanke, D. M., and Hanke, J. (1999) Progression of Alzheimer-related neuritic plaque pathology in the entorhinal region, perirhinal cortex and hippocampal formation. *Dement Geriatr Cogn Disord 10*, 70-6.
(172) Yoshiyama, Y., Higuchi, M., Zhang, B., Huang, S. M., Iwata, N., Saido, T. C., Maeda, J., Suhara, T., Trojanowski, J. Q., and Lee, V. M. (2007) Synapse loss and microglial activation precede tangles in a P301S tauopathy mouse model. *Neuron 53*, 337-51.
(173) Gotz, J., Chen, F., Barmettler, R., and Nitsch, R. M. (2001) Tau filament formation in transgenic mice expressing P301L tau. *J Biol Chem 276*, 529-34.
(174) Allen, B., Ingram, E., Takao, M., Smith, M. J., Jakes, R., Virdee, K., Yoshida, H., Holzer, M., Craxton, M., Emson, P. C., Atzori, C., Migheli, A., Crowther, R. A., Ghetti, B., Spillantini, M. G., and Goedert, M. (2002) Abundant tau filaments and nonapoptotic neurodegeneration in transgenic mice expressing human P301S tau protein. *J Neurosci 22*, 9340-51.
(175) Terwel, D., Lasrado, R., Snauwaert, J., Vandeweert, E., Van Haesendonck, C., Borghgraef, P., and Van Leuven, F. (2005) Changed conformation of mutant Tau-P301L underlies the moribund tauopathy, absent in progressive, nonlethal axonopathy of Tau-4R/2N transgenic mice. *J Biol Chem 280*, 3963-73.
(176) Tanemura, K., Akagi, T., Murayama, M., Kikuchi, N., Murayama, O., Hashikawa, T., Yoshiike, Y., Park, J. M., Matsuda, K., Nakao, S., Sun, X., Sato, S., Yamaguchi, H., and Takashima, A. (2001) Formation of filamentous tau aggregations in transgenic mice expressing V337M human tau. *Neurobiol Dis 8*, 1036-45.
(177) Tatebayashi, Y., Miyasaka, T., Chui, D. H., Akagi, T., Mishima, K., Iwasaki, K., Fujiwara, M., Tanemura, K., Murayama, M., Ishiguro, K., Planel, E., Sato, S., Hashikawa, T., and Takashima, A. (2002) Tau filament formation and associative memory deficit in aged mice expressing mutant (R406W) human tau. *Proc Natl Acad Sci U S A 99*, 13896-901.
(178) Ikeda, M., Shoji, M., Kawarai, T., Kawarabayashi, T., Matsubara, E., Murakami, T., Sasaki, A., Tomidokoro, Y., Ikarashi, Y., Kuribara, H., Ishiguro, K., Hasegawa, M., Yen, S. H., Chishti, M. A., Harigaya, Y., Abe, K., Okamoto, K., St George-Hyslop, P., and Westaway, D. (2005) Accumulation of filamentous tau in the cerebral cortex of human tau R406W transgenic mice. *Am J Pathol 166*, 521-31.
(179) Zhang, B., Higuchi, M., Yoshiyama, Y., Ishihara, T., Forman, M. S., Martinez, D., Joyce, S., Trojanowski, J. Q., and Lee, V. M. (2004) Retarded axonal transport of R406W mutant tau in transgenic mice with a neurodegenerative tauopathy. *J Neurosci 24*, 4657-67.
(180) Mocanu, M. M., Nissen, A., Eckermann, K., Khlistunova, I., Biernat, J., Drexler, D., Petrova, O., Schonig, K., Bujard, H., Mandelkow, E., Zhou, L., Rune, G., and Mandelkow, E. M. (2008) The potential for beta-structure in the repeat domain of tau protein determines aggregation, synaptic decay, neuronal loss, and coassembly with endogenous Tau in inducible mouse models of tauopathy. *J Neurosci 28*, 737-48.

(181) von Bergen, M., Friedhoff, P., Biernat, J., Heberle, J., and Mandelkow, E. (2000) Assembly of tau protein into Alzheimer paired helical filaments depends on a local sequence motif (306VQIVYK311) forming beta structure. *Proc Natl Acad Sci U S A 97*, 5129-5134.

(182) Schindowski, K., Bretteville, A., Leroy, K., Begard, S., Brion, J. P., Hamdane, M., and Buee, L. (2006) Alzheimer's disease-like tau neuropathology leads to memory deficits and loss of functional synapses in a novel mutated tau transgenic mouse without any motor deficits. *Am J Pathol 169*, 599-616.

(183) Lim, F., Hernandez, F., Lucas, J. J., Gomez-Ramos, P., Moran, M. A., and Avila, J. (2001) FTDP-17 mutations in tau transgenic mice provoke lysosomal abnormalities and Tau filaments in forebrain. *Mol Cell Neurosci 18*, 702-14.

(184) Oddo, S., Caccamo, A., Shepherd, J. D., Murphy, M. P., Golde, T. E., Kayed, R., Metherate, R., Mattson, M. P., Akbari, Y., and LaFerla, F. M. (2003) Triple-transgenic model of Alzheimer's disease with plaques and tangles: intracellular Abeta and synaptic dysfunction. *Neuron 39*, 409-21.

(185) Gotz, J., Tolnay, M., Barmettler, R., Chen, F., Probst, A., and Nitsch, R. M. (2001) Oligodendroglial tau filament formation in transgenic mice expressing G272V tau. *Eur J Neurosci 13*, 2131-40.

(186) Higuchi, M., Ishihara, T., Zhang, B., Hong, M., Andreadis, A., Trojanowski, J., and Lee, V. M. (2002) Transgenic mouse model of tauopathies with glial pathology and nervous system degeneration. *Neuron 35*, 433-46.

(187) Lin, W. L., Lewis, J., Yen, S. H., Hutton, M., and Dickson, D. W. (2003) Filamentous tau in oligodendrocytes and astrocytes of transgenic mice expressing the human tau isoform with the P301L mutation. *Am J Pathol 162*, 213-8.

(188) Higuchi, M., Zhang, B., Forman, M. S., Yoshiyama, Y., Trojanowski, J. Q., and Lee, V. M. (2005) Axonal degeneration induced by targeted expression of mutant human tau in oligodendrocytes of transgenic mice that model glial tauopathies. *J Neurosci 25*, 9434-43.

(189) Leroy, K., Boutajangout, A., Richardson, J., Octave, J. N., Lovestone, S., Anderton, B. H., and Brion, J. P. (2003) Mutant presenilin 1 proteins induce cell death and reduce tau-dependent processes outgrowth. *Neurosci Lett 353*, 226-30.

(190) Lewis, J., Dickson, D. W., Lin, W. L., Chisholm, L., Corral, A., Jones, G., Yen, S. H., Sahara, N., Skipper, L., Yager, D., Eckman, C., Hardy, J., Hutton, M., and McGowan, E. (2001) Enhanced neurofibrillary degeneration in transgenic mice expressing mutant tau and APP. *Science 293*, 1487-91.

(191) Noble, W., Olm, V., Takata, K., Casey, E., Mary, O., Meyerson, J., Gaynor, K., LaFrancois, J., Wang, L., Kondo, T., Davies, P., Burns, M., Veeranna, Nixon, R., Dickson, D., Matsuoka, Y., Ahlijanian, M., Lau, L. F., and Duff, K. (2003) Cdk5 is a key factor in tau aggregation and tangle formation in vivo. *Neuron 38*, 555-65.

(192) Tseng, B. P., Green, K. N., Chan, J. L., Blurton-Jones, M., and LaFerla, F. M. (2008) Abeta inhibits the proteasome and enhances amyloid and tau accumulation. *Neurobiol Aging 29*, 1607-18.
(193) Gotz, J., Chen, F., van Dorpe, J., and Nitsch, R. M. (2001) Formation of neurofibrillary tangles in P301l tau transgenic mice induced by Abeta 42 fibrils. *Science 293*, 1491-5.
(194) Carlson, S. W., Branden, M., Voss, K., Sun, Q., Rankin, C. A., and Gamblin, T. C. (2007) A complex mechanism for inducer mediated tau polymerization. *Biochemistry 46*, 8838-49.
(195) Sun, Q., and Gamblin, T. C. (2009) Pseudohyperphosphorylation causing AD-like changes in tau has significant effects on its polymerization. *Biochemistry 48*, 6002-11.
(196) Ballatore, C., Lee, V. M., and Trojanowski, J. Q. (2007) Tau-mediated neurodegeneration in Alzheimer's disease and related disorders. *Nat Rev Neurosci 8*, 663-72.
(197) Alonso, A. C., Zaidi, T., Grundke-Iqbal, I., and Iqbal, K. (1994) Role of abnormally phosphorylated tau in the breakdown of microtubules in Alzheimer disease. *Proc Natl Acad Sci U S A 91*, 5562-6.
(198) Eidenmuller, J., Fath, T., and Brandt, R. (1999) in *39th American Society for Cell Biology Annual Meeting* (Botstein, D., and Yamamoto, K., Eds.) pp 375a, The American Society for Cell Biology, Washington, DC.
(199) Vallee, R. B. (1982) A taxol-dependent procedure for the isolation of microtubules and microtubule-associated proteins (MAPs). *J Cell Biol 92*, 435-42.
(200) Mandelkow, E. M., Drewes, G., Biernat, J., Gustke, N., Van Lint, J., Vandenheede, J. R., and Mandelkow, E. (1992) Glycogen synthase kinase-3 and the Alzheimer-like state of microtubule-associated protein tau. *FEBS Lett 314*, 315-21.
(201) Voss, K., and Gamblin, T. C. (2009) GSK-3beta phosphorylation of functionally distinct tau isoforms has differential, but mild effects. *Mol Neurodegener 4*, 18.
(202) Khatoon, S., Grundke-Iqbal, I., and Iqbal, K. (1992) Brain levels of microtubule-associated protein tau are elevated in Alzheimer's disease: a radioimmuno-slot-blot assay for nanograms of the protein. *J Neurochem 59*, 750-3.
(203) Schneider, A., Biernat, J., von Bergen, M., Mandelkow, E., and Mandelkow, E. M. (1999) Phosphorylation that detaches tau protein from microtubules (Ser262, Ser214) also protects it against aggregation into Alzheimer paired helical filaments. *Biochemistry 38*, 3549-58.
(204) Chirita, C. N., Necula, M., and Kuret, J. (2003) Anionic micelles and vesicles induce tau fibrillization in vitro. *J Biol Chem 278*, 25644-50.
(205) Alonso, A. C., Grundke-Iqbal, I., and Iqbal, K. (1996) Alzheimer's disease hyperphosphorylated tau sequesters normal tau into tangles of filaments and disassembles microtubules. *Nat Med 2*, 783-7.

(206) Oosawa, F. a. A., Sho (1975) *Thermodynamics of the Polymerization of Protein*, Academic Press, London, New York, San Francisco.
(207) King, M. E., Gamblin, T. C., Kuret, J., and Binder, L. I. (2000) Differential assembly of human tau isoforms in the presence of arachidonic acid. *J Neurochem 74*, 1749-57.
(208) Iqbal, K., Grundke-Iqbal, I., Zaidi, T., Merz, P. A., Wen, G. Y., Shaikh, S. S., Wisniewski, H. M., Alafuzoff, I., and Winblad, B. (1986) Defective brain microtubule assembly in Alzheimer's disease. *Lancet 2*, 421-6.
(209) Braak, H. a. o. o. f., and Braak, E. (1995) Staging of Alzheimer's disease-related neurofibrillary changes. *Neurobiol Aging 16*, 271-8; discussion 278-84.
(210) Braak, H., Braak, E., and Strothjohann, M. (1994) Abnormally phosphorylated tau protein related to the formation of neurofibrillary tangles and neuropil threads in the cerebral cortex of sheep and goat. *Neurosci Lett 171*, 1-4.
(211) Goedert, M., Jakes, R., Crowther, R. A., Cohen, P., Vanmechelen, E., Vandermeeren, M., and Cras, P. (1994) Epitope mapping of monoclonal antibodies to the paired helical filaments of Alzheimer's disease: identification of phosphorylation sites in tau protein. *Biochem J 301*, 871-7.
(212) Jicha, G. A., Bowser, R., Kazam, I. G., and Davies, P. (1997) Alz-50 and MC-1, a new monoclonal antibody raised to paired helical filaments, recognize conformational epitopes on recombinant tau. *J Neurosci Res 48*, 128-32.
(213) Lin, Y. T., Cheng, J. T., Liang, L. C., Ko, C. Y., Lo, Y. K., and Lu, P. J. (2007) The binding and phosphorylation of Thr231 is critical for Tau's hyperphosphorylation and functional regulation by glycogen synthase kinase 3beta. *J Neurochem 103*, 802-13.
(214) Lu, P. J., Wulf, G., Zhou, X. Z., Davies, P., and Lu, K. P. (1999) The prolyl isomerase Pin1 restores the function of Alzheimer-associated phosphorylated tau protein. *Nature 399*, 784-8.
(215) Otvos, L., Jr., Feiner, L., Lang, E., Szendrei, G. I., Goedert, M., and Lee, V. M. (1994) Monoclonal antibody PHF-1 recognizes tau protein phosphorylated at serine residues 396 and 404. *J Neurosci Res 39*, 669-73.
(216) Augustinack, J. C., Schneider, A., Mandelkow, E. M., and Hyman, B. T. (2002) Specific tau phosphorylation sites correlate with severity of neuronal cytopathology in Alzheimer's disease. *Acta Neuropathol (Berl) 103*, 26-35.
(217) Drewes, G., Trinczek, B., Illenberger, S., Biernat, J., Schmitt-Ulms, G., Meyer, H. E., Mandelkow, E. M., and Mandelkow, E. (1995) Microtubule-associated protein/microtubule affinity-regulating kinase (p110mark). A novel protein kinase that regulates tau-microtubule interactions and dynamic instability by phosphorylation at the Alzheimer-specific site serine 262. *J Biol Chem 270*, 7679-88.
(218) Davies, C. A., Mann, D. M., Sumpter, P. Q., and Yates, P. O. (1987) A quantitative morphometric analysis of the neuronal and synaptic content of the frontal and temporal cortex in patients with Alzheimer's disease. *J Neurol Sci 78*, 151-64.

(219) Chee, F. C., Mudher, A., Cuttle, M. F., Newman, T. A., MacKay, D., Lovestone, S., and Shepherd, D. (2005) Over-expression of tau results in defective synaptic transmission in Drosophila neuromuscular junctions. *Neurobiol Dis 20*, 918-28.
(220) Eckermann, K., Mocanu, M. M., Khlistunova, I., Biernat, J., Nissen, A., Hofmann, A., Schonig, K., Bujard, H., Haemisch, A., Mandelkow, E., Zhou, L., Rune, G., and Mandelkow, E. M. (2007) The beta-propensity of Tau determines aggregation and synaptic loss in inducible mouse models of tauopathy. *J Biol Chem 282*, 31755-65.
(221) Yuan, A., Kumar, A., Peterhoff, C., Duff, K., and Nixon, R. A. (2008) Axonal transport rates in vivo are unaffected by tau deletion or overexpression in mice. *J Neurosci 28*, 1682-7.
(222) Brandt, R., Hundelt, M., and Shahani, N. (2005) Tau alteration and neuronal degeneration in tauopathies: mechanisms and models. *Biochim Biophys Acta 1739*, 331-54.
(223) Berger, Z., Roder, H., Hanna, A., Carlson, A., Rangachari, V., Yue, M., Wszolek, Z., Ashe, K., Knight, J., Dickson, D., Andorfer, C., Rosenberry, T. L., Lewis, J., Hutton, M., and Janus, C. (2007) Accumulation of pathological tau species and memory loss in a conditional model of tauopathy. *J Neurosci 27*, 3650-62.
(224) Bretteville, A., and Planel, E. (2008) Tau aggregates: toxic, inert, or protective species? *J Alzheimers Dis 14*, 431-6.
(225) Li, B., Chohan, M. O., Grundke-Iqbal, I., and Iqbal, K. (2007) Disruption of microtubule network by Alzheimer abnormally hyperphosphorylated tau. *Acta Neuropathol 113*, 501-11.
(226) Alonso Adel, C., Li, B., Grundke-Iqbal, I., and Iqbal, K. (2006) Polymerization of hyperphosphorylated tau into filaments eliminates its inhibitory activity. *Proc Natl Acad Sci U S A 103*, 8864-9.
(227) Rankin, C. A., and Gamblin, T. C. (2008) Assessing the toxicity of tau aggregation. *J Alzheimers Dis 14*, 411-6.
(228) LaPointe, N. E., Morfini, G., Pigino, G., Gaisina, I. N., Kozikowski, A. P., Binder, L. I., and Brady, S. T. (2009) The amino terminus of tau inhibits kinesin-dependent axonal transport: implications for filament toxicity. *J Neurosci Res 87*, 440-51.
(229) Hall, G. F., Chu, B., Lee, G., and Yao, J. (2000) Human tau filaments induce microtubule and synapse loss in an in vivo model of neurofibrillary degenerative disease. *J Cell Sci 113 (Pt 8)*, 1373-87.
(230) Gong, C. X., and Iqbal, K. (2008) Hyperphosphorylation of microtubule-associated protein tau: a promising therapeutic target for Alzheimer disease. *Curr Med Chem 15*, 2321-8.
(231) Huang, H. C., and Jiang, Z. F. (2009) Accumulated amyloid-beta peptide and hyperphosphorylated tau protein: relationship and links in Alzheimer's disease. *J Alzheimers Dis 16*, 15-27.

(232) Mudher, A., and Lovestone, S. (2002) Alzheimer's disease-do tauists and baptists finally shake hands? *Trends Neurosci 25*, 22-6.
(233) Muyllaert, D., Kremer, A., Jaworski, T., Borghgraef, P., Devijver, H., Croes, S., Dewachter, I., and Van Leuven, F. (2008) Glycogen synthase kinase-3beta, or a link between amyloid and tau pathology? *Genes Brain Behav 7 Suppl 1*, 57-66.
(234) Castellani, R. J., Nunomura, A., Lee, H. G., Perry, G., and Smith, M. A. (2008) Phosphorylated tau: toxic, protective, or none of the above. *J Alzheimers Dis 14*, 377-83.
(235) Arnold, C. S., Johnson, G. V., Cole, R. N., Dong, D. L., Lee, M., and Hart, G. W. (1996) The microtubule-associated protein tau is extensively modified with O-linked N-acetylglucosamine. *J Biol Chem 271*, 28741-4.
(236) Iqbal, K., Alonso Adel, C., Chen, S., Chohan, M. O., El-Akkad, E., Gong, C. X., Khatoon, S., Li, B., Liu, F., Rahman, A., Tanimukai, H., and Grundke-Iqbal, I. (2005) Tau pathology in Alzheimer disease and other tauopathies. *Biochim Biophys Acta 1739*, 198-210.
(237) Kuo, Y. M., Emmerling, M. R., Vigo-Pelfrey, C., Kasunic, T. C., Kirkpatrick, J. B., Murdoch, G. H., Ball, M. J., and Roher, A. E. (1996) Water-soluble Abeta (N-40, N-42) oligomers in normal and Alzheimer disease brains. *J Biol Chem 271*, 4077-81.
(238) Goedert, M., Jakes, R., Spillantini, M. G., Hasegawa, M., Smith, M. J., and Crowther, R. A. (1996) Assembly of microtubule-associated protein tau into Alzheimer-like filaments induced by sulphated glycosaminoglycans. *Nature 383*, 550-3.
(239) Chirita, C. N., and Kuret, J. (2004) Evidence for an intermediate in tau filament formation. *Biochemistry 43*, 1704-14.
(240) Sarthy, J., and Gamblin, T. C. (2006) A light scattering assay for arachidonic acid-induced tau fibrillization without interfering micellization. *Anal Biochem 353*, 150-2.
(241) Necula, M., and Kuret, J. (2004) A static laser light scattering assay for surfactant-induced tau fibrillization. *Anal Biochem 333*, 205-15.
(242) Tcatchoff, L., Nespoulous, C., Pernollet, J. C., and Briand, L. (2006) A single lysyl residue defines the binding specificity of a human odorant-binding protein for aldehydes. *FEBS Lett 580*, 2102-8.
(243) Brito, R. M., and Vaz, W. L. (1986) Determination of the critical micelle concentration of surfactants using the fluorescent probe N-phenyl-1-naphthylamine. *Anal Biochem 152*, 250-5.
(244) Sun, Q., and Gamblin, T. C. (2009) Pseudohyperphosphorylation Causing AD-like Changes in Tau Has Significant Effects on Its Polymerization. *Biochemistry*.
(245) R. Ranganathan, L. T., B. L. Bales. (2000) Surfactant- and salt- induced growth of normal sodium alkyl sulftate micelles well above their critical micelle concentrations. *J. Phys. Chem 104*, 2260-2264.

(246) Chirita, C., Necula, M., and Kuret, J. (2004) Ligand-dependent inhibition and reversal of tau filament formation. *Biochemistry 43*, 2879-87.
(247) von Bergen, M., Barghorn, S., Li, L., Marx, A., Biernat, J., Mandelkow, E. M., and Mandelkow, E. (2001) Mutations of tau protein in frontotemporal dementia promote aggregation of paired helical filaments by enhancing local beta-structure. *J Biol Chem 276*, 48165-74.
(248) Wang, W., and Hecht, M. H. (2002) Rationally designed mutations convert de novo amyloid-like fibrils into monomeric beta-sheet proteins. *Proc Natl Acad Sci U S A 99*, 2760-5.
(249) King, M. E., Ahuja, V., Binder, L. I., and Kuret, J. (1999) Ligand-dependent tau filament formation: implications for Alzheimer's disease progression. *Biochemistry 38*, 14851-9.